UNIVERSITY OF CALIFORNIA
RIVERSIDE

The Effects of Anthropogenic Emissions on Cloud Condensation Nuclei and Droplet Formation

A Dissertation submitted in partial satisfaction
of the requirements for the degree of

Doctor of Philosophy

in

Chemical and Environmental Engineering

by

Emmanuel Agyekum Fofie

June 2017

Dissertation Committee:
Dr. Akua A. Asa-Awuku, Chairperson
Dr. David Cocker III
Dr. Roya Bahreini

The Dissertation of Emmanuel Agyekum Fofie is approved:

_____

_____

_____

Committee Chairperson

University of California, Riverside

Acknowledgement

I am eternally grateful to my advisor, Dr. Akua A. Asa-Awuku. Thank you for your guidance throughout my graduate education. You were always on hand to guide me through my many struggles in laboratory and the classroom. When I had moments of uncertainty and felt overwhelmed by the burden of graduate school, you were on hand to provide advice and even material support. Thank you for your faith in my abilities and potential. Next, I owe a debt of gratitude to Dr. David Cocker. You were readily available when I needed somebody to run the odd research idea by. I will always be grateful for your academic guidance and your efforts that helped me transition into American culture. I am also grateful to Dr. Roya Bahreini, for her advice and experimental guidance. I truly appreciate the times we spent together on projects. You have been an admirable professor and inspirational dissertation advisor.

I would also like to thank Dr. J. Wayne Miller for his support and professional development advice throughout my graduate student years. Also, I must thank Dr. Kent Johnson and Dr. Georgios Karavalakis and the emissions and fuel research team; Edward O'Neil, Mark Villela and Kurt Burmiller. I am grateful for all the knowledge you transferred and the expertise I gained working on projects with you.

I am also grateful to my colleagues who provided assistance at various points during work on this dissertation, Carlos Espinoza, Dr. Dan Short, Dr. Michael Giordano,

Dr. Diep Vu, Ashley Vizenor, Weihua Li, Yu Jiang, Jiacheng Yang, Patrick Roth and Pedro Piqueras. I am also very grateful to my undergraduate student who worked for me, Vincent Castellucio, who was very instrumental in completing sections of this dissertation.

I am indepted to Dr. Athanasios Nenes of Georgia Institute of Technology for his advice on various projects for this dissertation. The advice and experiences you shared were very essential to completing this dissertation. I am thankful to Rick Drgac and his team at DMT Inc. for their assistance.

I am very grateful to Laurie Kelley of Project SHARE whose benevolence ensured my survival at the most critical point of my existence. I am eternally grateful to Yaa Amoabea Ansah-Adu, for her support and commitment, and lending her ears to my scientific gibberish.

Lastly but by far not the least, I would like to thank my parents who have devoted tremendous amounts of their time, energy and financial resources to enable me achieve success. I have always been able to count on your continuous encouragement and advice. I will forever be in your debts. Thank you!

The text in Chapter 2, part or in full, is a reprint of material that is cuurntly under review for publication in the Journal of Aerosol Science and Technology; Emmanuel Fofie, Vincent Castellucio and Akua Asa-Awuku ; Exploring CCN droplet kinetics with

a higher sensitivity optical particle counter. The text in Chapter 3, part or in full, is a reprint of material currently under review for publication in the Journal of Aerosol Science and Technology; Emmanuel Fofie, Niel Donahue, and Akua Asa-Awuku; Cloud condensation nuclei activity and droplet formation of primary and secondary organic aerosol mixtures. The text in Chapter 4, part or in full, is currently been prepared for publication in Atmospheric Chemistry and Physics; Emmanuel Fofie, Patrick Roth, Georgios Karavalakis, and Akua Asa-Awuku; CCN activity and droplet kinetics of aged emissions from new gasoline direct injection engines. The text in chapter 5, part or in full, is currently been prepared for publication; Emmanuel Fofie, Athanasios Nenes and Akua Asa-Awuku; Modifications in Droplet Kinetics by Ambient Gases.

To

Mercy Anane and Sampson Fofie

ABSTRACT OF THE DISSERTATION

The Effects of Anthropogenic Emissions on Cloud Condensation Nuclei and Droplet Formation

by

Emmanuel Agyekum Fofie

Doctor of Philosophy, Graduate Program in Chemical and Environmental Engineering
University of California, Riverside, June 2017
Dr. Akua A Asa-Awuku, Chairperson

Aerosols have a direct effect on climate, through reflection of solar radiation and indirectly as seeds for cloud formation; cloud condensation nuclei (CCN). There is however, a large uncertainty in our understanding of the contributions of aerosols to climate change. It is therefore imperative to explore the chemical and physical properties of aerosol that influence CCN activity and droplet kinetics. This dissertation investigates the effects of aerosol mixing states, chemical composition and photochemical aging on the CCN forming potential of ambient salts and combustion aerosol. Using customized instrumentation and algorithms, the CCN droplet kinetics of inorganic salts and photochemically aged combustion aerosol is also evaluated.

The droplet growth of inorganic and organic salts and the effects of cloud condensation nuclei concentrations on the final droplet sizes were explored with a

modified, higher sensitivity optical particle counter (OPC). From the higher sensitivity OPC data, the final droplet diameters of CCN appear independent of aerosol hygroscopicity but strongly dependent on the CCN concentration. We also evaluated the effects of excess non-condensable gases on the CCN activation and droplet kinetics in a cloud condensation nuclei counter (CCNc). Excess, heavier gases increased mass transfer of water vapor and modified the supersaturation in the CCNc column.

The CCN activity and droplet kinetics of aged anthropogenic primary and biogenic aerosol was evaluated. CCN activity and droplet kinetics of α-pinene SOA formed in an atmospheric reactor and mixed with diesel or motor oil-fuel primary organic aerosol (POA) was characterized by the single parameter κ-hygroscopicity. Results showed that a similarity in the CCN activity of organic aerosol may indicate a propensity for mixing. An empirical model developed using unit mass resolution (UMR) aerosol mass spectrometer data captures the complex CCN activity of the mixed systems. The hygroscopicity and droplet kinetics of fresh and aged emissions from new generation gasoline direct injection engines retrofitted with a gasoline particulate filter (GPF) was also evaluated. Photochemical aging and subsequent condensation of the SOA formed from the co-emitted gas phase SOA precursors increased the hygroscopicity of gasoline emissions. This body of work provides new insights into the current understanding of the effects of aerosol chemical composition, mixing state and hygroscopicity. The findings will help reduce the prevailing uncertainty in estimating anthropogenic radiative forcing.

Table of Contents

List of Figures

List of Tables

List of Acronyms and Symbols

CCN	Cloud Condensation Nuclie
CCNc	Cloud Condensation Nuclei counter
SMCA	Scaning mobility CCN analysis
CFSTGC	Continous flow streamwise thermal gradient CCN model
OPC	Optical particle counter
TDGA	Threshold droplet growth analysis
D_p	CCN droplet diameter
d_s	Dry aerosol diameter
M_w	Molecular weight
S	Ambient water vapor supersaturation
Sc	Critical supersaturation
α	Water vapor mass accommodation coefficient
σ_w	Surface tension of water
χ	Aerosol volume fraction
κ	Single parameter hygroscopicity term
GDI	Gasoline Direct Injection
LDV	Light duty vehicles

SMPS	Scaning mobility particle sizer
PM	Particulate matter
CPC	Condensation particle counter
HR-TOF-AMS	High resolution time of flight aerosol mass spectrometer
BC	Black carbon
SOA	Secondary organic aerosol
SA	Secondary aerosol
POA	Primary organic aerosol
HTDMA	Humidified tandem differential mobility analyzer

CHAPTER 1:INTRODUCTION

Climate change significantly affects the sustainability of life on earth. Climate change has consequential effects on human life ranging from health-related decrease in air quality, food production, and hydrological changes that affect available water resources. The main drivers of climate change are anthropogenic greenhouse gases and aerosol. Aerosols have a net cooling effect and counteract the warming effect of greenhouse gases. Aerosol directly scatters solar radiation back into the atmosphere, this is the aerosol direct effect. Aerosol also acts as seeds for cloud formation. Clouds have a cooling indirect effect; they reflect the solar radiation and reduce the total radiation budget. Black carbon, aerosol formed from combustion sources, however absorbs solar radiation and has a warming effect. There is high certainty that cloud-aerosol indirect effects offset the total radiative warming from greenhouse gases. However, cloud-aerosol indirect effects contribute the highest uncertainty to estimating radiative forcing (Figure 1-1)(Dockery et al., 1993; Lohmann & Feichter, 2005; Costello et al., 2009; Stocker, 2014).

Anthropogenic aerosol interactions with atmospheric water vapor are not well constrained in regards to their size distribution, mixing states, chemical composition, hygroscopicity, and cloud condensation nuclei (CCN) activity (Pilinis et al., 1995; Cubison et al., 2008). This is due to the absence or limitations in measuring these properties. High spatial and temporal variability in aerosol-cloud interactions make it challenging to measure and model aerosol indirect effects (Kerminen et al., 2005;

McComiskey et al., 2009). Providing new insights into the current understanding of the effects of aerosol chemical composition, mixing state and hygroscopicity will help reduce the prevailing uncertainty in estimating anthropogenic radiative forcing (Liu et al., 2012; Stubenrauch et al., 2013). This work provides novel analytical techniques, optimized instrumentation and experimentation essential to characterizing the chemical, physical and thermodynamic properties of anthropogenic aerosol that impact aerosol-cloud interactions.

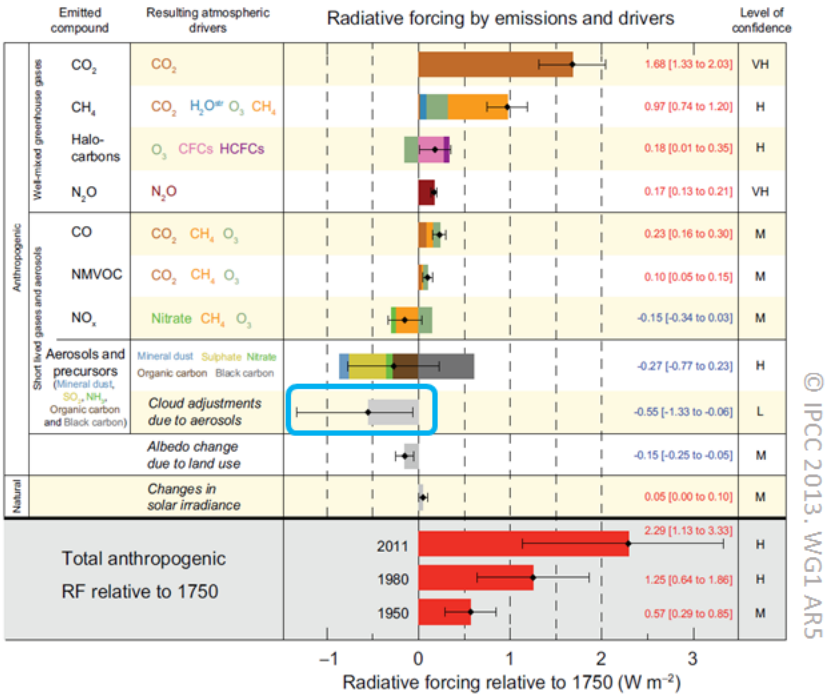

Figure 1.1. Radiative forcing estimates in 2011 relative to 1750. The best estimates of the net radiative forcing are shown as black diamonds with corresponding uncertainty intervals; the numerical values are provided on the right of the figure, together with the confidence level in the net forcing. Indirect radiative effects from clouds is circled in blue.

1.1 Aerosol Sources

Aerosols are suspensions of liquid or solid particles in a gas. The term "particulate matter" (PM) is conveniently used interchangeably with aerosol in literature. Aerosols are on the order of a few nanometers to tens of micrometers in size. Aerosols may form as a result of natural activities such as dust storms, sea spray (mainly NaCl and organic carbon), wildfires (mainly black carbon) and volcanoes (mainly ash and sulfates) (Andersson et al., 2013; Prather et al., 2013; Kumar, Barth, Madronich, et al., 2014; Kumar, Barth, Pfister, et al., 2014; Sommers et al., 2014; Mills et al., 2016). Secondary organic aerosol (SOA) forms from the photochemical oxidation of volatile biogenic and anthropogenic precursors (such as longifolene, isoprene, α-pinene). Biogenic SOA dominates the global atmospheric SOA loading (Carlton et al., 2010; Pöschl et al., 2010).

Human activities contribute a significant portion of the global aerosol budget. The main constituents of primary anthropogenic emissions include primary organic aerosol, industrial dust and black carbon (BC) (Kanakidou et al., 2005; McConnell et al., 2007; Hansson & Bhend, 2015). Secondary sulfate and nitrate aerosol form from anthropogenic emissions of SO_2 and NO_x, respectively (Martin et al., 2004). Combustion of fossil fuels, and biomass for energy generation for various applications, contribute the largest source of anthropogenic black carbon (Ramanathan & Carmichael, 2008).

1.2 Combustion Aerosol

Black carbon (BC), mainly from soot emissions, is the mostly light absorbing component of PM. BC is formed from the incomplete combustion of fossil fuels (gasoline, diesel and coal), biofuels, and biomass. BC absorbs solar radiation and has a warming effect second only to CO_2 (Bond et al., 2007). Additionally fine BC particles ($PM_{2.5}$) has adverse effects on health and regional visibility (Anenberg et al., 2012). In 2000 alone annual global BC emissions totalled 7600 Gg of which more than 60% was from anthropogenic combustion processes (Lamarque et al., 2010). In the United States, the EPA estimates more than 50% of all black carbon emissions are from transportation related combustion (Sasser et al., 2012).

When gasoline, diesel, and other high calorific oils are combusted to power transportation, BC is co-emitted with NO_x, aliphatic, and aromatic hydrocarbons (Gentner et al., 2012; May et al., 2014). In the atmosphere BC and its co-emissions undergo photochemical oxidation and form SOA (Gentner et al., 2017). In the daytime, the SOA formed forms mixtures with BC, this process has been shown to be quick, on the order of hours, making the influence of the emissions only a few kilometers away from the source (Wang et al., 2010). The formation of SOA from combustion has been explored through various laboratory chamber studies and ambient measurements. In chamber studies of mainly gasoline and diesel emissions, photochemical aging has been shown to modify the physical properties (mixing and size distribution), chemical composition, hygroscopicity and CCN activity of the initial emissions (Tritscher et al., 2011; Platt et al., 2013). However, in urban environments, gasoline emissions have been

shown to form more SOA than diesel emissions (Bahreini et al., 2012). In ambient aerosol measurements and chamber experiments, aerosol mass spectrometer (AMS) fragments associated with oxidized organic aerosol are used as markers to track the SOA formation and infer CCN activity and hygroscopicity (Duplissy et al., 2011; Lambe et al., 2011; Zhao et al., 2016).

The morphology and density of BC is modified with the incorporation of SOA coatings and primary organic aerosol (POA) during aging due to restructuring of agglomerates (Oshima et al., 2009; Nakao et al., 2011; Khalizov et al., 2013). Black carbon forms mixtures with inorganic salts, primary and secondary organic aerosol (Bond et al., 2013). The mixtures formed may be internal, external or core-shell structures. In internal mixtures organics, salts and BC are homogenously mixed to form single phase. External mixtures form from non-homogenous conglomerates of aerosol components. Core shell mixtures are formed when organics and inorganic species condense onto a BC core (Jacobson, 2001; Moffet & Prather, 2009).The formation of these mixtures depend on the miscibility, condensability and entropy of the aerosol species involved (Asa-Awuku et al., 2009; Vaden et al., 2010; Robinson et al., 2016). Due to the immiscibility of BC, however, BC mixtures are often assumed to be externally mixed (Cappa et al., 2012). The mixing state of BC assumed in cloud models is essential to the accurate estimation of aerosol direct and indirect effects (Jacobson, 2001; Wang et al., 2010). It is therefore essential to gain further insights into the mixing states of aged BC mixtures.

1.3 Cloud Formation and Droplet Kinetics

The formation of clouds from aerosols is adequately described by thermodynamic theory developed by Hilding Köhler in 1936. Köhler theory combines the Kelvin effects and Raoult's Law to relate the physical and chemical attributes of an activating aerosol (molecular mass, dissociation, dry size) to the environmental thermodynamic properties (vapor pressures/supersaturation) (Köhler, 1936). This theory is sufficient in describing ideal, soluble, and delinquent aerosol (i.e., simple inorganic salts such as NaCl and $(NH_4)_2SO_4$). It however has a few challenges when applied to complex systems of non-hygroscopic, insoluble and surface active aerosol. In such systems the CCN activity may be incorrectly estimated if these factors are not properly resolved (Asa-Awuku et al., 2008; Petters & Kreidenweis, 2008; Ruehl et al., 2012; Riipinen et al., 2015). Köhler theory is parametrized with a single κ-hygroscopicity parameter. This allows for the easy integration of hygroscopic growth and CCN activity data into cloud models (Petters & Kreidenweis, 2007).

The growth of cloud droplets after activation is constrained by the supersaturation, water vapor mass transfer and the density of CCN (Ruehl et al., 2008; Asa-Awuku et al., 2009; Ruehl et al., 2009; Lathem & Nenes, 2011).The droplet kinetics in ideal, well characterized aerosol such as NaCl and $(NH_4)_2SO_4$ is fairly simple and well understood. In complex aerosol systems however, the presence of slow dissolving, film-forming, and surface active sepcies may introduce kinetic limitations to droplet growth (Ruehl et al., 2008; Ruehl et al., 2016). These droplet kinetic limitations are most often parameterized by an apparent water vapor mass accommodation coefficient, α. The mass

accommodation coefficient has been used to constrain kinetic limitations in laboratory and ambient data with varying degrees of closure (Ruehl et al., 2008; Asa-Awuku et al., 2009; Lathem & Nenes, 2011; Raatikainen et al., 2013). Additionally, studies with ideal inorganic salt aerosols have shown modified droplet growth kinetics due to CCN density (Lathem & Nenes, 2011). Due to the limited sensitivity of currently available droplet measurement instruments however, quantifying changes in droplet diameters is challenging.

1.4 Dissertation Outline

The objectives of this dissertation were (a) to explore the CCN droplet growth kinetics with a higher sensitivity droplet measurement instrumentation and (b) investigate the CCN activity and droplet kinetics of vehicular emissions, considering aging, mixing states and chemical composition. To that end, in Chapter II, novel hardware and software techniques are employed to re-engineer the optical particle counter (OPC) on a DMT Inc. CCN counter to increase the sensitivity 2 fold. The higher sensitivity OPC is used in CCN growth experiments of well characterized inorganic salt aerosol to constraint the effects of CCN density and mass accommodation coefficient on the final droplet sizes. This chapter has been submitted for publication and is currently under review (Fofie et al., in review 2017). In Chapter III, we explore the effects of POA and biogenic SOA mixing on CCN activity and droplet kinetics. We develop a novel empirical relationship that captures complex CCN activity in anthropogenic and biogenic mixing systems using unit mass resolution (UMR) AMS data. This chapter has also been submitted for publication and is under review (Fofie et al, in review 2017b). In Chapter IV, we use

chemical composition and mixing data to constrain the hygroscopicity and droplet kinetics of fresh and photochemically aged vehicular soot. This work is in collaboration with vehicle emissions research conducted at the Center for Environmental Research Vehicle Emissions Laboratory. Soot from new generation light duty gasoline vehicles is aged in a novel mobile atmospheric reactor. A suit of online instrumentation provides high resolution compositional and physical state data. We explore the influence of particle seeding for perceived and predicted CCN hygroscopicity. Lastly, in Chapter V we use the optimized CCNc with higher resolution OPC to explore the droplet kinetics of aerosol system with an excess of heavier gases. We couple laboratory studies with a scaling analysis of the droplet growth equations to explore the influence of gases on the CCN droplet kinetics. This body of work is aimed at creating a better understanding of the effects of aerosol chemical composition, CCN density, mixing states, and aging on CCN formation and droplet kinetics and in turn reduce the uncertainty in estimating aerosol indirect effects.

1.5 Literature Cited

Andersson, S., Martinsson, B., Friberg, J., Brenninkmeijer, C., Rauthe-Schöch, A., Hermann, M., . . . Zahn, A. (2013). Composition and evolution of volcanic aerosol from eruptions of Kasatochi, Sarychev and Eyjafjallajökull in 2008–2010 based on CARIBIC observations. *Atmospheric Chemistry and Physics, 13*(4), 1781-1796.

Anenberg, S. C., Schwartz, J., Shindell, D. T., Amann, M., Faluvegi, G. S., Klimont, Z., . . . Vignati, E. (2012). Global air quality and health co-benefits of mitigating near-term climate change through methane and black carbon emission controls.

Asa-Awuku, A., Engelhart, G. J., Lee, B. H., Pandis, S. N., & Nenes, A. (2009). Relating CCN activity, volatility, and droplet growth kinetics of beta-caryophyllene secondary organic aerosol. *Atmospheric Chemistry and Physics, 9*(3), 795-812.

Asa-Awuku, A., Sullivan, A. P., Hennigan, C. J., Weber, R. J., & Nenes, A. (2008). Investigation of molar volume and surfactant characteristics of water-soluble organic compounds in biomass burning aerosol. *Atmospheric Chemistry and Physics, 8*(4), 799-812.

Bahreini, R., Middlebrook, A., Gouw, J. d., Warneke, C., Trainer, M., Brock, C., . . . Gilman, J. (2012). Gasoline emissions dominate over diesel in formation of secondary organic aerosol mass. *Geophysical Research Letters, 39*(6).

Bond, T. C., Bhardwaj, E., Dong, R., Jogani, R., Jung, S., Roden, C., . . . Trautmann, N. M. (2007). Historical emissions of black and organic carbon aerosol from energy-related combustion, 1850–2000. *Global Biogeochemical Cycles, 21*(2).

Bond, T. C., Doherty, S. J., Fahey, D. W., Forster, P. M., Berntsen, T., DeAngelo, B. J., . . . Zender, C. S. (2013). Bounding the role of black carbon in the climate system: A scientific assessment. *Journal of Geophysical Research-Atmospheres, 118*(11), 5380-5552. doi:10.1002/jgrd.50171

Cappa, C. D., Onasch, T. B., Massoli, P., Worsnop, D. R., Bates, T. S., Cross, E. S., . . . Zaveri, R. A. (2012). Radiative Absorption Enhancements Due to the Mixing State of Atmospheric Black Carbon. *Science, 337*(6098), 1078-1081. doi:10.1126/science.1223447

Costello, A., Abbas, M., Allen, A., Ball, S., Bell, S., Bellamy, R., . . . Kett, M. (2009). Managing the health effects of climate change. *The Lancet, 373*(9676), 1693-1733.

Cubison, M., Ervens, B., Feingold, G., Docherty, K., Ulbrich, I., Shields, L., . . . Jimenez, J. (2008). The influence of chemical composition and mixing state of Los Angeles urban aerosol on CCN number and cloud properties. *Atmospheric Chemistry and Physics, 8*(18), 5649-5667.

Dockery, D. W., Pope, C. A., Xu, X., Spengler, J. D., Ware, J. H., Fay, M. E., . . . Speizer, F. E. (1993). An association between air pollution and mortality in six US cities. *New England journal of medicine, 329*(24), 1753-1759.

Duplissy, J., DeCarlo, P. F., Dommen, J., Alfarra, M. R., Metzger, A., Barmpadimos, I., . . . Baltensperger, U. (2011). Relating hygroscopicity and composition of organic aerosol particulate matter. *Atmospheric Chemistry and Physics, 11*(3), 1155-1165. doi:10.5194/acp-11-1155-2011

Gentner, D. R., Isaacman, G., Worton, D. R., Chan, A. W., Dallmann, T. R., Davis, L., . . . Wilson, K. R. (2012). Elucidating secondary organic aerosol from diesel and gasoline vehicles through detailed characterization of organic carbon emissions. *Proceedings of the National Academy of Sciences, 109*(45), 18318-18323.

Gentner, D. R., Jathar, S. H., Gordon, T. D., Bahreini, R., Day, D. A., El Haddad, I., . . . de Gouw, J. (2017). Review of urban secondary organic aerosol formation from gasoline and diesel motor vehicle emissions. *Environmental science & technology, 51*(3), 1074-1093.

Hansson, H.-C., & Bhend, J. (2015). Causes of Regional Change—Aerosols *Second Assessment of Climate Change for the Baltic Sea Basin* (pp. 441-452): Springer.

Jacobson, M. Z. (2001). Strong radiative heating due to the mixing state of black carbon in atmospheric aerosols. *Nature, 409*(6821), 695-697.

Kanakidou, M., Seinfeld, J., Pandis, S., Barnes, I., Dentener, F., Facchini, M., . . . Nielsen, C. (2005). Organic aerosol and global climate modelling: a review. *Atmospheric Chemistry and Physics, 5*(4), 1053-1123.

Kerminen, V. M., Lihavainen, H., Komppula, M., Viisanen, Y., & Kulmala, M. (2005). Direct observational evidence linking atmospheric aerosol formation and cloud droplet activation. *Geophysical Research Letters, 32*(14).

Khalizov, A. F., Lin, Y., Qiu, C., Guo, S., Collins, D., & Zhang, R. (2013). Role of OH-initiated oxidation of isoprene in aging of combustion soot. *Environmental science & technology, 47*(5), 2254-2263.

Köhler, H. (1936). The nucleus in and the growth of hygroscopic droplets. *Transactions of the Faraday Society, 32*, 1152-1161.

Kumar, R., Barth, M., Madronich, S., Naja, M., Carmichael, G., Pfister, G., . . . Sarangi, T. (2014). Effects of dust aerosols on tropospheric chemistry during a typical pre-monsoon season dust storm in northern India. *Atmospheric Chemistry and Physics, 14*(13), 6813-6834.

Kumar, R., Barth, M., Pfister, G., Naja, M., & Brasseur, G. (2014). WRF-Chem simulations of a typical pre-monsoon dust storm in northern India: influences on aerosol optical properties and radiation budget. *Atmospheric Chemistry and Physics, 14*(5), 2431-2446.

Lamarque, J. F., Bond, T. C., Eyring, V., Granier, C., Heil, A., Klimont, Z., . . . Owen, B. (2010). Historical (1850–2000) gridded anthropogenic and biomass burning emissions of reactive gases and aerosols: methodology and application. *Atmospheric Chemistry and Physics, 10*(15), 7017-7039.

Lambe, A., Onasch, T., Massoli, P., Croasdale, D., Wright, J., Ahern, A., . . . Davidovits, P. (2011). Laboratory studies of the chemical composition and cloud condensation nuclei (CCN) activity of secondary organic aerosol (SOA) and oxidized primary organic aerosol (OPOA). *Atmospheric Chemistry and Physics, 11*(17), 8913-8928.

Lathem, T. L., & Nenes, A. (2011). Water Vapor Depletion in the DMT Continuous-Flow CCN Chamber: Effects on Supersaturation and Droplet Growth. *Aerosol Science and Technology, 45*(5), 604-615. doi:10.1080/02786826.2010.551146

Liu, X., Easter, R. C., Ghan, S. J., Zaveri, R., Rasch, P., Shi, X., . . . Vitt, F. (2012). Toward a minimal representation of aerosols in climate models: Description and evaluation in the Community Atmosphere Model CAM5. *Geoscientific Model Development, 5*(3), 709.

Lohmann, U., & Feichter, J. (2005). Global indirect aerosol effects: a review. *Atmospheric Chemistry and Physics, 5*(3), 715-737.

Martin, S., Hung, H.-M., Park, R., Jacob, D., Spurr, R., Chance, K., & Chin, M. (2004). Effects of the physical state of tropospheric ammonium-sulfate-nitrate particles on global aerosol direct radiative forcing. *Atmospheric Chemistry and Physics, 4*(1), 183-214.

May, A. A., Nguyen, N. T., Presto, A. A., Gordon, T. D., Lipsky, E. M., Karve, M., . . . Brandow, C. (2014). Gas-and particle-phase primary emissions from in-use, on-road gasoline and diesel vehicles. *Atmospheric Environment, 88*, 247-260.

McComiskey, A., Feingold, G., Frisch, A. S., Turner, D. D., Miller, M. A., Chiu, J. C., . . . Ogren, J. A. (2009). An assessment of aerosol-cloud interactions in marine stratus clouds based on surface remote sensing. *Journal of Geophysical Research: Atmospheres, 114*(D9).

McConnell, J. R., Edwards, R., Kok, G. L., Flanner, M. G., Zender, C. S., Saltzman, E. S., . . . Kahl, J. D. (2007). 20th-century industrial black carbon emissions altered arctic climate forcing. *Science, 317*(5843), 1381-1384.

Mills, M. J., Schmidt, A., Easter, R., Solomon, S., Kinnison, D. E., Ghan, S. J., . . . Bardeen, C. G. (2016). Global volcanic aerosol properties derived from emissions, 1990–2014, using CESM1 (WACCM). *Journal of Geophysical Research: Atmospheres, 121*(5), 2332-2348.

Moffet, R. C., & Prather, K. A. (2009). In-situ measurements of the mixing state and optical properties of soot with implications for radiative forcing estimates. *Proceedings of the National Academy of Sciences, 106*(29), 11872-11877.

Nakao, S., Shrivastava, M., Nguyen, A., Jung, H., & Cocker III, D. (2011). Interpretation of secondary organic aerosol formation from diesel exhaust photooxidation in an environmental chamber. *Aerosol Science and Technology, 45*(8), 964-972.

Oshima, N., Koike, M., Zhang, Y., Kondo, Y., Moteki, N., Takegawa, N., & Miyazaki, Y. (2009). Aging of black carbon in outflow from anthropogenic sources using a mixing state resolved model: Model development and evaluation. *Journal of Geophysical Research: Atmospheres, 114*(D6).

Petters, M., & Kreidenweis, S. (2007). A single parameter representation of hygroscopic growth and cloud condensation nucleus activity. *Atmospheric Chemistry and Physics, 7*(8), 1961-1971.

Petters, M. D., & Kreidenweis, S. M. (2008). A single parameter representation of hygroscopic growth and cloud condensation nucleus activity–Part 2: Including solubility. *Atmospheric Chemistry and Physics, 8*(20), 6273-6279.

Pilinis, C., Pandis, S. N., & Seinfeld, J. H. (1995). Sensitivity of direct climate forcing by atmospheric aerosols to aerosol size and composition. *Journal of Geophysical Research: Atmospheres, 100*(D9), 18739-18754.

Platt, S., Haddad, I. E., Zardini, A., Clairotte, M., Astorga, C., Wolf, R., . . . Ježek, I. (2013). Secondary organic aerosol formation from gasoline vehicle emissions in a new mobile environmental reaction chamber. *Atmospheric Chemistry and Physics, 13*(18), 9141-9158.

Prather, K. A., Bertram, T. H., Grassian, V. H., Deane, G. B., Stokes, M. D., DeMott, P. J., . . . Seinfeld, J. H. (2013). Bringing the ocean into the laboratory to probe the chemical complexity of sea spray aerosol. *Proceedings of the National Academy of Sciences, 110*(19), 7550-7555.

Raatikainen, T., Nenes, A., Seinfeld, J. H., Morales, R., Moore, R. H., Lathem, T. L., . . . Cerully, K. M. (2013). Worldwide data sets constrain the water vapor uptake coefficient in cloud formation. *Proceedings of the National Academy of Sciences, 110*(10), 3760-3764.

Ramanathan, V., & Carmichael, G. (2008). Global and regional climate changes due to black carbon. *Nature geoscience, 1*(4), 221-227.

Riipinen, I., Rastak, N., & Pandis, S. (2015). Connecting the solubility and CCN activation of complex organic aerosols: a theoretical study using solubility distributions. *Atmospheric Chemistry and Physics, 15*(11), 6305-6322.

Robinson, E. S., Donahue, N. M., Ahern, A. T., Ye, Q., & Lipsky, E. (2016). Single-particle measurements of phase partitioning between primary and secondary organic aerosols. *Faraday discussions*.

Ruehl, C., Chuang, P., & Nenes, A. (2008). How quickly do cloud droplets form on atmospheric particles? *Atmospheric Chemistry and Physics, 8*(4), 1043-1055.

Ruehl, C., Chuang, P., & Nenes, A. (2009). Distinct CCN activation kinetics above the marine boundary layer along the California coast. *Geophysical Research Letters, 36*(15).

Ruehl, C., Chuang, P., Nenes, A., Cappa, C., Kolesar, K., & Goldstein, A. (2012). Strong evidence of surface tension reduction in microscopic aqueous droplets. *Geophysical Research Letters, 39*(23).

Ruehl, C. R., Davies, J. F., & Wilson, K. R. (2016). An interfacial mechanism for cloud droplet formation on organic aerosols. *Science, 351*(6280), 1447-1450.

Sasser, E., Hemby, J., Adler, K., Anenberg, S., Bailey, C., Brockman, L., . . . Dawson, J. (2012). Report to Congress on Black Carbon. *Department of the Interior, Environment, and Related Agencies*.

Sommers, W. T., Loehman, R. A., & Hardy, C. C. (2014). Wildland fire emissions, carbon, and climate: science overview and knowledge needs. *Forest Ecology and Management, 317*, 1-8.

Stocker, T. (2014). *Climate change 2013: the physical science basis: Working Group I contribution to the Fifth assessment report of the Intergovernmental Panel on Climate Change*: Cambridge University Press.

Stubenrauch, C., Rossow, W., Kinne, S., Ackerman, S., Cesana, G., Chepfer, H., . . . Heidinger, A. (2013). Assessment of global cloud datasets from satellites: Project

and database initiated by the GEWEX radiation panel. *Bulletin of the American Meteorological Society, 94*(7), 1031-1049.

Tritscher, T., Jurányi, Z., Martin, M., Chirico, R., Gysel, M., Heringa, M. F., . . . Weingartner, E. (2011). Changes of hygroscopicity and morphology during ageing of diesel soot. *Environmental Research Letters, 6*(3), 034026.

Vaden, T. D., Song, C., Zaveri, R. A., Imre, D., & Zelenyuk, A. (2010). Morphology of mixed primary and secondary organic particles and the adsorption of spectator organic gases during aerosol formation. *Proceedings of the National Academy of Sciences, 107*(15), 6658-6663.

Wang, J., Cubison, M., Aiken, A., Jimenez, J., & Collins, D. (2010). The importance of aerosol mixing state and size-resolved composition on CCN concentration and the variation of the importance with atmospheric aging of aerosols. *Atmospheric Chemistry and Physics, 10*(15), 7267-7283.

Zhao, D., Buchholz, A., Kortner, B., Schlag, P., Rubach, F., Fuchs, H., . . . Watne, Å. (2016). Cloud condensation nuclei activity, droplet growth kinetics, and hygroscopicity of biogenic and anthropogenic secondary organic aerosol (SOA). *Atmospheric Chemistry and Physics, 16*(2), 1105-1121.

CHAPTER 2:EXPLORING CCN DROPLET KINETICS WITH A HIGHER SENSITIVITY OPC

2.1 Introduction

Warm clouds have a relative cooling effect on the atmosphere due to the reflection of solar radiation. Aerosol that activate into cloud droplets are called cloud condensation nuclei (CCN). The number and size of CCN droplets influence the amount of light reflected by the clouds; smaller droplets reflect more light than larger droplets. This is the cloud indirect effect (Twomey, 1974). The sizes of cloud droplets also determine the cloud optical depth which is the cloud's ability to modify incident light (Roeckner et al., 1987; Schwartz & Benkovitz, 2002; Rose et al., 2008). The estimation and modelling of these aerosol-cloud interactions are complex and currently incompletely constrained. This is due to the absence of fully resolved, global models that account for aerosol physical and chemical properties and spatial variations in atmospheric conditions (McFiggans et al., 2006; Rosenfeld et al., 2014). There is therefore a high uncertainty in predicting the anthropogenic radiative forcing resulting in variable estimations of global warming (Anderson et al., 2003; Stocker, 2014).

The ability of an aerosol to act as a cloud condensation nuclei is significantly influenced by the particle size and chemical composition (Dusek et al., 2006), the aerosol mixing state (Wang et al., 2010) and morphology (Giordano et al., 2015). The

hygroscopicity of the aerosol, its ability to absorb water vapor, depends on the factors above and can be represented by a single parameter κ-hygroscopicity (Petters & Kreidenweis, 2007, 2008). The singular κ-value accounts for the effects of aerosol chemistry and is easily incorporated into cloud models.

Droplet kinetic studies achieve a greater understanding of the chemical (e.g., surface active components, mass accommodation coefficient) and physical constraints (e.g., mixing states, aerosol loading) that influence droplet growth. Pioneering work by Nenes and co-authors explored the effects of the supersaturation, CCN droplet concentrations and instrument residence time on the growth of CCN droplets with the DMT CCNc. Studies further characterized the effects of the CCN concentrations on the final droplet diameters; higher CCN concentrations deplete the supersaturation and depress droplet sizes. The depression in droplet sizes were found to be uniform for most fast activating aerosol and negligible at CCN concentrations below $5000\ cm^{-3}$ (Nenes, Ghan, et al., 2001; Lathem & Nenes, 2011). By comparing ambient droplets measured with a phase Doppler interferometer and laboratory generated CCN, *Ruehl et al.(2008)* characterized the droplet growth rate and kinetic limitations with an apparent mass accommodation coefficient and found differences in the droplet kinetics attributed to slow-dissolving and film forming compounds. However, *Raatikainen et al*, (2013) using worldwide DMT CCNc data sets, suggest that ubiquitous rapidly activating aerosol ($\alpha > 0.1$) are omnipresent and indicate there is a minimal uncertainty in the water vapor accommodation. Thus aerosol should grow to the same droplet sizes at similar saturation conditions (i.e., flowrate and temperature gradient).

Various instruments have been developed to characterize CCN and droplet kinetics. The first of such instruments was a batch, wetted parallel plate, static thermal diffusion chamber designed by Twomey (Twomey, 1963). It achieved a low supersaturation of 0.2% by applying a temperature differential across the two wetted parallel plates. Several minutes are required to obtain a full CCN spectrum over several supersaturations. There were also challenges with the confidence in the resolution obtained with this design. Improvements on the parallel plate were made by making the flow continuous thereby eliminating the low resolution and data constrains of the initial batch design (Sinnarwalla & Alofs, 1973). In the more recent CCNc design, a wetted cylindrical column is sectionally heated and cooled to obtain a streamwise flow supersaturation in the centerline of the column (Hoppel et al., 1979; Chuang et al., 2000; Nenes, Chuang, et al., 2001).

Based on work by *Roberts and Nenes (2005)*, Droplet Measurement Technologies Inc. (DMT) developed a fast, real-time continuous flow streamwise thermal gradient CCN. The DMT CCNc became commercially available in 2005 and has since provided prolific data on the nature of CCN. DMT CCNc data has provided insight into the CCN activity and hygroscopicity of various aerosol systems (Petters & Kreidenweis, 2007; Engelhart et al., 2008; Asa-Awuku et al., 2009; Giordano et al., 2015). The DMT CCNc has also been employed in visibility studies and haze formation as well as in droplet optical properties measurement (Shinozuka et al., 2009; Leng et al., 2016). Cloud microphysics and droplet growth kinetics has also been explored. The number of studies

exploiting the data from the DMT CCNc to infer droplet kinetics and characterize CCN droplets is however paltry compared to the total data available.

The DMT CCNc develops a supersaturation at the centerline of a cylindrical alumina bisque column. The water from the alumina bisque diffuses faster in air than heat and creates a thermodynamically unstable regime at the centerline resulting in a supersaturated regime. The superstation is modified by sample flowrate, Q, and temperatures gradient, ΔT. Aerosol with a critical supersaturation, S_c less than the column centerline supersaturation, *SS* will activate into cloud condensation nuclei and are counted by the optical particle counter (OPC) at the exit of the column (Roberts & Nenes, 2005; Lance et al., 2006; Seinfeld & Pandis, 2016).

The standard DMT CCNc measures CCN using an OPC with a 660nm wavelength laser with up to 50 mW power. The growing CCN droplets scatters the light at an angle of 27- 153° and is detected by a photodiode at 1 Hz resolution. The CCN concentration is inferred from the frequency of the beam pulses. A proprietary Mie theory based algorithm converts the intensity of the scattered light into droplet sizes (Bohren & Huffman, 1983). The standard CCN counter is fitted with an OPC with a minimum detection threshold of 0.75 μm and maximum detection limit of 10 μm. The counts are separated into 20 bins, with the first two bins having a 0.25 μm bin width. The remaining bins have a 0.5 μm bin width. The size detection limits are sufficient for the characterization of the CCN activity of laboratory generated and ambient aerosol for the instrument flowrates (0.2 – 1 LPM) and operational supersaturations (0.07 – 2.0%).

However, any droplet size difference less than 0.5μm is not detected within the standard OPC sensitivity (Roberts & Nenes, 2005; DMT, 2012a, 2012b).

Will droplet data from a DMT CCNc counter with a higher sensitivity optical particle counter provide additional insight into our current understanding of CCN droplet kinetics? In this study we customized a CCNc with a higher sensitivity optical particle counter (OPC-β). We use data from the modified CCN and the standard commercially available DMT CCN counter to evaluate the CCN activity and droplet kinetics of organic and inorganic salts. The effects of solute composition and CCN concentrations on the final droplet sizes is measured. We use dry aerosol size information and CCN spectrum data from the higher sensitivity OPC-β CCNc and the continuous flow streamwise thermal gradient CCN (CFSTGC) model to estimate the mass accommodation coefficient, α.

2.2 Experimental Methods

The OPC hardware and CCN proprietary software is re-engineered in this study. The laser, internal optics and the main body of the two OPCs are identical, except for the electronics and the algorithm used to estimate the droplet diameters. In the standard OPC, the lowest signal threshold is set at 0.5 μm, noise level, and the highest signal at 10 μm. The signal between the two thresholds are quantized into 20 bins. In the modified OPC (hereon defined as OPC-β), the lower threshold is set to less than 3 μm and the highest threshold is at 8 μm with the 20 bins maintained. The bin size width is therefore reduced from 0.5 μm to 0.25 μm. A decrease in the bin size width increases the sensitivity of the

measurements. The instrument LabVIEW® code was modified to integrate these changes.

Both OPCs were calibrated with National Institute of Standards and Technology (NIST) certified borosilicate glass beads (Thermo Scientific) and the CFSTGC model (Lance et al., 2006; Lathem & Nenes, 2011; Raatikainen et al., 2012). Previous work shows that glass beads have a comparable refraction to water droplets and do not influence the OPC sizing (Raatikainen et al., 2012). Four borosilicate glass spheres of mean diameters 1.9 μm ± 0.5 μm, 5.4 μm ±0.3 μm, 8.0 μm ± 0.4 μm and 10 μm ± 1.0 μm, were injected into the CCNc column with a custom bead injector. The CCNc was operated at 0°K temperature gradient. The bead injector was placed in-line with the sample flow (between the top of the column and the low pressure end of the laminar flow) and a filter was placed at the open CCNc inlet. The set-up reduces coincident errors. (Raatikainen et al., 2012)

The standard OPC calibration with the glass beads showed a ~30% under-sizing error (Fig. 1, blue triangles). As such, the laser baseline was adjusted and the calibration repeated until a near perfect fit was attained. A concurrent setup of the two CCN counters, one fitted with a standard calibrated OPC and the other with the modified OPC-β was done with laboratory generated $(NH_4)_2SO_4$ aerosol. The dry aerosol size and number, sample and inlet temperatures, flowrates, pressure and the calibrated supersaturation from ammonium sulfate experiments are inputs for the CFSTGC model.

The hygroscopicity parameter, κ of 0.605 and a mass accommodation coefficient, α = 0.2 were used. The CCN number was ~$500\ cm^{-3}$ (Lathem & Nenes, 2011). Both the

software (CFSTGC model) and the hardware (glass beads) calibration agree for the standard OPC (Fig 2-1. blue circles) and either calibration method can be used. Here we use the CFSTGC model to calibrate OPC-β. The droplet diameters from the OPC-β and that of the CFSTGC model also agree (R^2 = 0.99) with only a ~10% under-sizing error (Fig. 2 - 1, green squares).

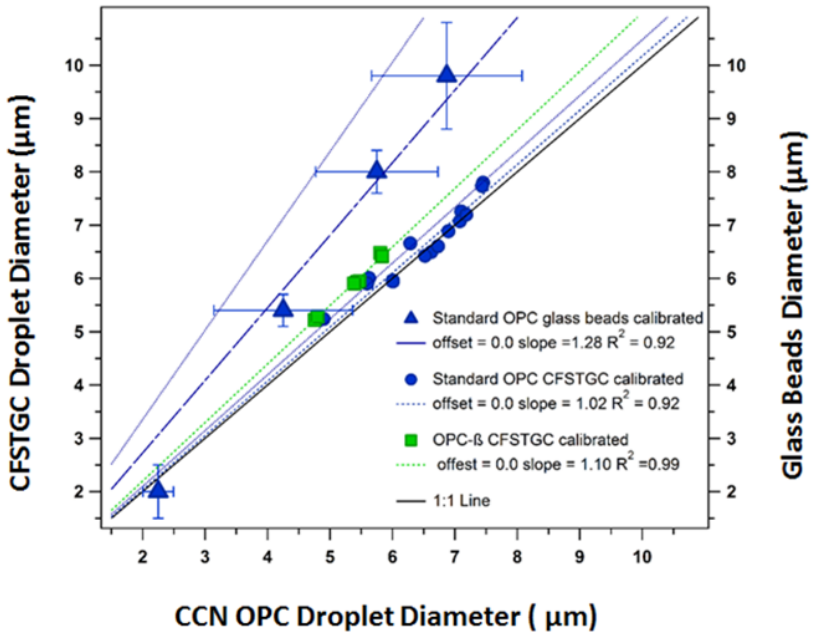

Figure 2.1. Calibration of the CCN optical particle counters. Calibration of the standard OPC with borosilicate glass beads (blue filled triangles). The glass beads-corrected standard OPC (blue circles) and OPC-β (green squares) are concurrently calibrated with the CFSTGC model. Both CCN counters were operated at 0.4- 0.8% *SS*, 0.5 LPM and 100 nm dry diameter ammonium sulfate.

Aerosol of known chemical composition with κ-hygroscopicity ranging from 0.2 to 1.3 (Table 2-1) was atomized using a custom-built Collison atomizer. The experimental set-up is shown in Fig. 2-2. A dry diameter, higher than the critical diameter, dp_{50}, (80 or 100 nm) was selected with an Scanning Mobility Particle Sizing (SMPS) system (TSI DMA 3081 and CPC 3772). The dry size concentration was also kept below $2500\ cm^{-3}$. The size selected dry aerosol was activated with the OPC-β CCNc. The instrument supersaturation was also calibrated with $(NH_4)_2SO_4$ aerosol using the scanning mobility CCN analysis (SMCA) approach (Moore et al., 2010). The CCNc flowrates were calibrated within ±5% of the set point, as per instrument manufacturer recommendations. The OPC first stage monitor was kept below the recommended manufacturer voltage to eliminate fogging. The CCNc supersaturation was from 0.1 – 0.8% whiles the flowrate was 0.25 and 0.5 lpm. The droplet diameters at each supersaturation and flowrate were estimated from the frequency of the signal in each of the 20 bins. The same conditions in supersaturation and flowrate were maintained in a separate experiment to assess the effects of CCN concentration on droplet size. The CCN concentration was increased from 200 to 10000 cm^{-3} by modifying the atomizer pressure and solute concentration. The mass accommodation coefficient, α , for each chemical composition was estimated using the CFSTGC model (Lance et al., 2006; Lathem & Nenes, 2011). CFSTGC simultaneously solves the droplet growth equations using an assumed mass accommodation coefficient (which we vary in this work), the CCN variables (flowrate, supersaturation, flow ratio, pressure, and temperature), the dry particle size and the κ-hygroscopicity

Table 2.1 CCN derived κ-hygroscopicity.[1]

Chemical Composition	***κ-hygroscopicity***
Sodium chloride	1.28
Ammonium chloride	1.20
Ammonium nitrate	0.75
Ammonium sulfate	0.61
Oxalic acid	0.33
Malonic acid	0.22
Succinic acid	0.23

[1]Petters and Kreidenweis (2007) and references therein; κ was adapted from Table 1

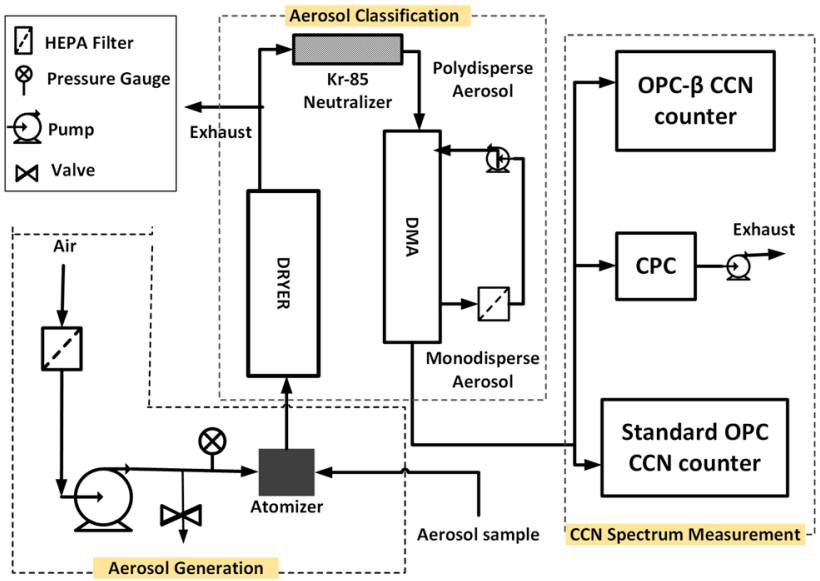

Figure 2.2 Experimental setup for measuring CCN activity and droplet diameter. The atomized aerosol is dried, charged and classified with the Differential Mobility Analyzer (DMA). 80 and 100 nm dry sizes are selected for droplet experiments. The DMA stream is split between a Condensation Particle Counter (CPC), a CCN with the standard OPC and the CCN with the OPC-β.

2.3 Results and Discussion

Simulations from the CFSTGC model provide insights into the rate of water uptake of the growing droplet characterized by the water vapor mass accommodation, α. Simulated droplet sizes for solutes of different chemical composition (varying κ-hygroscopicity) and constant instrument settings (flowrate, temperature gradient, supersaturation) are similar (Fig. A-1).

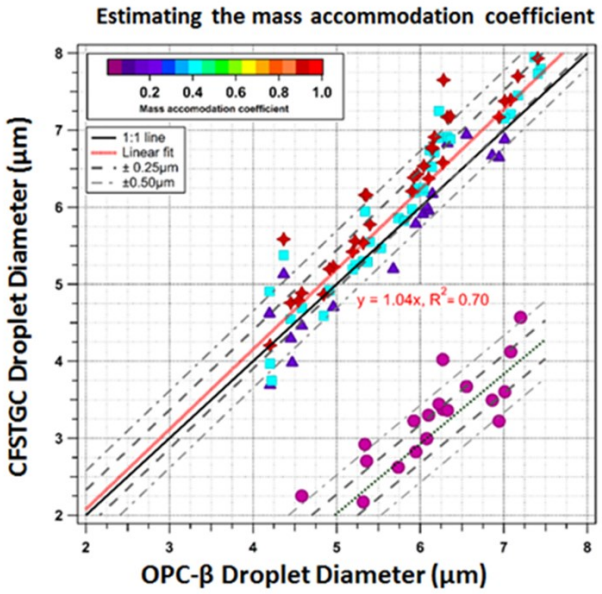

Figure 2.3. Droplets simulated with the CFSTGC model for mass accommodation coefficients from 0.01 – 1 and compared with the experimentally derived CCN droplets. A best fit line is provided for α > 0.1

Figure 2.3 summarizes the simulated droplet diameter for all compositions, supersaturations (0.2 – 0.8%), and flowrates considered. There were no significant differences between the experimental OPC-β and simulated droplet diameters for $\alpha \geq 0.1$ (S = 1.04, R^2 =0.7). The simulations under-predict the droplet diameter by ~40% for $\alpha = 0.01$. Therefore mass accommodation values, $0.1 \geq \alpha \leq 1$, yield the best convergence for all compositions. Hence, lower mass accommodation values do not adequately predict the droplet kinetics of simple compounds.

In figure 2.4, we evaluate the dependence of the CCN droplet diameter on the CCN concentration. The droplet diameters for all the aerosol species (at 80 and 100 nm dry diameters) were evaluated for CCN concentrations from 500 -10000 cm^{-3} and

flowrates between 0.25 and 0.50 lpm. We observe a suppression in the droplet diameter as the CCN concentration increased for all hygroscopicities and at all supersaturations and flowrates considered. In both the standard OPC and OPC-β, a ~0.2 μm decrease in the droplet diameter per $1000cm^{-3}$ was observed. The decrease in the droplet sizes was present at lower CCN concentrations; lower than the previously suggested 5000 cm^{-3} CCN threshold for fast activating simple salts (Lathem & Nenes, 2011). Changes in droplet diameters are also observed for CCN less than 1500 cm^{-3} in the higher sensitivity OPC-β (with 0.25μm bin width).

In the standard OPC however, a more significant change in the CCN concentration (>> 2500 cm^{-3}) is required to see droplet depression. The depression in the droplet diameters was observed for all dry aerosol sizes, flowrates and supersaturations evaluated. The dependence of CCN droplet diameter on the solute composition is evaluated in Figure 2-5. The droplet diameter of $(NH_4)_2SO_4$ is commonly used as a reference and compared to the droplet diameters of aerosol of different composition at the same dry size, supersaturation and flowrate. This method, known as threshold droplet growth analysis (TDGA) has previously been applied to ambient and laboratory data sets (Asa-Awuku et al., 2008; Engelhart et al., 2008; Raatikainen et al., 2012). TDGA was previously published with an uncertainty of ± 0.5 μm. However, OPC-β has ± 0.25 μm bin widths and uncertainty. The droplet diameters from the OPC-β of activated 100 nm aerosol with varying hygroscopicities at 0.25 and 0.5 lpm for supersaturations from 0.15 to 0.6% are compared in figure 2-5. Additionally, total CCN concentrations are < 3000 cm^{-3}. 80 nm data (not shown) produces similar results. For both flowrates considered,

the droplet sizes of all aerosol are within one bin deviation (± 0.25μm) of the $(NH_4)_2SO_4$) reference. Where differences exist, they are usually less than 2 bin sizes and are inconsistent over the supersaturation range. There are therefore no statistically relevant changes in the CCN droplet diameters due to differences in the aerosol chemical composition (and κ- hygroscopicity).

Final droplet diameters of TDGA should be re-evaluated accounting for droplet depletion (Fig. 2-5b and 2-5d). Significant depressions in the droplet diameters occur well below 5000 cm^{-3} (Fig. 2-4). The previously stated 0.2 μm per 1000 cm^{-3} is used to normalize the droplet data in Fig 2.5a and 2.5c. The normalized droplet diameters exhibit smaller variability. In the 0.25 lpm experiments, Fig. 2.5a, the average standard deviation, σ, is decreased from 0.17 to 0.11 in Fig. 2-5b. σ also decreased from 0.16 to 0.13 in the 0.50 lpm experiments (Figs. 2.5c and 2.5d). Although CCN concentrations are below 3000 cm^{-3} in Fig. 2.5 (i.e., concentrations are well below the suggested 5000 cm^{-3} threshold) droplet size corrections are required and make the data more robust.

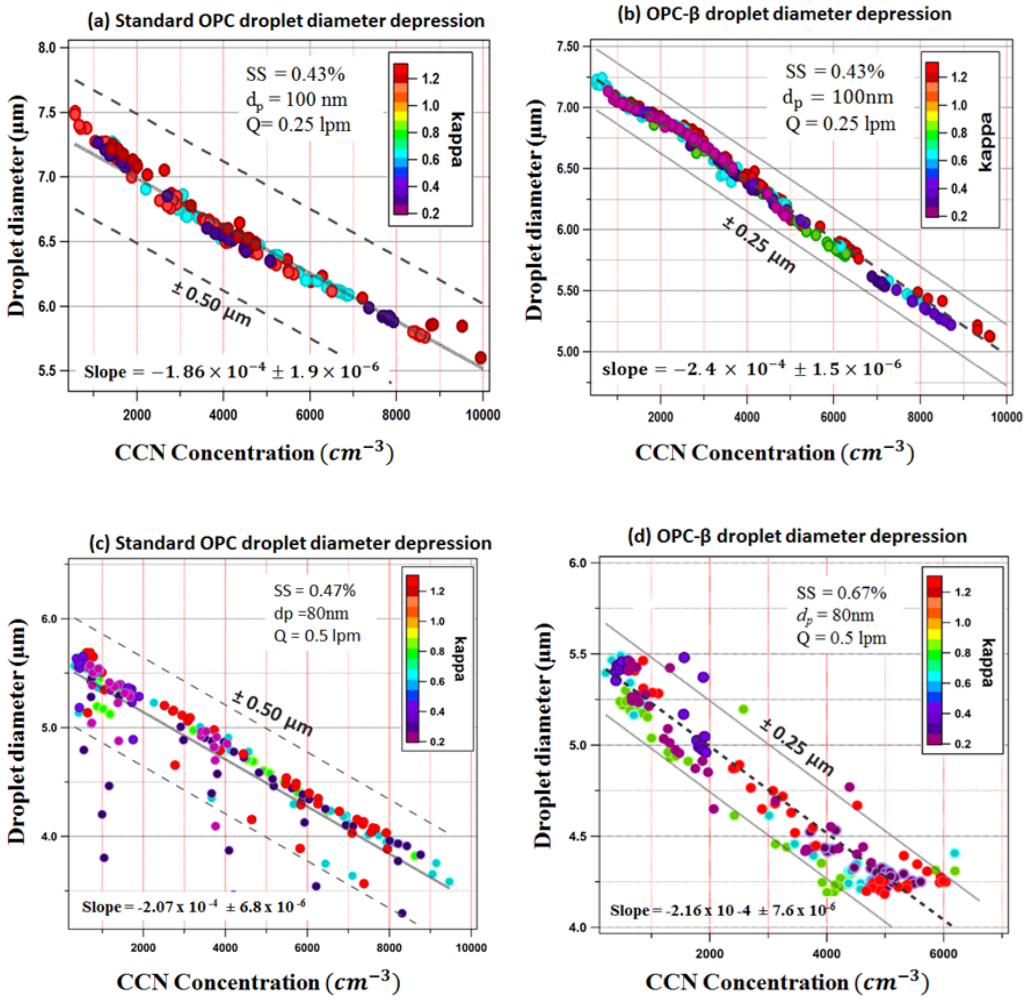

Figure 2.4. Decreases in droplet diameter with increasing CCN concentrations. In (a) & (c), the droplet diameter is measured with the standard OPC. In (b) & (d) the droplet diameter is measured with the modified the OPC. Aerosol chemistry is indicated by changing κ-hygroscopicity

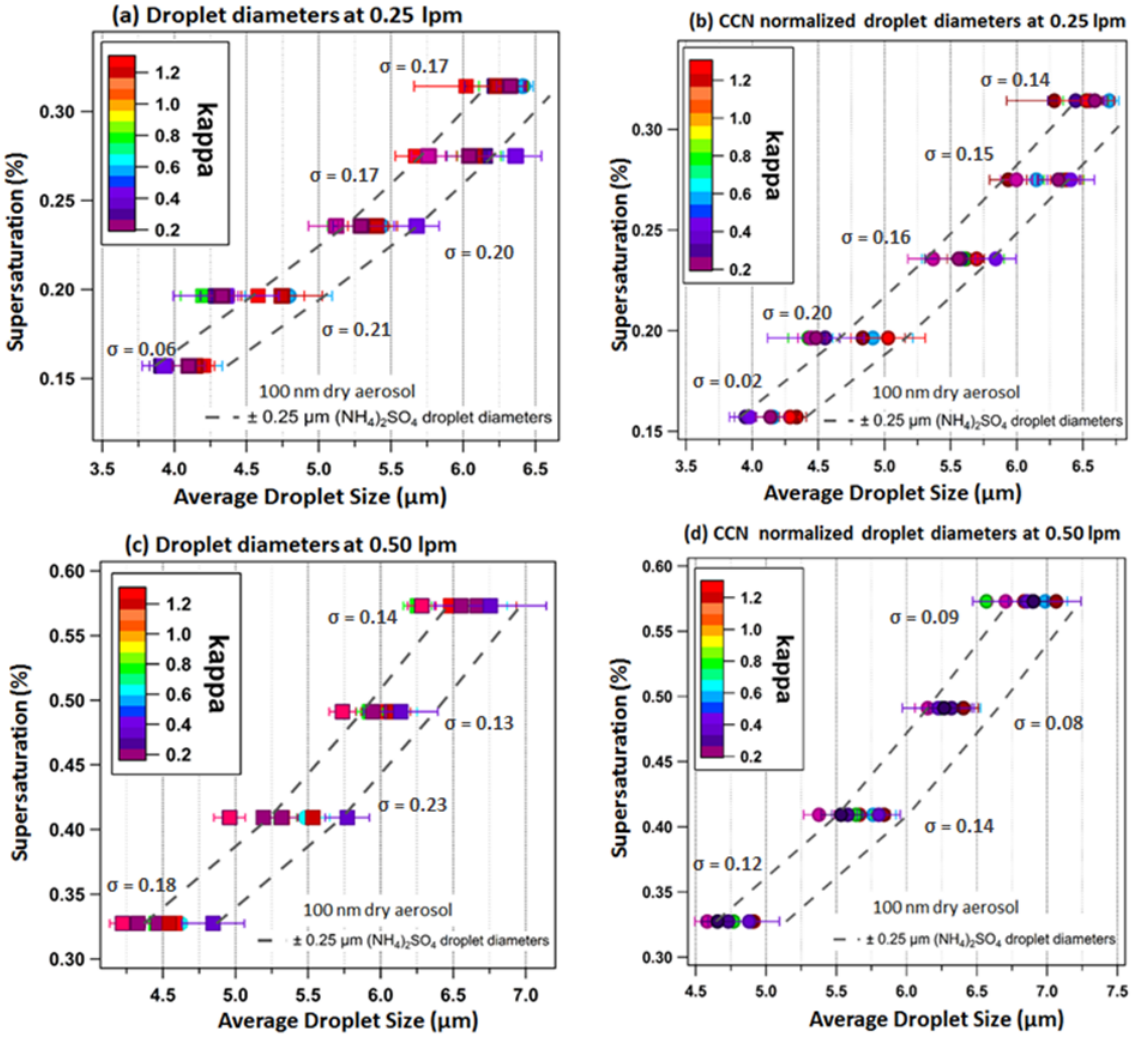

Figure 2.5. TDGA Droplet sizes for 100nm dry aerosol at different solute compositions (a) 0.25 lpm and for supersaturations ranging from 0.15 - 0.35% and (c) 0.50 lpm and 0.30 – 0.60% supersaturation. Dashed vertical lines are OPC bin widths. In (b) and (d) droplet sizes for 100nm dry aerosol are normalized by CCN concentration. Droplet diameters are compared with those of $(NH_4)_2SO_4$ at the same conditions with ± 0.25 µm deviation from the mean (grey dashed line).

2.4 Summary and Implications

All standard CCNc built by DMT, Inc. come with an optical particle counter (OPC) with a bin range of 0.75 -10 μm and a bin size of 0.5 μm. To date, CCNc published works employ these settings for CCN droplet size and depletion studies. In this study, we have shown that the sensitivity of the standard OPC can be improved with modifications in the electronics. By re-engineering the OPC-β to have a 0.25 μm bin width, a 2-fold increase in sensitivity is achieved at the expense of a smaller droplet size measurement range. The higher sensitivity in the OPC-β allows for a more accurate measurement in droplet sizes and provides a robust means of comparing CCN droplet growth.

The data from the new OPC-β indicates that the suppression in CCN droplet sizes due to the CCN number depletion effects are more prevalent than previously thought. Throughout the CCN concentration range, there is an observed 0.2 μm change per $1000\ cm^{-3}$ in the OPC- β data. The depletion is persistent even below $\ll 5000\ cm^{-3}$ (Lathem & Nenes, 2011). This indicates a more universal influence of the CCN concentration on CCN droplet diameters than previously published. The suppression in the droplet diameter is independent of aerosol dry size and droplet growth time (flowrate). The suppression of droplet diameters is likely present for all measured CCN concentrations; its observation may however be limited by the sensitivity of currently available optical counters.

The improved OPC-β however did not provide much improvement for estimating the water vapor mass accommodation coefficient. The plausible values $(0.1 > \alpha \leq 1)$ for a wide range of aerosol hygroscopicities are consistent with previously estimated mass accommodation coefficients from hygroscopicity tandem differential mobility analyser data, CCN and electronic dynamic balance experiments studies (Ruehl et al., 2008; Raatikainen et al., 2013; Emanuelsson et al., 2016; Rovelli et al., 2016). Our findings agree with an increasing body of work that suggests that simple aerosol (those absent film-forming compounds, slow solute dissolution and viscous glass-like compounds) have α greater than 0.1 (Raatikainen et al., 2013; Langridge et al., 2016; Noziere, 2016; Ruehl et al., 2016).

CCN experiments with the high sensitivity OPC-β show no significant differences in the droplet sizes due to chemical composition (indicated by κ-hygroscopicity). Simple salts and organic acids exhibit similar final droplet diameters when depletion corrected. The chemistry of the aerosol (and hygroscopicity) however has a more direct influence on the CCN concentration than on the droplet diameter. Hence the chemistry of the aerosol species will influence the CCN number whiles the CCN number determines the final cloud droplet diameters.

These observations are consistent with previous inferences drawn from ambient and laboratory measurement of mainly inorganic salt systems which showed no difference in the droplet diameters (Lathem & Nenes, 2011) but fails to provide further insight into observed divergence in droplet diameters observed in secondary organic aerosol generated from chamber photochemical reactions (Asa-Awuku et al., 2009). The

improved quantification of droplet depletion effects of CCN concentrations from the higher sensitivity OPC-β data suggests that the current understanding of aerosol droplet kinetics may be gravely limited by droplet measurement instrument sensitivity. Efforts must therefore be made to optimize and improve the sensitivity of currently available OPC sizing in CCN droplet counters.

2.5 Acknowledgements

The authors particularly thank Rick Drgac and Athanasios Nenes for their technical OPC advice and development of the CFSTGC model, respectively. In addition, funding for this project has been supported by the National Science Foundation Award (1151893). This work is the sole responsibility of the grantee and does not represent the official views of any funding agencies.

2.6 Literature Cited

Anderson, T. L., Charlson, R. J., Schwartz, S. E., Knutti, R., Boucher, O., Rodhe, H., & Heintzenberg, J. (2003). Atmospheric science. Climate forcing by aerosol--a hazy picture. *Science, 300*(5622), 1103-1104. doi:10.1126/science.1084777

Asa-Awuku, A., Engelhart, G. J., Lee, B. H., Pandis, S. N., & Nenes, A. (2009). Relating CCN activity, volatility, and droplet growth kinetics of beta-caryophyllene secondary organic aerosol. *Atmospheric Chemistry and Physics, 9*(3), 795-812.

Asa-Awuku, A., Sullivan, A. P., Hennigan, C. J., Weber, R. J., & Nenes, A. (2008). Investigation of molar volume and surfactant characteristics of water-soluble organic compounds in biomass burning aerosol. *Atmospheric Chemistry and Physics, 8*(4), 799-812.

Bohren, C. F., & Huffman, D. R. (1983). Absorption and scattering by a sphere. *Absorption and Scattering of Light by Small Particles*, 82-129.

Chuang, P. Y., Nenes, A., Smith, J. N., Flagan, R. C., & Seinfeld, J. H. (2000). Design of a CCN instrument for airborne measurement. *Journal of Atmospheric and Oceanic Technology, 17*(8), 1005-1019. doi:Doi 10.1175/1520-0426(2000)017<1005:Doacif>2.0.Co;2

DMT. (2012a). Cloud Condensation Nuclei Counter; Manual for Single-Column CCNs. *DOC-0086*(Revision I-2).

DMT. (2012b). Cloud Droplet Probe Manual. *DOC-0029*(Rev O).

Dusek, U., Frank, G. P., Hildebrandt, L., Curtius, J., Schneider, J., Walter, S., . . . Andreae, M. O. (2006). Size matters more than chemistry for cloud-nucleating ability of aerosol particles. *Science, 312*(5778), 1375-1378. doi:10.1126/science.1125261

Emanuelsson, E. U., Tschiskale, M., & Bilde, M. (2016). Phase State and Saturation Vapor Pressure of Submicron Particles of meso-Erythritol at Ambient Conditions. *The Journal of Physical Chemistry A, 120*(36), 7183-7191.

Engelhart, G., Asa-Awuku, A., Nenes, A., & Pandis, S. (2008). CCN activity and droplet growth kinetics of fresh and aged monoterpene secondary organic aerosol. *Atmospheric Chemistry and Physics, 8*(14), 3937-3949.

Giordano, M., Espinoza, C., & Asa-Awuku, A. (2015). Experimentally measured morphology of biomass burning aerosol and its impacts on CCN ability. *Atmospheric Chemistry and Physics, 15*(4), 1807-1821. doi:10.5194/acp-15-1807-2015

Hoppel, W., Twomey, S., & Wojciechowski, T. (1979). A segmented thermal diffusion chamber for continuous measurements of CN. *Journal of Aerosol Science, 10*(4), 369-373.

Lance, S., Nenes, A., Medina, J., & Smith, J. (2006). Mapping the operation of the DMT continuous flow CCN counter. *Aerosol Science and Technology, 40*(4), 242-254.

Langridge, J. M., Richardson, M. S., Lack, D. A., & Murphy, D. M. (2016). Experimental evidence supporting the insensitivity of cloud droplet formation to the mass accommodation coefficient for condensation of water vapor to liquid water. *Geophysical Research Letters, 43*(12), 6650-6656.

Lathem, T. L., & Nenes, A. (2011). Water Vapor Depletion in the DMT Continuous-Flow CCN Chamber: Effects on Supersaturation and Droplet Growth. *Aerosol Science and Technology, 45*(5), 604-615. doi:10.1080/02786826.2010.551146

Leng, C., Duan, J., Xu, C., Zhang, H., Wang, Y., Wang, Y., . . . Zhang, R. (2016). Insights into a historic severe haze event in Shanghai: synoptic situation, boundary layer and pollutants. *Atmospheric Chemistry and Physics, 16*(14), 9221-9234.

McFiggans, G., Artaxo, P., Baltensperger, U., Coe, H., Facchini, M. C., Feingold, G., . . . Lohmann, U. (2006). The effect of physical and chemical aerosol properties on warm cloud droplet activation. *Atmospheric Chemistry and Physics, 6*(9), 2593-2649.

Moore, R. H., Nenes, A., & Medina, J. (2010). Scanning Mobility CCN Analysis—A Method for Fast Measurements of Size-Resolved CCN Distributions and Activation Kinetics. *Aerosol Science and Technology, 44*(10), 861-871. doi:10.1080/02786826.2010.498715

Nenes, A., Chuang, P. Y., Flagan, R. C., & Seinfeld, J. H. (2001). A theoretical analysis of cloud condensation nucleus (CCN) instruments. *Journal of Geophysical Research, 106*(D4), 3449-3474.

Nenes, A., Ghan, S., ABDUL-RAZZAK, H., Chuang, P. Y., & Seinfeld, J. H. (2001). Kinetic limitations on cloud droplet formation and impact on cloud albedo. *Tellus B, 53*(2), 133-149.

Noziere, B. (2016). Don't forget the surface. *Science, 351*(6280), 1396-1397.

Petters, M. D., & Kreidenweis, S. M. (2007). A single parameter representation of hygroscopic growth and cloud condensation nucleus activity. *Atmospheric Chemistry and Physics, 7*(8), 1961-1971.

Petters, M. D., & Kreidenweis, S. M. (2008). A single parameter representation of hygroscopic growth and cloud condensation nucleus activity–Part 2: Including solubility. *Atmospheric Chemistry and Physics, 8*(20), 6273-6279.

Raatikainen, T., Moore, R. H., Lathem, T. L., & Nenes, A. (2012). A coupled observation – modeling approach for studying activation kinetics from measurements of CCN activity. *Atmospheric Chemistry and Physics, 12*(9), 4227-4243. doi:10.5194/acp-12-4227-2012

Raatikainen, T., Nenes, A., Seinfeld, J. H., Morales, R., Moore, R. H., Lathem, T. L., . . . Cerully, K. M. (2013). Worldwide data sets constrain the water vapor uptake coefficient in cloud formation. *Proceedings of the National Academy of Sciences, 110*(10), 3760-3764.

Roberts, G., & Nenes, A. (2005). A continuous-flow streamwise thermal-gradient CCN chamber for atmospheric measurements. *Aerosol Science and Technology, 39*(3), 206-221.

Roeckner, E., Schlese, U., Biercamp, J., & Loewe, P. (1987). Cloud optical depth feedbacks and climate modelling. *Nature, 329*(6135), 138-140.

Rose, D., Gunthe, S., Mikhailov, E., Frank, G., Dusek, U., Andreae, M. O., & Pöschl, U. (2008). Calibration and measurement uncertainties of a continuous-flow cloud condensation nuclei counter (DMT-CCNC): CCN activation of ammonium sulfate and sodium chloride aerosol particles in theory and experiment. *Atmospheric Chemistry and Physics, 8*(5), 1153-1179.

Rosenfeld, D., Sherwood, S., Wood, R., & Donner, L. (2014). Climate effects of aerosol-cloud interactions. *Science, 343*(6169), 379-380.

Rovelli, G., Miles, R. E., Reid, J. P., & Clegg, S. L. (2016). Accurate Measurements of Aerosol Hygroscopic Growth Over a Wide Range in Relative Humidity. *The Journal of Physical Chemistry A*.

Ruehl, C. R., Chuang, P. Y., & Nenes, A. (2008). How quickly do cloud droplets form on atmospheric particles? *Atmospheric Chemistry and Physics, 8*(4), 1043-1055.

Ruehl, C. R., Davies, J. F., & Wilson, K. R. (2016). An interfacial mechanism for cloud droplet formation on organic aerosols. *Science, 351*(6280), 1447-1450. doi:10.1126/science.aad4889

10.1126/science.aad4889.

Schwartz, S. E., & Benkovitz, C. M. (2002). Influence of anthropogenic aerosol on cloud optical depth and albedo shown by satellite measurements and chemical transport modeling. *Proceedings of the National Academy of Sciences, 99*(4), 1784-1789.

Seinfeld, J. H., & Pandis, S. N. (2016). *Atmospheric chemistry and physics: from air pollution to climate change*: John Wiley & Sons.

Shinozuka, Y., Clarke, A., DeCarlo, P., Jimenez, J.-L., Dunlea, E., Roberts, G., . . . Kapustin, V. (2009). Aerosol optical properties relevant to regional remote sensing of CCN activity and links to their organic mass fraction: airborne observations over Central Mexico and the US West Coast during MILAGRO/INTEX-B. *Atmospheric Chemistry and Physics, 9*(18), 6727-6742.

Sinnarwalla, A., & Alofs, D. (1973). A cloud nucleus counter with long available growth time. *Journal of Applied Meteorology, 12*(5), 831-835.

Stocker, T. (2014). *Climate change 2013: the physical science basis: Working Group I contribution to the Fifth assessment report of the Intergovernmental Panel on Climate Change*: Cambridge University Press.

Twomey. (1963). Measurements of natural cloud nuclei. *J. Rech. Atmos, 1*, 101-105.

Twomey, S. (1974). Pollution and the planetary albedo. *Atmospheric Environment (1967), 8*(12), 1251-1256.

Wang, J., Cubison, M., Aiken, A., Jimenez, J., & Collins, D. (2010). The importance of aerosol mixing state and size-resolved composition on CCN concentration and the variation of the importance with atmospheric aging of aerosols. *Atmospheric Chemistry and Physics, 10*(15), 7267-7283.

CHAPTER 3:CCN ACTIVITY AND DROPLET FORMATION OF POA AND SOA MIXTURES

3.1 Introduction

Ambient aerosol are complex mixtures. The formation of aerosol mixtures from secondary organic plus primary organic aerosol sources is influenced by miscibility, condensability, polarity and entropy (Asa-Awuku et al., 2009; Vaden et al., 2010). *Vaden et al* (2010) showed that secondary organic aerosol (SOA) can condense onto hydrophobic primary organic aerosol (POA) and form metastable coated shells. *Asa-Awuku et al* (2009) evaluated the formation of mixtures from SOA, diesel POA and motor oil fuel POA. They found more volatile diesel POA and α-pinene SOA formed "strong-phase" mixtures whiles β-caryophyllene SOA and motor oil fuel POA formed a "weak-phase" mixture. They defined "strong-phase" mixtures as readily entropically mixed systems and "weak-phase" as the opposite. The use of weak and strong phase mixtures, employed in this work, is therefore not indicative of the viscous phase states or phase-state terminology employed in the description of aerosol physical properties reported elsewhere (Saukko et al., 2012; Lu et al., 2014). We apply the same terminology as applied to the SOA and POA mixing systems in Asa-Awuku et al, [2009], with the new addition of CCN activity and droplet formation.

The cloud condensation nuclei (CCN) activity of unmixed POA and SOA is relatively well studied (Dusek et al., 2006; Petters & Kreidenweis, 2007, 2008; Ruehl et

al., 2008; Koehler et al., 2009). Freshly emitted soot is only slightly hygroscopic but can become more CCN active due to oxidation and condensation of hydrophilic co-emitted vapors (Khalizov et al., 2013). In SOA, there is a direct correlation between the oxidized fraction and the CCN κ-hygroscopicity in ambient and smog chamber data sets (Jimenez et al., 2009; Massoli et al., 2010). However, when POA and SOA are mixed, predicting the CCN activity becomes more challenging (Nenes & Seinfeld, 2003; King et al., 2007). Wang et al., observed a rapid mixing of ambient urban non-hygroscopic POA and BC with photochemically aged organic aerosol during the MILAGRO field campaign. CCN activity increased in the subsequent mixtures and κ-hygroscopicity increased from 0 to 0.1. CCN activity was found to be sensitive to the mixing states, especially when non-hygroscopic species ($\kappa < 0.1$) contributed significantly to the volume (Wang et al., 2010).

In this study we explore the CCN activity and droplet formation of mixtures of α-pinene biogenic SOA plus diesel primary organic aerosol (DL POA) as well as α-pinene SOA plus motor-oil fuel primary organic aerosol (MOF POA). We characterize the extent of mixing, if any, on the CCN activity. We further discuss changes in the single parameter κ-hygroscopicity due to mixing the SOA and the POA and explore subsequent droplet kinetics.

3.2 Experimental Methods and Instrumentation

The aerosol formation procedure is similar to *Asa-Awuku et al* (2009) and is briefly described here. The experiments were performed in a 12 m^3 temperature and humidity controlled Teflon environmental chamber. SOA was formed by dark ozonolysis of α-

pinene at 21°C and < 5% RH. The SOA mass formation reached completion in the first hour of the reaction before the injection of the POA. POA was derived from two sources. Motor oil and diesel fuel (MOF POA) was flash vaporized and injected into the reactor; the mixture is a controlled surrogate for unburnt diesel emissions (Sakurai et al., 2003). The second POA was generated from local commercial diesel combusted in a 4.5 kW single-engine generator at low load. The resulting diesel POA (DL POA) was injected into the reactor.

Aerosol chemical composition was measured with an Aerodyne Quadrupole Aerosol Mass Spectrometer (Q-AMS).The Q-AMS ion fragments (mass to charge ratio, (m/z)) are unit mass resolution (UMR) (Zhang et al., 2005). The Q-AMS also provides particle time-of-flight (PTOF) data for size distributions (Fig. S1). The contributions POA and SOA can be observed with UMR data. (McFiggans et al., 2005) showed that the evolution of POA and SOA mixing in urban and rural sites was demonstratively traced with the *m/z 44* and *m/z 57* ion fragments. (Mohr et al., 2009) observe *m/z 44* for predominantly oxygenated organic aerosol (OOA) such as α-pinene SOA, and trace *m/z 57* for the hydrocarbon-like organic aerosol (HOA) from diesel and MOF POA. *m/z 44* and *m/z 57* are aptly applied to the mixed SOA and POA in this study.

The aerosol size distribution was measured with a scanning mobility particle sizer (SMPS, TSI 3081) and a condensation particle counter (CPC, TSI 3772). A DMT cloud condensation nuclei counter (CCNc) was operated downstream of the SMPS and in parallel with the CPC. The theory and operation of the CCNc is thoroughly described elsewhere (Roberts & Nenes, 2005; Rose et al., 2008). The size selected aerosol is sampled by the

CCNc at a 0.5 lpm flowrate. The activated fraction (the CCN concentration divided by aerosol number concentration) is measured between supersaturations of 0.3 – 1.5% for different particle dry diameters. Scanning mobility CCN analysis (SMCA) is employed and calculates the critical activation diameters (d_{p50}) for each supersaturation every 2.25 minutes (Moore et al., 2010). The CCNc is calibrated with $(NH_4)_2SO_4$ aerosol for the same experimental supersaturations and flowrate following procedures outlined in (Rose et al., 2008) (Table, S1 Supplemental Information).

The CCN activity of aerosol can be characterized by the single-parameter Köhler theory hygroscopicity parameter, κ. κ-hygroscopicity is calculated for each d_{p50} and supersaturation. (Petters & Kreidenweis, 2007) and is dependent on aerosol chemistry. The average final droplet diameters are measured at the critical dry diameters (d_{p50}). The reported droplet diameter is the average of the final droplet diameters of the total aerosol activated fraction. The impacts of mixing are assessed on droplet growth by using the threshold droplet growth analysis (TDGA) method (Asa-Awuku et al., 2008; Engelhart et al., 2008; Raatikainen et al., 2012). In TDGA the average droplet sizes of the mixture systems are compared to the droplet size of calibration $(NH_4)_2SO_4$ aerosol at the same experimental conditions. Differences in droplet size indicate changes in droplet kinetics.

3.3 Results and Discussion

3.3.1 CCN Activity and Droplet Measurement

The α-pinene SOA was the most hygroscopic ($\kappa = 0.15$) of the three species. The MOF POA was the least hygroscopic ($\kappa = 0.022 \pm 0.002$) while the diesel POA had a

hygroscopicity closer to that of SOA (κ = 0.11 ± 0.03) (Figure 1). The similarity in the hygroscopicity of α-pinene SOA and DL POA could be attributed to a significant presence of *m/z 44* ion, an indication of oxygenated organic components (Lambe et al., 2011). It is noted that *m/z 43* signals also indicate oxygenation and are found in all three systems. However, only *m/z 44* signal can be found in the more hygroscopic α-pinene SOA and DL POA PTOF spectra (Asa-Awuku et al., 2009).

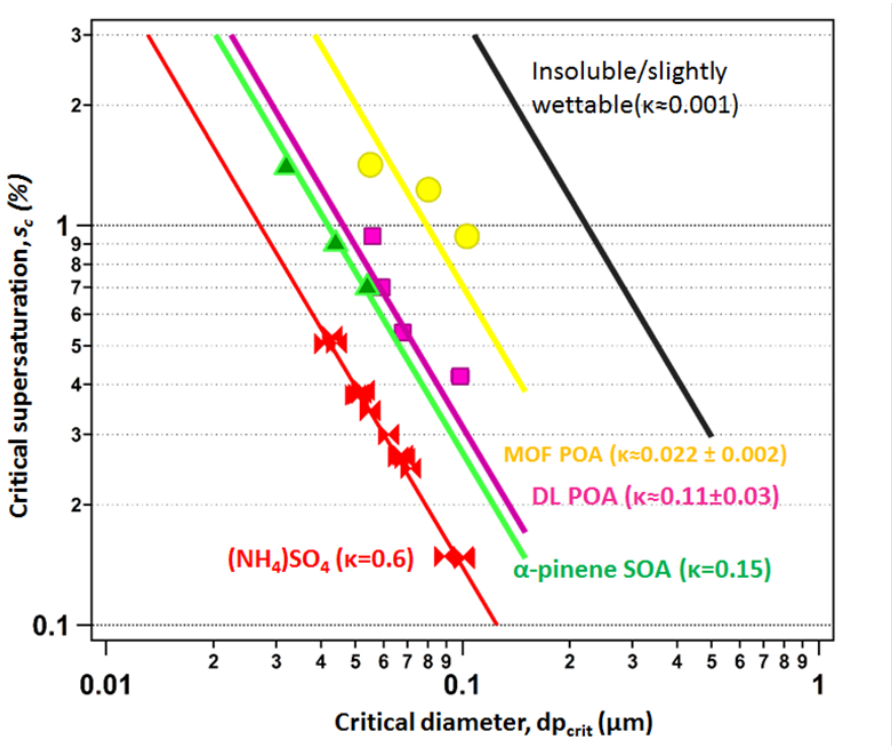

Figure 3.1. Measured CCN activity of α-pinene SOA (green triangles, κ=0.15), DL POA (pink squares, κ=0.11) and MOF POA (yellow circles, κ=0.022) compared with $(NH_4)SO_4$ (κ = 0.6) and hypothetical insoluble but slightly wettable aerosol (κ = 0.0001)

The unimodal SOA distribution was modified after the injecting the DL POA and MOF POA (Figure B-1). In the DL + α-pinene SOA experiment, a short-lived bimodal distribution was formed immediately after injecting the POA. The bimodal distribution, however converged into a single distribution after ~ 1 hour. Asa-Awuku et al, (2009) define this process as "strong mixing into a single phase". In the MOF POA + α-pinene SOA, two distinct distributions were formed immediately after the injection of the MOF POA and persisted throughout the experiment (Figure B-1). Asa-Awuku et al, (2009) define this process as a "weak two-phase mixture". More recently, light-scattering single-particle measurements (LSSP) on similar mixtures confirm that the MOF - SOA mixtures remain largely distinct for hours while DL - SOA mixtures show limited exchange of marker fragments between the two populations (Robinson et al., 2016). Again, the terminology "strong and weak phase mixtures" refers to the aerosol miscibility and does not refer to the chemical viscosity of the particles (Saukko et al., 2012; Lu et al., 2014).

In the α-pinene SOA plus diesel-exhaust POA mixture experiments (Figure 3.2a), the CCN activity decreased immediately after the injection of the DL POA. The hygroscopicity of the mixture was significantly depressed (from κ = 0.15 to κ =0 .06); below that of α-pinene SOA and DL POA. The non-linear depression in κ values is likely due to the presence of non-hygroscopic aerosol. In the first hour more volatile aerosol components of DL POA evaporate and condense on the larger α-pinene SOA (Fig. B-2). The resulting low volatility material has hygroscopicity ~0.06. The mixture attained equilibrium and formed a "single-phase" ~ 1 hour after the DL POA injection. As

coagulation and condensation occurs, κ-hygroscopicity values increase to 0.12. In the α-pinene SOA plus motor oil-fuel POA experiments (Fig. 3.2b), there was a rapid decrease in the CCN activity of the mixture when the MOF POA was injected (from $\kappa = 0.15$ to $\kappa = 0.022$). The mixture remained a "weak two-phase" system (Figure B-1). However, the CCN activity increased ($\kappa = 0.10$). Both cases (DL POA and MOF POA plus α-pinene SOA) showed a steady increase in CCN activity after mixing equilibrium was established; 1 hour after injection of the DL POA and immediately for MOF POA. The increase in CCN activity is likely due to continued chemical oxidation in both systems.

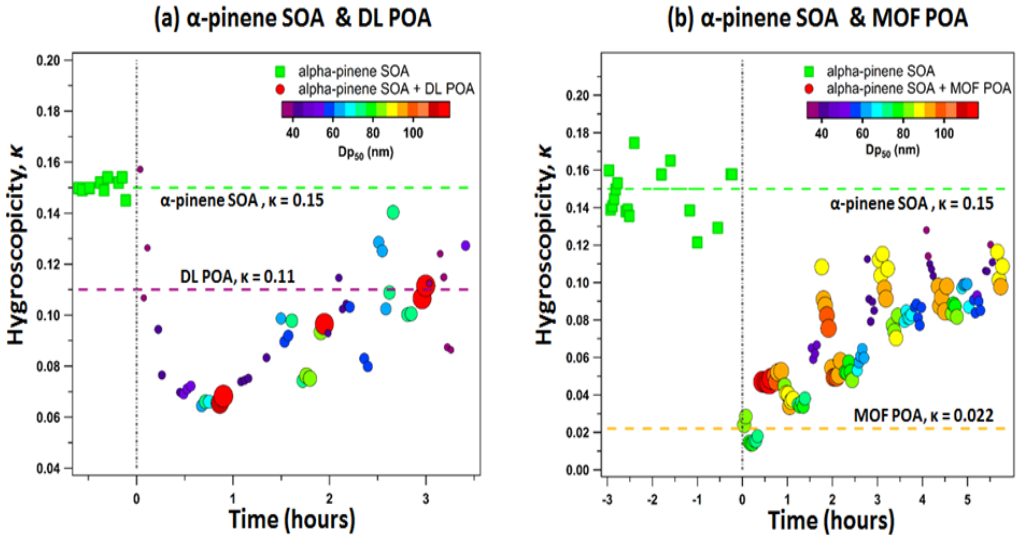

Figure 3.2. Measured CCN κ-hygroscopicity of (a) α-pinene SOA (green squares) and DL POA (filled circles) and (b) α-pinene SOA (green squares) and MOF POA (filled circles). In (a) the hygroscopicity decreases from the α-pinene SOA average (horizontal green dashed line, $\kappa = 0.15$) when the DL MOF is injected but increases after equilibrium to

values above DL POA (horizontal purple dashed line). In (b) the injection of the MOF POA causes an instantaneous decrease in the hygroscopicity. Immediately after injection, hygroscopicity increases, within the average kappa-values of α-pinene SOA (horizontal green dashed line) and MOF POA (horizontal yellow dashed line). Dashed vertical lines indicate time of POA injection.

Figure 3.3 evaluates the effects of mixing on the droplet kinetics at 0.94% supersaturation and 0.5 lpm CCNc flowrate. (Additional droplet information at other SS are presented in Fig. B-3). In all cases, the droplet diameter is evaluated at the critical particle diameter, dp_{50}. The single system average droplet sizes are compared to the two-phase mixed system. The α-pinene SOA average droplet size ($5.98 \pm 0.20\ \mu m$) is larger than those of both DL POA ($5.2 \pm 0.18\ \mu m$) and MOF POA ($4.9 \pm 0.21\ \mu m$). The difference in droplet sizes is within 1 (0.5μm) and 2 (1μm) bins for DL POA and MOF POA, respectively. α-pinene SOA and (NH4)2SO4 ($5.8 \pm 0.05\ \mu m$) form comparable droplet sizes at the same *SS* and flowrate conditions. For the DL POA plus α-pinene SOA mixture, the droplet diameters 20 minutes after injection are reduced by ~12% to sizes similar to that of the DL POA alone; at this point the "single-phase" mixing has not been attained (Fig 3.3a). Over time the droplet diameter increases and converges towards the α-pinene SOA droplet size (within measurement uncertainty of the OPC). In the MOF POA plus α-pinene SOA system, the droplet diameter ($6.07 \pm 0.04\ \mu m$) is similar to the α-pinene SOA at the point of injection (Fig. 3.3b). Overall the droplet diameters in the MOF POA plus α-pinene SOA did not vary significantly during the course of the experiment($6.01 \pm 0.13\ \mu m$).

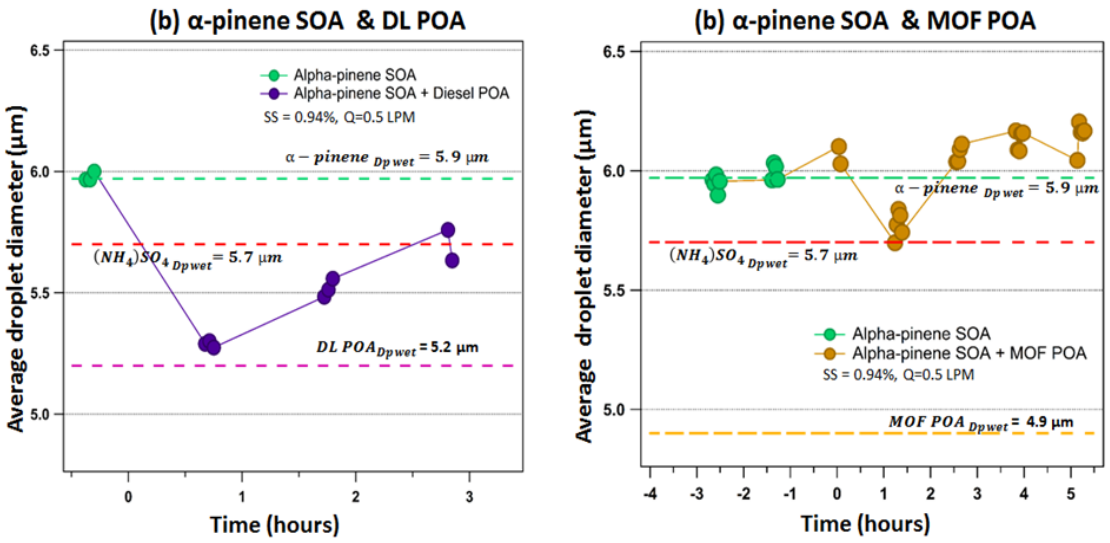

Figure 3.3. Average droplet diameters at 0.94% supersaturation and 0.5 lpm flowrate. (a) α-pinene SOA + DL POA droplet diameters (b) α-pinene SOA + MOF POA droplet sizes.

3.3.2 CCN Prediction of Complex Mixtures

The above observations of CCN activity suggest that *a)* the organic aerosol water-uptake is sensitive to the differences in the *m/z 44* ion signal and *b)* kappa values after equillibrium are consistent with volume additive mixtures of the SOA and POA. Here, we hypotheisze and test a framework to predict the CCN activity of mixtures derived from these observations and previous work that show:

- the oxidized, water-soluble fraction of complex organic aerosol (OA) is soluble and hygroscopic. OA can depress the surface tension of the activating droplet up to 10% (Moore et al., 2008; Ruehl et al., 2012). The m/z 44 ion fragment can be

used to trace the level of OA oxidation; researchers have observed a linear relationship between OA oxidation and the κ-hygroscipicity in ambient, as well as smog-chamber, aerosol (Jimenez et al., 2009; Duplissy et al., 2011).

- for multiple-component systems, a solubility influenced, volume additive approach reasonably estimates the κ-hygroscopicity (Petters & Kreidenweis, 2008). Solublility limitations are assumed negligible. Recent work by Riipinen et al (2015) suggests that, in aerosol mixtures, resolving the aerosol solubility outside a limited solubilty range ($0.1 - 100\ gL^{-1}$) does not improve CCN predictions.
- α-pinene SOA is mostly hygroscopic and soluble material (Englehart, 2008). Thus the contribution of non-hygroscopic mass is injected with the POA. Moreover, the POA can be traced with the *m/z 57* fragment ion (Alfarra et al., 2004; McFiggans et al., 2005; Canagaratna et al., 2010).

If the above tenants hold, then UMR data can predict CCN activity of the SOA and POA mixtures. We propoose to model the experimental observations with the following equation,

$$x_{hygroscopic} = \frac{m/z\ 44}{m/z\ 57} \quad [3.1]$$

$$k_{mixture} = x_{hygroscopic}k_{hygroscopic} + \left(1 - x_{hygroscopic}\right)k_{non-hygroscopic} \quad [3.2]$$

Where $x_{hygroscopic}$ is the realtive molar contribution of the more hygroscopic, soluble organic component *(m/z 44)* to the non-hygroscopic but wettable organic component *(m/z 57).* Here the volume additive hygroscopicity, $\kappa_{mixture}$ is simplified into a binary mixture of the more hygroscopic soluble organics, $\kappa_{hygroscopic} = 0.15$, and a non-hygroscopic but wettable component with $\kappa_{non-hygroscopic} = 0.001$. It is assumed that hygroscopic and non-hygroscopic OA is of similar density and thus molar ratios are equivalent to volume ratios.

In Figure 3.4, *κ*-hygroscopicity values estimated from Equation [3.2] are compared to measured CCN κ-hygroscopicity. The timeseries plots (Figs. 4a and b) show that the prediction follows the trends of the observed CCN acitivity.

In the DL POA plus α-pinene SOA mixture the modeled hygroscopicity captures the non-linearity observed in the first hour; non-hygroscopic material *(m/z 57)* is injected with DL POA and reduces the apparent *κ* to 0.08, less than the κ of DL POA but slightly greater than the measured value of 0.06. The minimum predicted and measured hygroscopicity differ; the AMS signal does not account for the entire non-volatile and non-hygroscopic material at the smaller dry diameters in the range of CCN activity (35 – 70nm, Comapre Fig. B-1a to B-2a). The CCN predicted values become more hygroscopic after equillibrum, as the *m/z* 44 signal increases with time (Fig 3.4a).

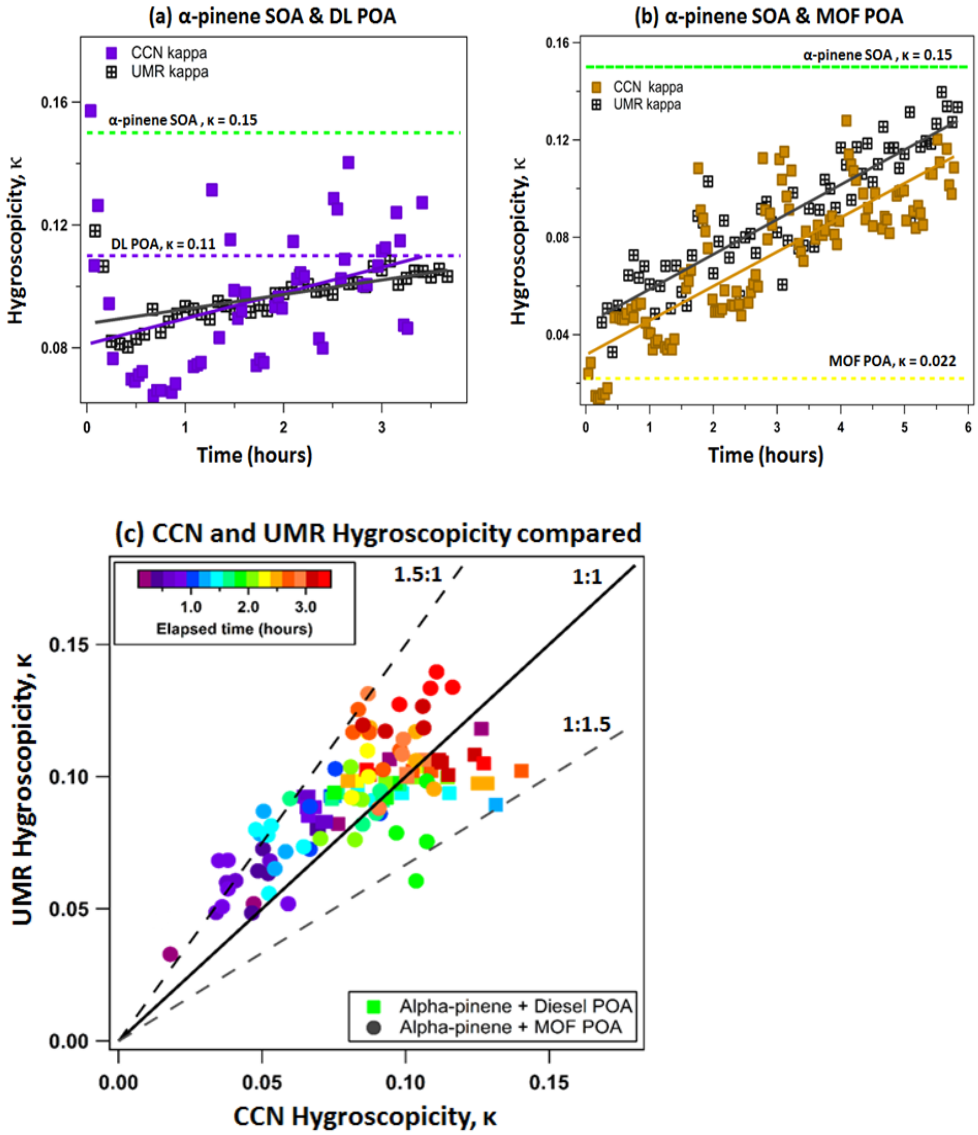

Figure 3-3.4. Modeled UMR κ-hygroscopicity compared with CCN meausred *κ*-hygroscopicity. (a) α-pinene SOA + DL POA. (b) α-pinene SOA + MOF POA. (c) Predicted UMR *κ*-hygroscopicity is compared with that measured CCN *κ*-hygroscopicity.

The predicted and measured hygroscopicity also increases in the MOF POA plus α-pinene SOA mixture; suggesting that even MOF POA and SOA continue to experience chemical oxidation as the relative contribution of *m/z* 44 to *m/z* 57 increases over time. The prediction tends to overpredict the MOF POA plus α-pinene system. The simple UMR model (Eq. [2]) predicts hygroscopicity to within ~50% uncertainty (Fig. 4c) and captures evolving chemical changes that influence hygroscopcity.

3.4 Implications

Asa-Awuku et al (2009) were able to conclusively show that organics from anthropogenic and biogenic origins can exist in multiple phase mixing states. The propensity of these "weak and strong phase" mixtures to form droplets in the supersaturated regime is significantly modified with chemical ageing. Here we observed that the hygroscopicity of motor oil POA (κ =0.022) and diesel exhaust POA (κ = 0.11) are remarkably different from each other even though the chemical fingerprint (Fig. 3 in Asa-Awuku e al, 2009) are similar. Thus the previous elemental composition information from the higher resolution AMS mass spectrum (unavailble here) did not provide sufficient information to describe the molecular force interactions that govern mixing state, phase miscibility or separation. However, how molecules driving miscibility also interact with water, and their propensity to form droplets is likely a better indication of whether the aerosol phases will mix (Robinson et al., 2016). Simply put, like dissolves like. The apparent hygroscopicities of diesel exhaust and α-pinene SOA are similar and the two components readily mixed to form a strong well-mixed aerosol.

Hence, the comparison of the CCN activity maybe a better indicator of the propensity of the aerosol to form mixtures.

The process of aerosol mixing is time dependent and we observe the effects of strong and weak mixing in CCN activity. The measured and predicted κ-hygroscopicity of the MOF POA + α-pinene SOA and DL POA + α-pinene SOA mixtures are transient; yet after phase equilibrium is established particles become more CCN active. The increase in the κ-hygroscopicity is attributed to the formation of more oxidized material after equillibrium as indicated by the increase in the *m/z* 44 signal.

From threshold droplet growth analysis (TDGA), DL POA and MOF POA grow to similar average droplet sizes. This is consistent with the similarity in "chemical fingerprints" as described by *Asa-Awuku et al*. (2009). The modifications in hygroscopicity observed upon mixing the POA with the α-pinene SOA does not translate into significant difference in droplet growth. In the α-pinene SOA + DL POA, the observed suppression in the droplet sizes upon injecting the POA may be due to the formation of mixtures with lower mass accommodation coefficients. This may slow down the water uptake and hence result in smaller final droplet sizes (Ruehl et al., 2008). The co-condensation of the initially volatile DL POA may have influenced the slight increase in the droplet diameters after entropic mixing equilibrium was attained (Topping et al., 2013). The differences in the droplet diameters observed for both systems are all within two bin sizes hence the changes may not be significant considering optical particle counter sizing sensitivity (Moore et al., 2010). Improvements in the CCNc optical

particle counter sensitivity are therefore needed to enable a robust exploration of droplet kinetics in the future.

The proposed UMR model method is different than other AMS-CCN techniques. The UMR method applies the ratio of fragments; an absolute amount (typically requireing density and wall-loss correction) is not required. It should also be noted that simultaneous CCN and High-Resolution AMS data was not avilable for this study. Although, a direct relationship exists between *m/z 44* ion and O:C (Ng et al., 2010), this UMR-CCN model also accounts for the contribution of non-hygroscopic material (as traced with *m/z* 57). However all AMS coupled CCN predictions have limitations. The AMS bulk information is applied to the entire distribution and does not account for size-resolved mixing state. In addition, AMS-CCN models work best after equillbrium is established and as particles move to larger sizes above the detection range of the AMS aerodynamic lense.

Nonetheless, the ability to predict CCN activity from UMR AMS fragment ions and the nature of mixing from the the CCN hygroscopicity may be a promising tool to gain further insight into the evolution of organic aerosol mixtures and their interaction with water vapor. When available, CCN information coupled with fragment ion data will provide both hygroscopicity and mixing insights that can lead to the robust modeling of CCN activity and droplet growth kinetics in transient aerosol systems.

3.5 Acknowledgements

The authors would like to thank the United States National Science Foundation (NSF) and the University of California Transportation Research Fellowship for their support in this work. Specifically, the publication of this work was supported by the NSF grant 1151893. Its contents are solely the responsibility of the grantees and do not necessarily represent the official views of the NSF or UCTC. Further, the NSF does not endorse the purchase of any commercial products or services mentioned in the publication. Additioanlly, AAA and NMD thank the Dreyfus Post-doctoral fellowship for their support in data collection.

3.6 Literature Cited

Alfarra, M. R., Coe, H., Allan, J. D., Bower, K. N., Boudries, H., Canagaratna, M. R., . . . Worsnop, D. R. (2004). Characterization of urban and rural organic particulate in the lower Fraser valley using two aerodyne aerosol mass spectrometers. *Atmospheric Environment, 38*(34), 5745-5758. doi:10.1016/j.atmosenv.2004.01.054

Asa-Awuku, A., Sullivan, A. P., Hennigan, C. J., Weber, R. J., & Nenes, A. (2008). Investigation of molar volume and surfactant characteristics of water-soluble organic compounds in biomass burning aerosol. *Atmospheric Chemistry and Physics, 8*(4), 799-812.

Asa-Awuku, A., Miracolo, M., Kroll, J., Robinson, A., & Donahue, N. (2009). Mixing and phase partitioning of primary and secondary organic aerosols. *Geophysical Research Letters, 36*(15).

Canagaratna, M. R., Onasch, T. B., Wood, E. C., Herndon, S. C., Jayne, J. T., Cross, E. S., . . . Worsnop, D. R. (2010). Evolution of vehicle exhaust particles in the atmosphere. *J Air Waste Manag Assoc, 60*(10), 1192-1203.

Duplissy, J., DeCarlo, P. F., Dommen, J., Alfarra, M. R., Metzger, A., Barmpadimos, I., . . . Baltensperger, U. (2011). Relating hygroscopicity and composition of organic aerosol particulate matter. *Atmospheric Chemistry and Physics, 11*(3), 1155-1165. doi:10.5194/acp-11-1155-2011

Dusek, U., Reischl, G., & Hitzenberger, R. (2006). CCN activation of pure and coated carbon black particles. *Environmental science & technology, 40*(4), 1223-1230.

Engelhart, G., Asa-Awuku, A., Nenes, A., & Pandis, S. (2008). CCN activity and droplet growth kinetics of fresh and aged monoterpene secondary organic aerosol. *Atmospheric Chemistry and Physics, 8*(14), 3937-3949.

Jimenez, J., Canagaratna, M., Donahue, N., Prevot, A., Zhang, Q., Kroll, J. H., . . . Ng, N. (2009). Evolution of organic aerosols in the atmosphere. *Science, 326*(5959), 1525-1529.

Khalizov, A. F., Lin, Y., Qiu, C., Guo, S., Collins, D., & Zhang, R. (2013). Role of OH-initiated oxidation of isoprene in aging of combustion soot. *Environmental science & technology, 47*(5), 2254-2263.

King, S. M., Rosenoern, T., Shilling, J. E., Chen, Q., & Martin, S. T. (2007). Cloud condensation nucleus activity of secondary organic aerosol particles mixed with sulfate. *Geophysical Research Letters, 34*(24).

Koehler, K. A., Kreidenweis, S. M., DeMott, P. J., Petters, M. D., Prenni, A. J., & Carrico, C. M. (2009). Hygroscopicity and cloud droplet activation of mineral dust aerosol. *Geophysical Research Letters, 36*(8). doi:10.1029/2009gl037348

Lambe, A., Onasch, T., Massoli, P., Croasdale, D., Wright, J., Ahern, A., . . . Davidovits, P. (2011). Laboratory studies of the chemical composition and cloud condensation nuclei (CCN) activity of secondary organic aerosol (SOA) and oxidized primary organic aerosol (OPOA). *Atmospheric Chemistry and Physics, 11*(17), 8913-8928.

Lu, J. W., Rickards, A. M., Walker, J. S., Knox, K. J., Miles, R. E., Reid, J. P., & Signorell, R. (2014). Timescales of water transport in viscous aerosol: measurements on sub-micron particles and dependence on conditioning history. *Physical Chemistry Chemical Physics, 16*(21), 9819-9830.

Massoli, P., Lambe, A., Ahern, A., Williams, L., Ehn, M., Mikkilä, J., . . . Jayne, J. (2010). Relationship between aerosol oxidation level and hygroscopic properties of laboratory generated secondary organic aerosol (SOA) particles. *Geophysical Research Letters, 37*(24).

McFiggans, G., Alfarra, M. R., Allan, J., Bower, K., Coe, H., Cubison, M., . . . Facchini, C. (2005). Simplification of the representation of the organic component of atmospheric particulates. *Faraday discussions, 130*, 341-362.

Mohr, C., Huffman, J. A., Cubison, M. J., Aiken, A. C., Docherty, K. S., Kimmel, J. R., . . . Jimenez, J. L. (2009). Characterization of primary organic aerosol emissions from meat cooking, trash burning, and motor vehicles with high-resolution aerosol mass spectrometry and comparison with ambient and chamber observations. *Environmental science & technology, 43*(7), 2443-2449.

Moore, R., Ingall, E., Sorooshian, A., & Nenes, A. (2008). Molar mass, surface tension, and droplet growth kinetics of marine organics from measurements of CCN activity. *Geophysical Research Letters, 35*(7).

Moore, R. H., Nenes, A., & Medina, J. (2010). Scanning Mobility CCN Analysis—A Method for Fast Measurements of Size-Resolved CCN Distributions and Activation Kinetics. *Aerosol Science and Technology, 44*(10), 861-871. doi:10.1080/02786826.2010.498715

Nenes, A., & Seinfeld, J. H. (2003). Parameterization of cloud droplet formation in global climate models. *Journal of Geophysical Research: Atmospheres, 108*(D14).

Ng, N., Canagaratna, M., Zhang, Q., Jimenez, J., Tian, J., Ulbrich, I., . . . Bahreini, R. (2010). Organic aerosol components observed in Northern Hemispheric datasets from Aerosol Mass Spectrometry. *Atmospheric Chemistry and Physics, 10*(10), 4625-4641.

Petters, M., & Kreidenweis, S. (2007). A single parameter representation of hygroscopic growth and cloud condensation nucleus activity. *Atmospheric Chemistry and Physics, 7*(8), 1961-1971.

Petters, M., & Kreidenweis, S. (2008). A single parameter representation of hygroscopic growth and cloud condensation nucleus activity–Part 2: Including solubility. *Atmospheric Chemistry and Physics, 8*(20), 6273-6279.

Raatikainen, T., Moore, R., Lathem, T., & Nenes, A. (2012). A coupled observation–modeling approach for studying activation kinetics from measurements of CCN activity. *Atmospheric Chemistry and Physics, 12*(9), 4227-4243.

Roberts, G., & Nenes, A. (2005). A continuous-flow streamwise thermal-gradient CCN chamber for atmospheric measurements. *Aerosol Science and Technology, 39*(3), 206-221.

Robinson, E. S., Donahue, N. M., Ahern, A. T., Ye, Q., & Lipsky, E. (2016). Single-particle measurements of phase partitioning between primary and secondary organic aerosols. *Faraday discussions*.

Rose, D., Gunthe, S. S., Mikhailov, E., Frank, G. P., Dusek, U., Andreae, M. O., & Pöschl, U. (2008). Calibration and measurement uncertainties of a continuous-flow cloud condensation nuclei counter (DMT-CCNC): CCN activation of ammonium sulfate and sodium chloride aerosol particles in theory and experiment. *Atmospheric Chemistry and Physics, 8*(5), 1153-1179.

Ruehl, C., Chuang, P., & Nenes, A. (2008). How quickly do cloud droplets form on atmospheric particles? *Atmospheric Chemistry and Physics, 8*(4), 1043-1055.

Ruehl, C., Chuang, P., Nenes, A., Cappa, C., Kolesar, K., & Goldstein, A. (2012). Strong evidence of surface tension reduction in microscopic aqueous droplets. *Geophysical Research Letters, 39*(23).

Sakurai, H., Tobias, H. J., Park, K., Zarling, D., Docherty, K. S., Kittelson, D. B., . . . Ziemann, P. J. (2003). On-line measurements of diesel nanoparticle composition and volatility. *Atmospheric Environment, 37*(9), 1199-1210.

Saukko, E., Lambe, A., Massoli, P., Koop, T., Wright, J., Croasdale, D., . . . Davidovits, P. (2012). Humidity-dependent phase state of SOA particles from biogenic and

anthropogenic precursors. *Atmospheric Chemistry and Physics, 12*(16), 7517-7529.

Topping, D., Connolly, P., & McFiggans, G. (2013). Cloud droplet number enhanced by co-condensation of organic vapours. *Nature geoscience, 6*, 443-446. doi:doi:10.1038/ngeo1809

Vaden, T. D., Song, C., Zaveri, R. A., Imre, D., & Zelenyuk, A. (2010). Morphology of mixed primary and secondary organic particles and the adsorption of spectator organic gases during aerosol formation. *Proceedings of the National Academy of Sciences, 107*(15), 6658-6663.

Wang, J., Cubison, M., Aiken, A., Jimenez, J., & Collins, D. (2010). The importance of aerosol mixing state and size-resolved composition on CCN concentration and the variation of the importance with atmospheric aging of aerosols. *Atmospheric Chemistry and Physics, 10*(15), 7267-7283.

Zhang, Q., Alfarra, M. R., Worsnop, D. R., Allan, J. D., Coe, H., Canagaratna, M. R., & Jimenez, J. L. (2005). Deconvolution and quantification of hydrocarbon-like and oxygenated organic aerosols based on aerosol mass spectrometry. *Environmental science & technology, 39*(13), 4938-4952.

CHAPTER 4:CCN ACTIVITY AND DROPLET KINETICS OF AGED GDI EMISSIONS

4.1 Introduction

Soot, formed from the incomplete combustion of fossil fuels, biofuel and biomass, forms a significant portion of the global aerosol budget; with an estimated 7600 Gg yr^{-1} emitted in 2000 alone (Lamarque et al., 2010; Sasser et al., 2012). Soot is mainly composed of spherules of black carbon mixed with nitrates, sulfates and other organic and inorganic salts (Adachi & Buseck, 2008; Adachi et al., 2010). Soot particles have a net warming effect and when assumed to be internally mixed have warming effect second only to CO_2 (Ramanathan & Carmichael, 2008; Bond et al., 2013). Globally, about 20% of all black carbon emissions are from combustion related fossil fuel burning. The US Environmental Protection Agency (EPA) estimates more than 50% of black carbon emissions are from transportation sources (Sasser et al., 2012). Combustion soot, which vehicular soot makes up significant fraction of, may contribute up to 64% of the global CCN budget (Spracklen et al., 2011). It is therefore imperative to constrain the evolution and CCN potential of vehicular soot to improve our current estimation of anthropogenic direct and indirect forcing.

Fresh vehicular soot (combusted from various fuel sources) has exhibited no significant hygroscopic growth and CCN activity (Vu et al., 2017). The CCN concentration of combustion aerosol is mainly determined by the size distribution (Dusek et al., 2006), chemical composition (Jimenez et al., 2009) and morphology (Giordano et

al., 2015). Tailpipe emissions are often assumed to be largely nucleation mode particles, mostly externally mixed, fractal composites with a significant insoluble volume fraction (Andreae & Rosenfeld, 2008). Little data exists on the aged CCN activity of complex vehicular emissions. *Tristcher et al (2011)* photochemically aged diesel soot and showed that secondary aerosol (mainly secondary organic aerosol and nitrates) formed form volatile organic carbon co-emitted with soot. Furthermore, the formation of secondary aerosol (SA) lead to changes in aerosol density, and increased both the sub-saturated (0.06 – 0.12) and supersaturated (0.09 – 0.14) hygroscopicity of the aerosol mixture. The hygroscopicity of aged diesel emissions was comparable to the hygroscopicity of chamber generated and ambient organic aerosol data sets (Chirico et al., 2010; Duplissy et al., 2011; Lance et al., 2013)

The secondary aerosol (SA) formed from both diesel and gasoline emission sources has been shown to be chemically similar (Presto et al., 2014). Thus the sub-saturated and supersaturated hygroscopicity and CCN activity of aged gasoline-generated soot are assumed to be similar to that of aged diesel, with kappa < 0.1 (Zaveri et al., 2010). To our knowledge, the subsaturated and supersaturated hygroscopicity of aged gasoline emissions has yet to be fully explored. Particularly, those from advanced gasoline engine technologies, (i.e gasoline direct engines) that now dominate the gasoline vehicle market share.

During photochemical aging of vehicular emissions the aerosol size distribution and morphology of the aerosol is significantly modified by the condensing SA. The

condensation of the denser SA material increases the effective density of the aerosol and the volume equivalent diameter (Khalizov et al., 2013; Rissler et al., 2013; Giordano et al., 2016). Depending on the miscibility, condensability, polarity and entropy, black carbon may form core shells, internal or external mixtures with the condensing SA and other atmospheric salts (nitrates, sulfates) (Asa-Awuku, Engelhart, et al., 2009; Vaden et al., 2010; Robinson et al., 2016). External mixtures are assumed to be weak non-homogenous conglomerates formed between the aerosol components. In internal mixtures, the aerosol components form a single-phase homogenous aerosol species. Black carbon is however solid and assumed immiscible and form multiphase core shell structures. External mixtures of BC and SA and salts are therefore more probable, especially after atmospheric transportation and aging (Jacobson, 2001; Moffet & Prather, 2009; Cappa et al., 2012).

Transportation emissions are a significant fraction of the total global PM emissions. One of the largest sources of vehicular emissions in the US is from light duty vehicles (LDV); passenger and trucks (Lamarque et al., 2010; Xing et al., 2013). With increasing LDV usage, the US Environmental Protection Agency (EPA) and the National Highway Transportation Safety Administration has promulgated legislation to increase the corporate average fuel economy(CAFE) and concurrently decrease the greenhouse gas emissions from LDV (Hula et al., 2015). The automobile industry responded to these new regulatory standards by developing and manufacturing more fuel efficient light duty vehicles. Improvements in fuel economy however modify emissions. For example, fuel

efficient diesel vehicles incorporate diesel particulate filters to effectively remove enhanced soot emissions (EPA, 2012; Maricq et al., 2012).

Currently, gasoline direct injection (GDI) engines provide the best approach to meet both the new CAFE and GHG emissions standards (Yi et al., 2009; Hula et al., 2015; Ellies et al., 2016) . In GDI engines, the fuel and air is injected into the combustion chamber separately (Iwamoto et al., 1997; Zhang et al., 2012). This engine design provides higher power output, better fuel economy and fewer greenhouse gases. GDI engines however generate more particulate matter and number (PM/PN) as compared to equivalent port fuel injection engines. The reported higher PM and PN from GDI engines has been attributed to reduced time for inhomogeneous fuel air mixing, liquid gasoline impingement on the cylinder walls and piston resulting in regional fuel-rich combustion in the cylinder (Karavalakis et al., 2014; Wang et al., 2014). Efforts are therefore being made to integrate technologies and calibrate GDI engines to meet new, more stringent emissions standards. Proposals include modifications to the engine injector geometry and position to reduce fuel impingement, increasing fuel pressure and minimizing fuel droplet size, improve injection timing, engine downsizing and turbocharging and integrating gasoline particulate filters (GPF) (Yi et al., 2009; Piock et al., 2011; Whitaker et al., 2011).

Gasoline particulate filters (GPF) can remove up to 85% in applications with different gasoline blends over US EPA certified drive cycles (Chan et al., 2012; Chan et al., 2014). *Roth et al* (2017, in preparation) showed that the filtration of particulate black

carbon by the GPF results in changes in the composition, morphology, density and size distribution of secondary aerosol mixtures formed from photochemical aging of the filtrate. With these changes in both physical and chemical properties, it is important to constrain the corresponding subsaturated and supersaturated hygroscopicity, CCN activity and droplet kinetics of emissions from GDI vehicles with and without a GPF. This work complements the work of *Roth et al* (2017, in preparation) who during the same campaign characterized the secondary aerosol formation.

In this study, the first of its kind, we investigate the cloud condensation nuclei activity of freshly emitted and photochemically aged gasoline emissions from two light duty vehicles fitted with a GPF. Using CCN counter measurements and hygroscopicity tandem differential mobility analyzer (HTDMA) measurements, we characterize the evolution of the aerosol sub- and super-saturated hygroscopicity during the photochemical aging of the unfiltered soot and filtered, $(NH_4)_2SO_4$-seeded soot in a mobile atmospheric reactor. The impacts of organics, sulfates and nitrates fractional compositions on the CCN activity and hygroscopicity is also explored through aerosol particle composition data from an aerosol mass spectrometer. Changes in the droplet kinetics is characterized with threshold droplet growth analysis (TDGA).

4.2 Theory and Closure Analysis

4.2.1 Supersaturated Hygroscopicity

Aerosol activate into cloud droplets and act as cloud condensation nuclei when exposed to a critical water vapor supersaturation, s_c. The critical supersaturation depends,

mainly, on the aerosol dry size and chemical composition. Köhler theory incorporates the solute and curvature effects on equilibrium water vapor pressure. Köhler theory relates the thermodynamic and physical properties of aerosol to predict the critical supersaturation, $s_{c,}$ at which an aerosol of dry size $D_{d,}$ will activate into CCN (Köhler, 1936; Seinfeld & Pandis, 2006). Kohler theory can be defined as:

$$\ln S_c = \left(\frac{4A^3\rho_w M_s}{27\nu\rho_s M_w d_s^3}\right)^{\frac{1}{2}}, \text{ where } A = \frac{4\sigma_{s/a}M_W}{RT\rho_w} \qquad [4.1]$$

Where S_c is the critical water-vapor saturation ratio for a dry-particle critical diameter d_s. The particle has a density ρ_s, a molecular weight M_s, and the Kelvin effect is represented by A. M_w and ρ_w are the molecular weight and density of water respectively and ν is the number of ions resulting from the dissociation of one solute molecule, $\sigma_{s/a}$ is the surface tension, R is the universal gas constant and T is the sample temperature. S_c, the critical saturation is greater than 1, the critical supersaturation $s_{c,}$ is defined as $s_c = S_c - 1$.

In the absence of available solute and aerosol composition data, especially for ambient aerosol, Köhler theory is parameterized by a single hygroscopicity parameter, κ. The single parameter, κ integrates aerosol compositional, size distribution and ambient water vapor concentration data. This enables an easy, robust representation of CCN activity in CCN models. Inorganic salts, such as ammonium sulfate and sodium chloride, which are generally highly hygroscopic, have a κ between 0.5 and 1.2 whereas slightly hygroscopic to hygroscopic organic salts and secondary organic aerosol have a κ between

0.01 and 0.5. Non-hygroscopic but wettable aerosol such as black carbon has a near zero κ (Petters & Kreidenweis, 2007). The single parameter supersaturated CCN hygroscopicity, κ_{CCN} can be defined by:

$$\kappa_{CCN} = \frac{4A^3}{27d_s^3 ln^2 S_c} \quad [4.2]$$

4.2.2 Sub-saturated Hygroscopicity

The subsaturated water uptake by dry aerosol can be studied with the humidified tandem differential mobility analyzer (HTDMA) technique. An initial differential mobility analyzer (DMA) scans mono-dispersed, diffusion-dried aerosol, the aerosol distribution is then exposed to an elevated relative humidity (RH) in a conditioner where the particle takes up water. A second DMA is used to obtain a the humidified aerosol distribution and the ration between the peak dry distribution mobility diameter, D_{in} and peak humidified aerosol distribution mobility diameter, D_{RH} is the diameter growth factor (Schwarz et al.) which indicates the increase in the radial thickness of the aerosol (Rader & McMurry, 1986; Gysel et al., 2009).

HTDMA data can be fitted to obtain a single parameter hygroscopic factor similar to the fit for CCN data by fitting the GF as a function of RH (Petters & Kreidenweis, 2007; Kreidenweis & Asa-Awuku, 2014). Parameterization of HTDMA growth factor data with the single parameter κ allows for the integration of HTDMA data into climate models. The single hygroscopic factor, κ can be defined as:

$$\kappa_{HTDMA} = [GF^3 - 1]\left[\frac{100}{RH}\ exp\left(\frac{4\sigma_{s/a}M_w}{RT\rho_w D_{in}}\right) - 1\right] \quad [4.3]$$

If the Kelvin effects, the change in the water vapor pressure due to the curvature of the growing droplet, and κ is assumed constant over a given RH range (valid for RH > 85%) (Khvorostyanov & Curry, 2007; Petters & Kreidenweis, 2007), then κ_{HTDMA} can be estimated as follows:

$$\kappa_{HTDMA} = 0.111[(GF)^3 - 1] \quad [4.4]$$

4.2.3 κ-hygroscopicity Closure

The assumptions used to estimate the simplified Köhler theory-based relationships for CCN activity information from sub-saturated and supersaturated instruments are extensive. CCN closure studies allows for the evaluation of these assumptions for suitability and robustness. Several studies have sought closure between the κ_{CCN} and κ_{HTDMA} in ambient and laboratory-generated aerosol with varying degrees of discrepancy observed (Prenni et al., 2007; Alfarra et al., 2013; Whitehead et al., 2014; Zhao et al., 2016). The estimated subsaturated, κ_{HTDMA} is almost always lower than the supersaturated, κ_{CCN} . This may be attributed to surface tension, volatilization of organics, non-spherical dry aerosol and short residence times in the HTDMA (Massoli et al., 2010; Dusek et al., 2011; Frosch et al., 2011). Organic species may volatize between the first and second DMA and this may affect the initial dry aerosol size, D_{in} (Prenni et al., 2001) . Non-spherical aerosol, prevalent in combustion, from the first DMA may collapse and

restructure resulting in un-conserved aerosol dry volume and inaccurate growth factor prediction and κ estimation (Mikhailov et al., 2009). The short residence time in subsaturated HTDMA may also limit aerosol dissolution, especially in coated aerosol and delay the equilibrium, thereby limiting the mass transfer of water vapor to the surface of the aerosol (Chan & Chan, 2007; Modini et al., 2010). Closure studies allow for the quantification of these factors on the hygroscopicity and CCN activity of the aerosol.

The focus of many supersaturated CCN closure studies compares ambient CCN activity with predictions by coupling compositional, size and CCN data from available fast resolution instrumentation. These studies are done to constrain the effects of aerosol mixing states, size dependent composition and droplet kinetics. The mixing state of aerosols has significant influences on the CCN activity and droplet concentrations (Cubison et al., 2008; Asa-Awuku et al., 2011). Assuming internal mixtures enables the use of bulk chemical composition properties but may result in an over-prediction of CCN concentrations and hygroscopicity (Lance et al., 2009; Wang et al., 2010). Incorporating hygroscopic and organic composition data can improve the agreement between the predicted CCN number and the hygroscopicity (Gunthe et al., 2009; Chang et al., 2010). CCN activity constrained with composition data (such as from an aerosol mass spectrometer) enables the evaluation of the influence of mixing states and bulk chemical composition assumptions on the estimated hygroscopicity and CCN activity.

4.3 Experimental and Analytical Methods

4.3.1 Setup and Instrumentation

The experiments were done at University of California, Riverside's Center for Environmental Research and Technology as part of a multi-agency funded study. The study evaluated tailpipe particulate matter emissions, secondary organic aerosol (SOA) formation and CCN activity of aged emissions from gasoline direct injection (GDI) light duty vehicles (LDV) prevalent in the California fleet. The secondary aerosol generation and characterization experiments from these specific vehicles are more elaborately described in Roth et al (2017, in preparation). Here, we only dwell on the aspects of the data and experimental setup that are pertinent to explaining CCN formation and hygroscopicity. The experimental setup of pertinent instruments and facilities is shown in Figure 4.1.

Two LDV wall-guided GDI vehicles, 2016 Ford Fusion and 2016 Mazda 3, were run on a Burke E. Porter light duty chassis dynamometer on the California Unified Cycle. The tailpipe emissions were sampled via constant volume sampler and diluted. An AVL Micro soot sensor and a suite of other particle and gas measurement instrumentation was used to characterize the primary soot emissions. The soot was sampled directly from the dilution system into a portable mobile atmospheric reactor. In another setup, the vehicle's exhaust system was modified to include a gasoline particulate filter (GPF). The GPF can remove about 90% of the PM (Chan et al., 2012; Chan et al., 2014) In the GPF-fitted

experiments, atomized aerosol $(NH_4)_2SO_4$ was injected into the reactor to serve as seeds (additional surface area) for secondary aerosol formation.

The primary emissions were aged in a 30 m^3 fluorinated ethylene propylene mobile film reactor. The primary tailpipe emissions; soot only or GPF-filtered soot + $(NH_4)_2SO_4$, is photo-oxidized for an average of 8 hours under ultra-violet lights and with hydrogen peroxide oxidant (70 – 140 μL) (Roth et al 2017, in preparation). The particulate mass, mainly SOA and nitrates, generated during photochemical oxidation are herein collectively referred to as secondary aerosol (SA). The SA formed during photooxidation experiments from the default engine after-treatment configuration without GPF, Mazda 3 and Ford Fusion experiments, are hereafter referred to as BCSA I and BCSA II, respectively. The secondary aerosol formed from the $(NH_4)_2SO_4$-seeded experiments are SSA I and SSA II, respectively. Each experimental iteration was done in triplicates; 12 unique experiments were performed. Results presented here are averages of at least two runs of one vehicle setup. The particle composition of the aerosol mixture was characterized by a high-resolution time-of-flight mass spectrometer (HR-TOF-AMS; Aerodyne Research Inc.) (Canagaratna et al., 2007). The aerosol effective density, ρ_{eff}, was measured with a customize-built aerosol particle mass analyzer (APM) –Scanning mobility particle sizer (SMPS) system. It has a 75s resolution. A custom LabVIEW® program actively optimized the instrument response by determining the peak diameter form two parallel SMPS to correct the mass of the particle estimated by the APM (Malloy et al., 2009).

The subsaturated hygroscopic growth of the BCSA and SSA is continuously measured with a custom-built HTDMA. Based on the Radar and McCurry design, the initial dry aerosol size distribution is measured by the first SMPS and then humidified (RH 85% - 95%) for about 1 min. A second SMPS measures the post-humidification size distribution. The ratio of the peaks of the lognormal size distributions is the GF (Rader & McMurry, 1986; Cocker et al., 2001; Qi et al., 2010). The CCN activity was measured with a DMT Inc. CCN counter (CCNc) coupled with a TSI Inc. SMPS system. The size distribution from the SMPS (10 – 500 nm) operating in scanning mode, is exposed to scanning superstation (0.8 - 1.8%) in the CCN counter (CCNc) at a sample flowrate of 0.5 lpm. The CCN counter provides CCN concentration and droplet size information at 1Hz resolution. This is inverted with the SMPS dry size data to infer the CCN activity and hygroscopicity. The CCNc flowrates and supersaturation was calibrated within 10% of the flowrate and supersaturation set points before the experiments with laboratory-generated $(NH_4)_2SO_4$ (Lance et al., 2006; Rose et al., 2008).

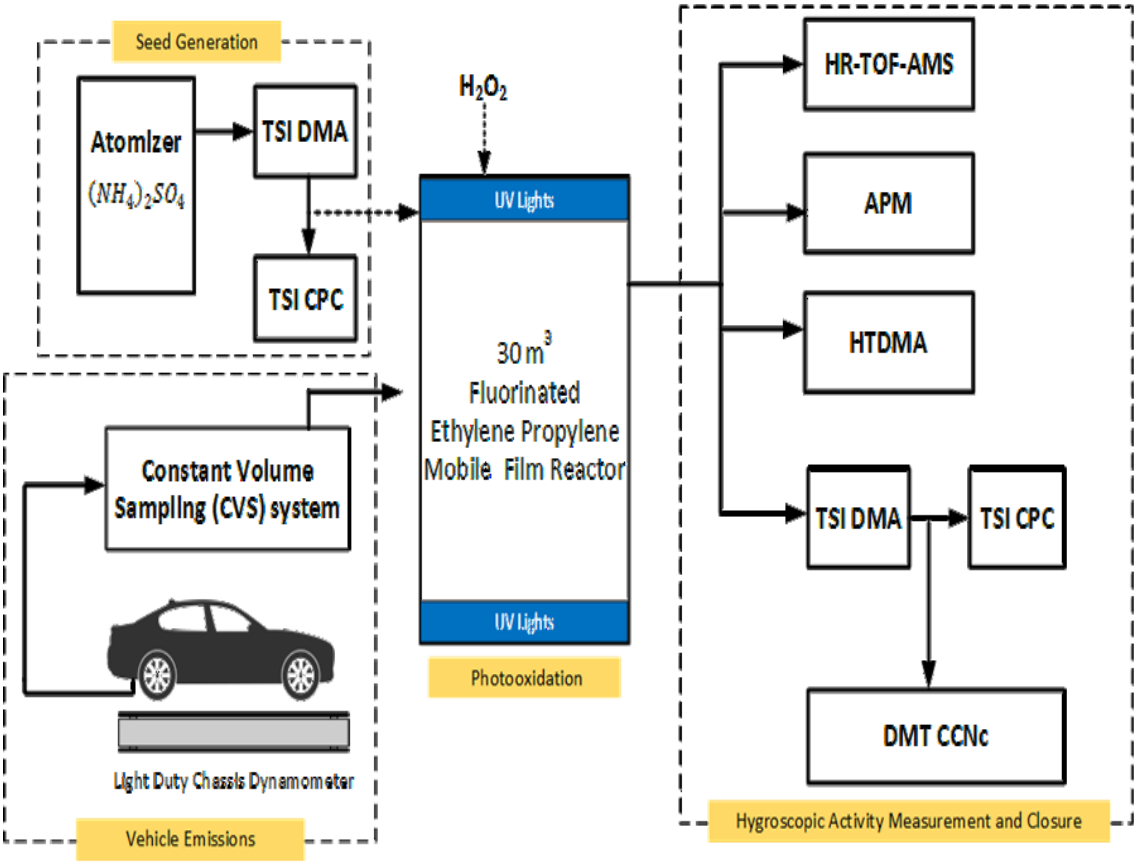

Figure 4.1. Experimental setup for tailpipe emissions measurement, SA generation and hygroscopicity measurement

4.3.2 Determining κ-hygroscopicity

An apparent CCN hygroscopicity parameter, κ_{CCN} was measured from the CCN counter and SMPS data with scanning mobility CCN analysis, SMCA (Moore et al., 2010). The dry aerosol number, CN is derived from inverting the aerosol time series data from the SMPS. Multiple charge-corrected dry size distribution and CCN time series are synchronized to estimate an activation ratio (CCN/CN). The critical diameter, dp_{50}, is the diameter at which more than half of the aerosol dry size distribution activates at a

specific supersaturation, s_c (Moore et al., 2010). The dp_{50} is equivalent to D_d in equation [4.2]. In using equation [4.2] to estimate κ_{CCN}, we assumed SSA and BCSA were internally mixed or formed core-shell structures, respectively.

Equation [4.3] is employed to estimate the subsaturated HTDMA hygroscopicity parameter, κ_{HTDMA}. Only positive hygroscopicity values are reported. Negative κ_{HTDMA} are not shown and indicate shrinkage in the aerosol size; as a likely a result of restructuring when exposed to the higher RH environment (Mikhailov et al., 2009; Ma et al., 2013). In calculating the κ_{CCN} and κ_{HTDMA}, the surface tension of pure water in the growing droplet was constrained with the instrument water vapor temperature (Pruppacher & Klett, 1997).

From *Petters et al (2007)*, the average volume-weighted κ of a mixture can be calculated from the individual volume fractions of the constituent species:

$$\kappa = \sum_i \varepsilon_i \kappa_i \qquad [4.5]$$

Where ε_i is the volume fraction of component i^{th} of the aerosol mixture. Inorganic nitrate measured by the AMS was assumed ammonium nitrate with κ of 0.75. The sulfates from the salt seeded experiments were assumed to be ammonium sulfate with a κ of 0.6 and κ of 0.15 was used for the organic fraction in line with chamber generated SOA (Petters & Kreidenweis, 2007; Suda et al., 2012). The total aerosol mass was assumed to be composed of refractory and non-refractory aerosol. Thus the total mass is estimated from the initial black carbon mass (measured before

photooxidation from the AVL micro soot sensor) and the secondary aerosol mass measured by the AMS. The total aerosol volume is estimated from this mass and the effective density, ρ_{eff} from the APM-SMPS system. The residual volume after accounting for the AMS organics and inorganics is considered the volume of the black carbon component. An average hygroscopicity, κ_{BC} of 0.001 was applied to freshly emitted soot (Zaveri et al., 2010; Vu et al., 2015). Assuming simple mixing (Petters & Kreidenweis, 2007), the average hygroscopicity based on the aerosol mass fractions as follows:

$$\kappa_{AMS} = \varepsilon_{inorg}.\kappa_{inorg} + \varepsilon_{org}.\kappa_{org} + \kappa_{BC}.(1 - \varepsilon_{inorg} + \varepsilon_{org}) \quad [4.6]$$

Where *inorg* and *org* are the inorganic and organic property values respectively.

4.3.3 Determining Droplet Kinetics

The droplet growth and kinetics effects of the condensing SA on either the BC or $(NH_4)_2SO_4$ is evaluated through threshold growth analysis (TDGA) (Engelhart et al., 2008; Asa-Awuku, Engelhart, et al., 2009). TGDA detects the presence of slowly activating components during the evolution of both SSA and BCSA. This method has been applied to various ambient and laboratory-generated aerosol to varying effect. In TDGA the average droplet diameter of activated CCN exiting the CCN counter optical particle counter (OPC) is compared to a standard aerosol with rapid activation kinetics at the same supersaturation S_c and instrument settings. In this study laboratory-generated $(NH_4)_2SO_4$ aerosol is used as the reference. Absent mass transfer limitations, slow activating and surface active fractions and depletion effects, the reference aerosol and the

BCSA and SSA should all grow to similar droplet sizes (Padró et al., 2010; Asa-Awuku et al., 2011; Engelhart et al., 2011; Ruehl et al., 2016; Fofie, Castellucio, et al., 2017). The reported droplet diameters are corrected for droplet size depletion by the CCN number (Lathem & Nenes, 2011). It should also be noted that the optical particle counter on the CCNc has a bin width of 0.5 μm hence any droplet size differences less than 1 μm are not be robustly differentiated (Fofie, Castellucio, et al., 2017).

4.4 Results

4.4.1 Supersaturated Hygroscopicity

The supersaturated $\kappa_{CCN}$was estimated using the methods and assumptions described in section 3.2 and equation [4.2]. The average apparent κ_{CCN} for the BCSA mixtures over the entire experiment, after the UV lights were turned on, was 0.11 ± 0.07. This is within the range of previously reported CCN hygroscopicity for laboratory-aged combustion soot (Zaveri et al., 2010; Tritscher et al., 2011). Whiles the average SSA κ_{CCN} before the UV lights were turned on was 0.50 ± 0.07 and 0.42 ± 0.09 after the UV lights are turned on. This is also consistent with previously documented hygroscopicities of SOA coated salt mixtures from chamber experiments (Huff Hartz et al., 2005; King et al., 2009; Shantz et al., 2010).

In figure 4.2, we observe changes in the hygroscopicity as a function of time and dry diameter. In the BCSA I and BCSA II experiments (fig. 4.2a and 4.2b), the first 30 minutes show hygroscopicities similar to unaged vehicle soot, $\kappa_{CCN} = 0.0014 \pm 0.0006$ (Tritscher et al., 2011; Vu et al., 2017). As the emissions age, however, the SA formed

from the co-emitted gas phase precursors condense onto the BC core (Roth 2017, in preparation) and increase the hygroscopicity. In the BCSA II experiments, the CCN hygroscopicity increases to levels above that of average SOA (peak $\kappa_{CCN} = 0.3$) indicating the formation of species more hygroscopic than slightly soluble organics. *Roth et al (2017*) shows the formation of elevated amounts of nitrates may account for the sudden spike in hygroscopicity. In BCSA I there is a gradual increase in the hygroscopicity during the course of the experiment but the maximum κ_{CCN} ($\kappa_{CCN} = 0.125$) remains below that of SA indicating the dominance of the black carbon component on the hygroscopicity. In the SSA experiments (fig. 4.2c and d), the hygroscopicity is significantly dominated by the ammonium sulfate seeds.

The formation of SA however, does significantly suppress the average κ_{CCN}, reducing it from 0.55 to 0.42. This suggests an internally mixed aerosol of ammonium sulfate, BC and SA as consistent with previous ambient and experimental observations (Wang et al., 2010).

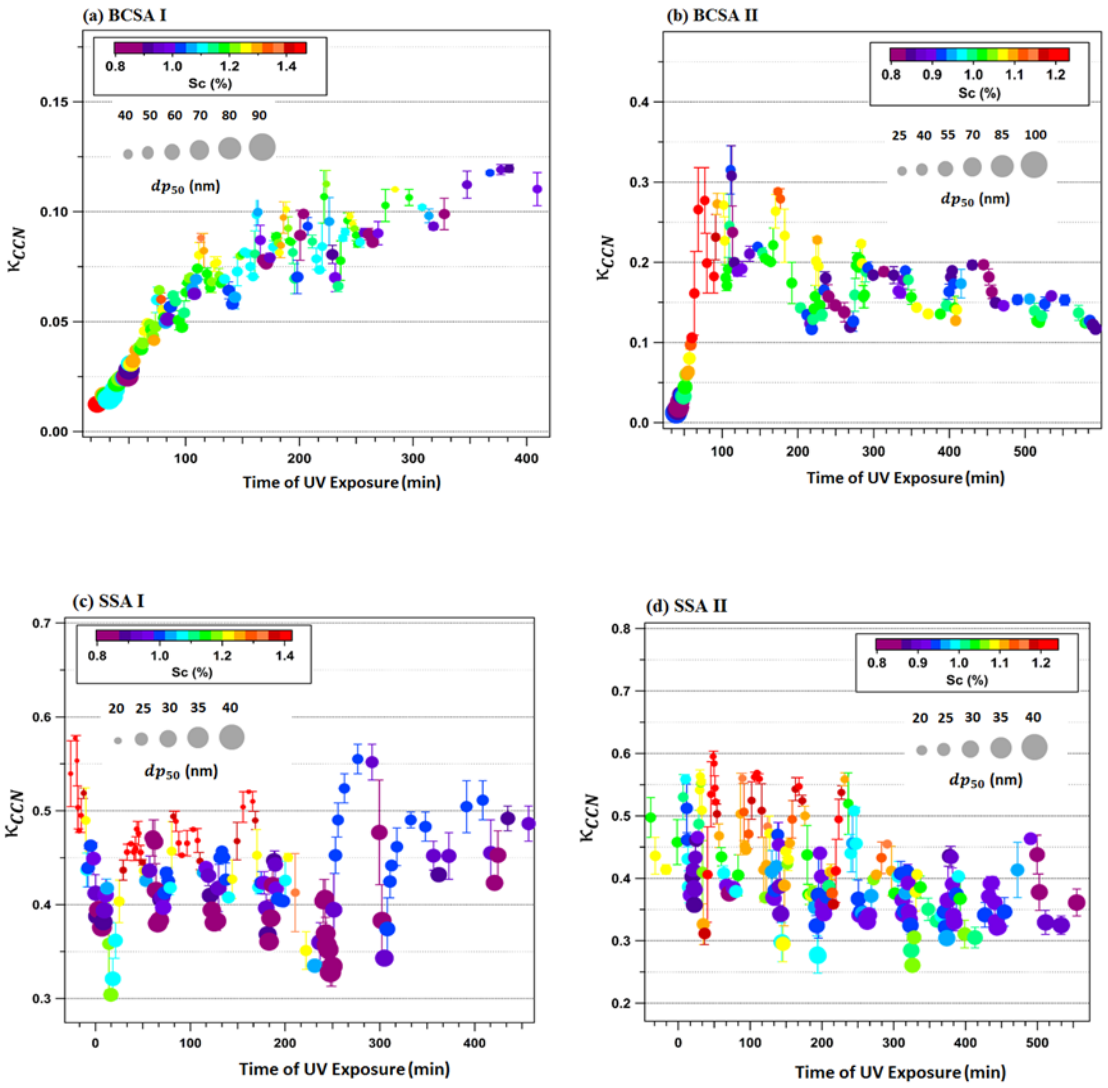

Figure 4.2. Evolution of the CCN hygroscopicity, κ_{CCN} with experimental time. The UV lights are turned on at time = 0 minutes

There is a sensitivity of the hygroscopicity to the critical dry diameter, dp_{50} . In the SSA systems, irrespective of the experimental elapsed time, the larger dry aerosol ($dp_{50} = 40\ nm$) were the least hygroscopic ($\kappa_{CCN} = 0.3$) and more hygroscopic ($\kappa_{CCN} = 0.5$) at the smaller critical diameters ($dp_{50} = 20\ nm$). This suggests that at the smaller dry SSA sizes the more soluble, hygroscopic $(NH_4)_2SO_4$ volume faction dominates the CCN activity. In the BCSA system, the hygroscopicity is relatively insensitive at $dp_{50} \gg 60\ nm$. The more hygroscopic nitrates and organics have a higher propensity to condense onto the smaller size BC particles. The resultant BCSA are less fractal with a greater CCN active surface area, thus the apparent supersaturated hygroscopicity increases (Fig. 4.2 a & b).

4.4.2 Sub-saturated Hygroscopicity

The sub-saturated hygroscopicity, κ_{HTDMA} was calculated from the HTDMA data using equation [4.4]. The HTDMA was operated at $RH = 0.93 \pm 0.04$. The BCSA particles had a $GF = 1.06 \pm 0.02$ and $\kappa_{HTDMA} = 0.006 \pm 0.005$ before the UV lights were turned on. The GF reduced to 1.007 ± 0.005 with $\kappa_{HTDMA} = 0.015 \pm 0.036$ after the lights were turned on. In the SSA the average GF before the UV lights were turned on was 1.31 ± 0.21 and $\kappa_{HTDMA} = 0.18 \pm 0.04$ with a reduced growth factor of 1.26 ± 0.17 and $\kappa_{HTDMA} = 0.10 \pm 0.14$ after the lights were turned on. The κ_{HTDMA} was evaluated for aerosol dry sizes, D_{in}, from 60 to 260 nm initially selected by the first DMA.

In figure 4.3, we observe changes in the subsaturated hygroscopicity, κ_{HTDMA} during the evolution of the emissions. In the BCSA I and II (Fig. 4.3a and b) aerosol is initially very non-hygroscopic ($\kappa_{HTDMA} = 0.002 \pm 0.0007$ for BCSA I and $\kappa_{HTDMA} = 0.0003 \pm 0.007$ for BCSA II).The formation and condensation of SA from the co-emitted gas phase components onto the BC core increases the κ_{HTDMA}. The variation in κ_{HTDMA} is highly sensitive to the peak of the dry aerosol distribution, D_{in} selected by the first DMA. In the BCSA I, the κ_{HTDMA} increases to as much as 0.11 ± 0.03 after 500 minutes of photochemical oxidation at an average peak dry diameter, $D_{in}$of 120 nm. In the BCSA II however, after 600 minutes of photochemical oxidation the κ_{HTDMA} increases to 0.03 ± 0.0074 at an average peak dry diameter of 260 nm. In the SSA however, there was an observed depression in the measured κ_{HTDMA} with increase in the peak dry size. In the SSA I mixture the low hygroscopicity ($\kappa_{HTDMA} = 0.024 \pm 0.001$) was observed for the large dry sizes of 225 nm whiles the mixture is most hygroscopic ($\kappa_{HTDMA} = 0.19 \pm 0.02$) at an average dry size of 115nm before the UV lights were turned on.

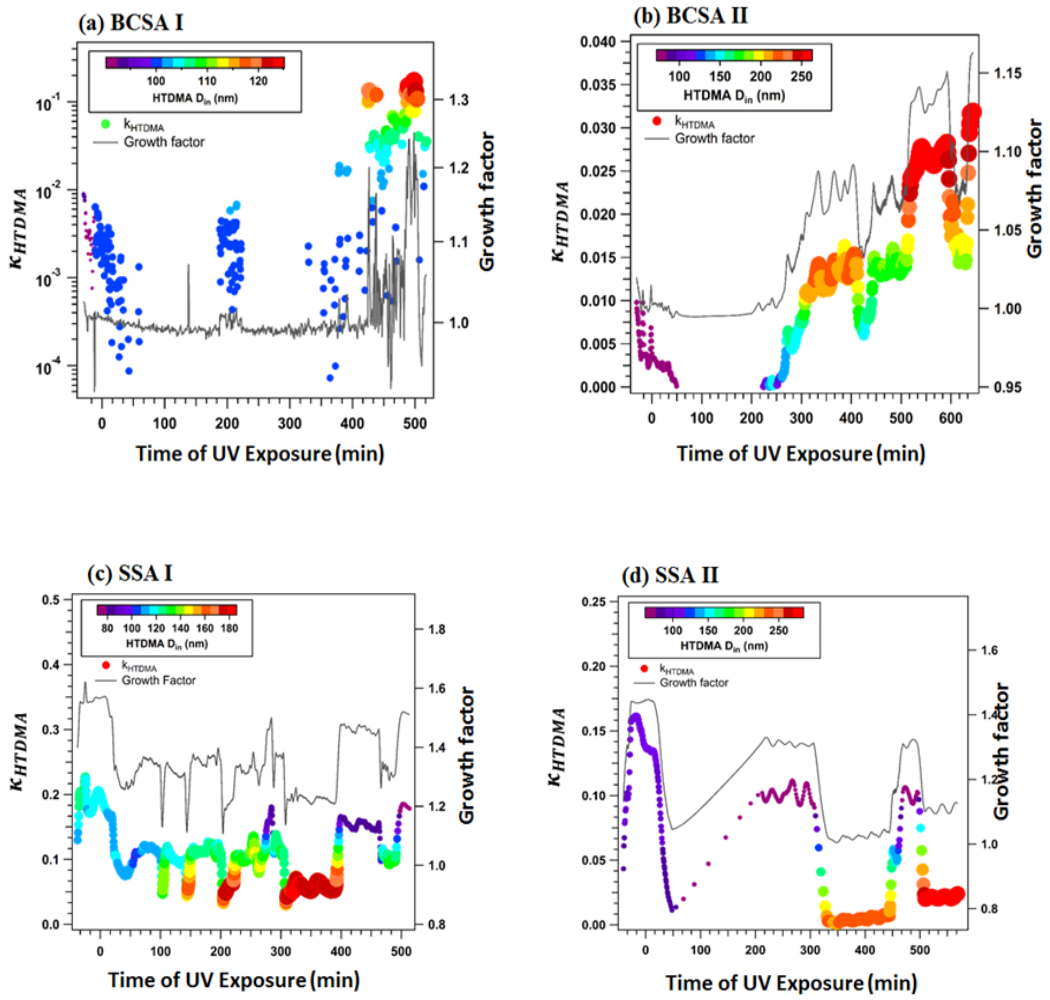

Figure 4.3. Evolution of the HTDMA hygroscopicity, κ_{HTDMA} with experimental time. The UV lights are turned on at Time = 0 min. Only positive κ_{HTDMA} values are shown.

We observe similar trends in the secondary aerosol formed from the 2nd vehicle (SSA II). The SSA II mixture is the least hygroscopic ($\kappa_{HTDMA} = 0.021 \pm 0.002$) at a peak average dry size of 280nm. SSAII was the most hygroscopic ($\kappa_{HTDMA} = 0.15 \pm 0.02$) at an average dry size of 100nm before the UV lights were turned on. The higher hygroscopicity observed in the SSA before the lights were turned on is consistent with

the presence of greater volume fractions of more soluble $(NH_4)_2SO_4$. The formation and condensation of SA onto the salt core depresses the solubility and hygroscopicity of SSA. The lowest κ_{HTDMA} in the SSA is equivalent to the largest hygroscopicity in the BCSA confirming the more soluble secondary material is the main driver of hygroscopicity in the subsaturated regime. The quantitative contributions of the secondary aerosol to supersaturated and subsaturated particle hygroscopicity are evaluated with a closure study in Section 4.5

4.4.3 Droplet Kinetics

In Figure 4.4 the droplet sizes of the mixtures is compared to the droplet sizes of laboratory-generated $(NH_4)_2SO_4$ aerosol. The droplets are evaluated at 0.5 lpm CCNc flowrate and 0.8 – 1.6% supersaturation. The droplets sizes are corrected for depressions due to the CCN concentrations (Lathem & Nenes, 2011; Fofie, Castellucio, et al., 2017).

In fig. 4.4a, the condensation of the SA onto the BCSA does not seem to modify the droplet kinetics. The average final droplet diameters of BCSA, for all supersaturations evaluated, was within $\pm 4\%$ of the $(NH_4)_2SO_4$ reference diameters. Changes in the volume fraction of the secondary aerosol (NO_3 + organics) does not significantly modify the droplet sizes. These results suggest that the integration of BC into the SA to form core shell structures does not substantially modify the kinetics of the SA. In Fig. 4.4b, there is a more significant modification of the SSA droplet kinetics. The average final droplet diameters for SSA, for all supersaturations evaluated, were an average of one bin size and up to 7% smaller than the $(NH_4)_2SO_4$ reference diameters (Fofie, Castellucio, et al.,

2017). This suggests that the integration of the $(NH_4)_2SO_4$ and SA into internal mixtures results in relatively slower droplet kinetics.

These results are in agreement with previously reported droplet kinetics from chamber SOA (Engelhart et al., 2008; Zhao et al., 2016) and ambient data sets (Bougiatioti et al., 2009). Contrary to previous observations in ambient aerosol, the presence of the insoluble BC fraction does not seem to significantly retard the droplet growth kinetics in BCSA (Padró et al., 2010; Asa-Awuku et al., 2011). The modifications in droplet kinetics in SSA may not be statistically insignificant since they are within one bin width (0.5 μm) of the optical particle counter (Fofie, Castellucio, et al., 2017).

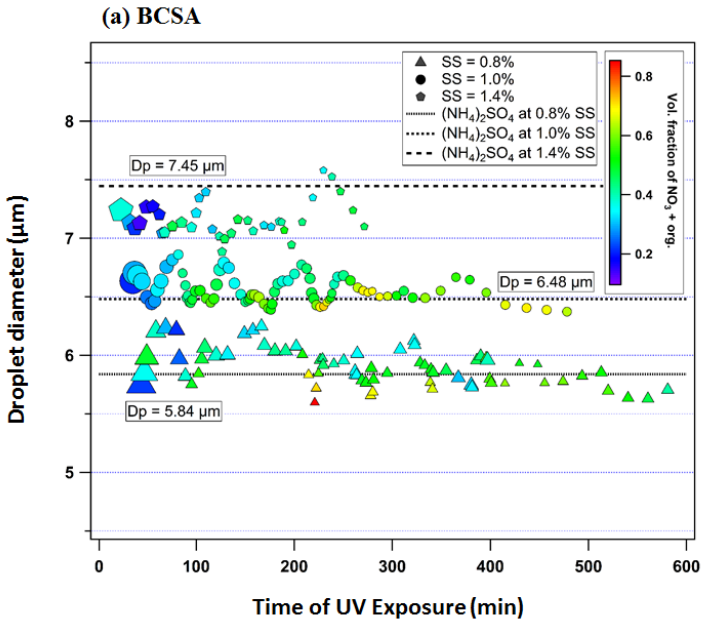

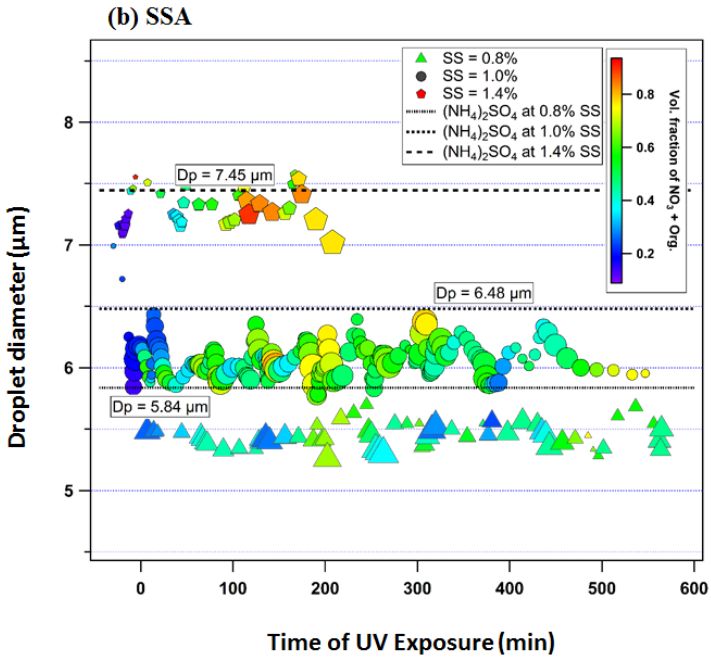

Figure 4.4. The droplet diameters of (a) BCSA and (b) SSA compared to that of $(NH_4)_2SO_4$. Each point is the mean droplet diameter at the specified supersaturation over the course of the experiment.

4.5 Closure Analysis

4.5.1 Closure between CCN Measured and AMS Derived κ-Hygroscopicity

The κ-hygroscopicity parameter measured from the CCN experiments is compared to hygroscopicity,κ_{AMS} values calculated from HR-TOF-AMS and APM data using equation [4.6]. In figure 4.5, by comparing the slopes, S of the fits, there is an observed general convergence of the bulk κ-hygroscopicities, κ_{AMS} and κ_{CCN} for all systems (S= 1.005 to $S = 1.13$) except in BCSA II ($S = 1.91$) (fig 4.5b).

The influence of the dry aerosol size on the CCN analysis seems to be minimal in both BCSA and SSA. The aerosol shows a uniform, size-independent chemical

composition (except in BCSA II). The higher dry aerosol detection limit of the AMS does not therefore seem to adversely bias the closure. The convergence in the mobility diameter derived κ_{CCN} and the mass fraction based κ_{AMS} hygroscopicities indicates that the bulk composition assumptions inherent in CCN SMCA analysis are sound for this aerosol system. Constraining the aerosol volume with the effective density, ρ_{eff} data from the APM-SMPS system ensured a robust prediction of the aerosol volume. ρ_{eff} accounts for the mixture morphology and fractal nature as SA condenses onto the core (DeCarlo et al., 2004; Nakao et al., 2011; Giordano et al., 2015).

The non-closure observed in BCSA II may be due to a non-uniform, size dependent chemical composition of the aerosol mixture. *Roth et al* (2017) observed a nucleation burst after 100 min accompanied by a significant formation of nitrates. The nitrate-rich nucleation formed mainly larger dry aerosol beyond the scope of CCN measurements. The BCSA II κ_{AMS} is size-dependent and is driven by the higher nitrate volume fraction, hence the non-convergence observed.

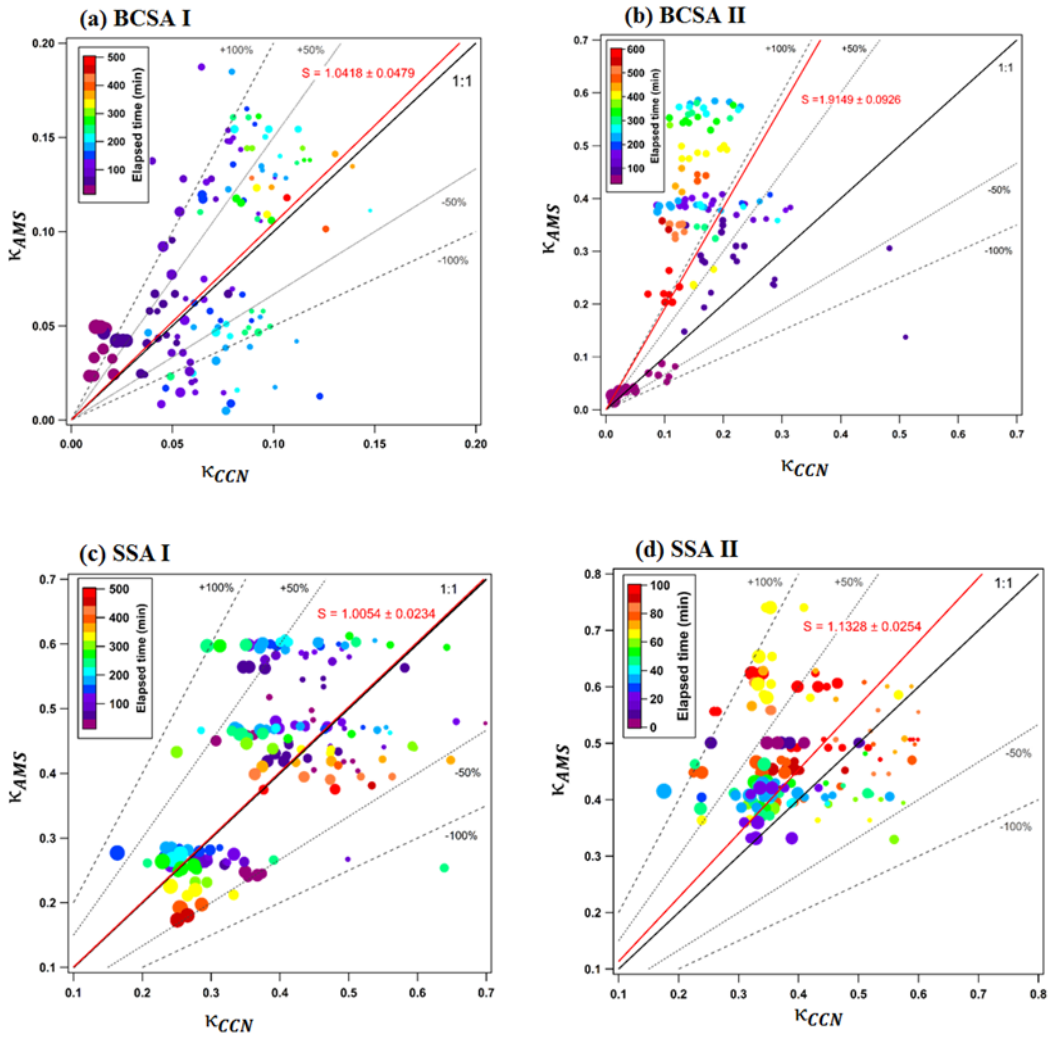

Figure 4.5. Closure analysis of CCN hygroscopicity with AMS data. Solid red line represent the slope, *S* of the fit. Dashed lines represent ±50% and ±100% prediction error.

4.5.2 Closure between CCN and HTDMA κ-hygroscopicity

The *κ*-hygroscopicity parameter computed from the supersaturated CCNc and the subsaturated HTDMA is compared to evaluate the convergence of the two approaches in

figure 4.6. There is significant difference between the κ_{HTDMA} and κ_{CCN}. The κ_{HTDMA} was lower than κ_{CCN} in both systems. The ratio of $\kappa_{HTDMA}/\kappa_{CCN}$ in BCSA I and BCSA II is 0.10 and 0.42, respectively. The of $\kappa_{HTDMA}/\kappa_{CCN}$ for SSA is 0.27 and 0.13, respectively. There is therefore a larger difference between the hygroscopicities in the SSA than in BCSA. The non-closure observed in the measured sub- and super-saturated can be attributed to various factors including solubility, nonsphericity, non-conservation of morphology, and volatilization of volatile organic components (Prenni et al., 2007; Petters et al., 2009; Massoli et al., 2010; Alfarra et al., 2013).

The solubility of the aerosol has a significant effect on both the subsaturated and supersaturated hygroscopicity. The solubility effects have however been observed to be more noticeable in the subsaturated HTDMA measurement. (Petters & Kreidenweis, 2008). The SSA κ_{HTDMA} although higher than that of BCSA is not equivalent to that of κ_{CCN}. The presence of the condensed, less soluble SOA fraction on the BC and $(NH_4)_2SO_4$ may supress the influence of the more soluble $(NH_4)_2SO_4$ on κ_{HTDMA}. Less soluble aerosol require higher relative humidity to activate into the droplets. The higher supersaturations (0.8 - 1.6%) at which the CCN was operated activated smaller aerosol into droplets as compared to the HTDMA (~ RH = 94%). The κ_{CCN} is based on bulk average chemical composition hence the effects of the non-uniform, size dependent chemical composition on hygroscopicity, as suggested by κ_{HTDMA}, are absent. The lower solubility coupled with a lower residence time and larger sizes in the HTDMA results in the lower measured hygroscopicities in both BCSA and SSA.

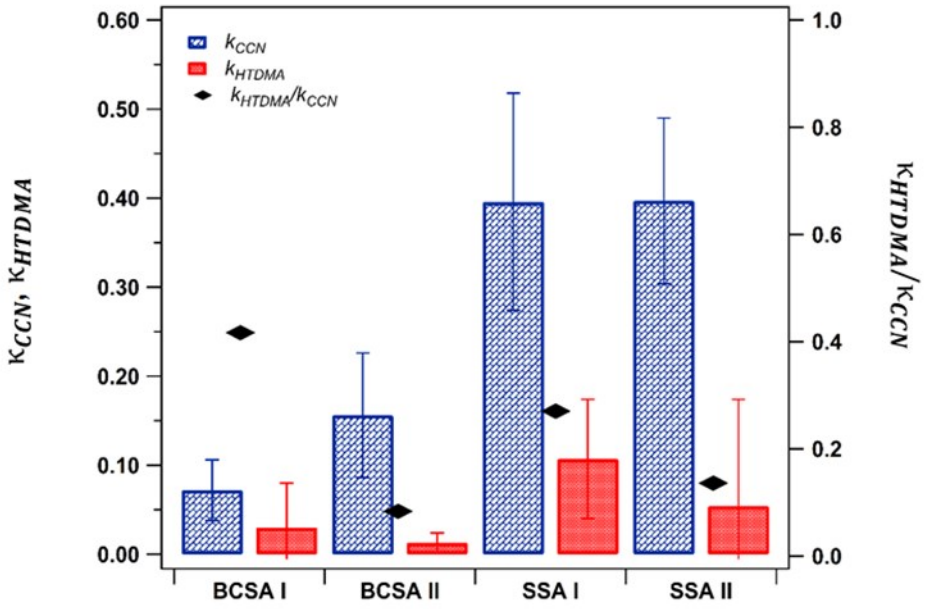

Figure 4.6. Comparison between κ_{CCN} and κ_{HTDMA}.

4.5.3 Effects of the Aerosol Volume Fraction on CCN hygroscopicity

In aerosol mixtures, the hygroscopicity has been shown to be volume additive and solubility influenced. This is well characterized in known, simple aerosol mixtures of salts and organic aerosol (Riipinen et al., 2015). In photochemically aged combustion aerosol and SOA however, the more complex chemical composition and mixing states makes constraining the hygroscopicity with the volume fractions challenging (Asa-Awuku, Miracolo, et al., 2009; Fofie, Donahue, et al., 2017).

In figure 4.7, the complex aerosol mixtures formed are constrained by the component volume fractions. In fig. 4.7a, the organic aerosol fraction in BCSA remains relatively unchanged. The bulk of the secondary aerosol volume is from the nitrates.

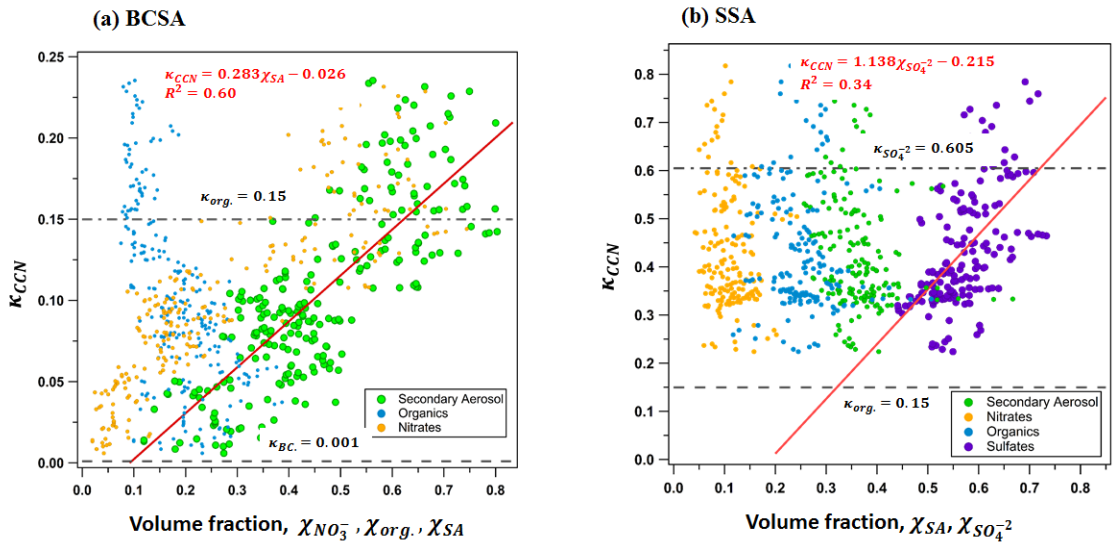

Figure 4.7. Effects of the aerosol volume fractions on the κ_{CCN} . Solid red line is the linear fit.

The BC fraction limits the supersaturated hygroscopicity, κ_{CCN} of the mixture when the secondary aerosol volume fraction $\chi_{SA} < 0.1$ of the total aerosol volume. Thereafter, the hygroscopicity increases linearly with increasing SA volume fraction ($\kappa_{CCN} = 0283_{\chi_{SA}} - 0.026, R^2 = 0.60$). When $\chi_{SA} = 0.6$, the κ_{CCN} is equivalent to that of secondary organic aerosol ($\kappa_{SOA} = 0.15$) although more than 0.4 of the χ_{SA} fraction is from the more soluble, hygroscopic nitrates. In fig. 4.7b, the sampled SSA aerosol showed unchanged SA volume fractions. The $(NH_4)_2SO_4$ fraction reduced with increasing formation and condensation of SA. The formation of nearly equi-volume

fractions of the components suggest homogenous, internally mixed aerosol. The hygroscopicity is higher than κ_{SOA} and $\kappa_{(NH_4)_2SO_4}$ but shows no distinct correlation between one fraction and hygroscopicity.

4.6 Summary and Implications

In this study we investigated the hygroscopicity and droplet kinetics of secondary aerosol (BCSA and SSA) formed from emissions of light-duty vehicles with new engine technology. BCSA was formed from the photo-oxidation of the whole soot wiles SSA was formed from GPF-filtered, $(NH_4)_2SO_4$ – seeded soot. The sub- and super-saturated hygroscopic activity is characterized with HTDMA and CCN counter respectively. The aerosol chemical composition, mixing states and morphology are constrained with information an AMS and APM-SMPS system. We found that aged soot from light duty vehicles are hygroscopic in supersaturated and subsaturated environments.

In supersaturated CCNc experiments, BCSA and SSA showed significant increase in hygroscopicity with photochemical aging (κ_{CCN} = 0.001 – 0.32 in BCSA and $\kappa_{CCN} = 0.55 - 0.25$ in SSA). In the BCSA, condensation of nitrates onto the BC core is driving the hygroscopicity. The CCN activity in BCSA increases incrementally with the formation of SA. *Tritscher et al* (2011) recently observed similar trends in hygroscopicity in aged diesel soot. The condensation of the SA fills the void in the non-spherical freshly emitted soot (Nakao et al., 2011), the BC fractions however limits the κ_{CCN} to levels less than the SA alone. This suggests a core-shell mixture with the SOA

condensing onto a BC core (Wittbom et al., 2014). In BCSA I, with relatively lower mass of SOA forming, the black carbon component drives the hygroscopicity. There is a strong closure between κ_{CCN} and κ_{AMS} ($S = 1.0418 \pm 0.0479$). In BCSA II however, there is weak closure between the κ_{CCN} and κ_{AMS} ($S = 1.9149 \pm 0.0926$). The formation of high amounts of organics and nitrates modified the effective density ($\rho_{eff} = 0.66 - 1.87$) and morphology of BCSA II significantly (King et al., 2009). This results in an over-estimated electrical mobility diameter, dp_{50} and under-prediction in κ_{CCN}. This core-shell assumption is buttressed by the sensitivity of κ_{CCN} to larger aerosol dry sizes which have a higher nitrate fraction in BCSA II.

In SSA, the presence of the more hygroscopic $(NH_4)_2SO_4$ core drives κ_{CCN} to levels higher than the SA. The continual condensation of SA onto the salt core depresses the hygroscopicity. The decrease in κ_{CCN} with SA formation, but not to levels equal to SA alone, indicates the likely formation of an internal mixture of SA + $(NH_4)_2SO_4$ as observed and inferred in previous ambient and laboratory data sets (Riemer et al., 2004; Adachi & Buseck, 2008). The internal mixture hypothesis is confirmed by the robust closure between the κ_{CCN} and the AMS-derived κ_{AMS} (SSA I $S = 1.0054 \pm 0.0234$, SSA II $S = 1.1328 \pm 0.0254$) which assumes the aerosol is internally mixed and homogenous bulk properties. Similar trends in hygroscopic behavior has been observed in laboratory studies of salt-seeded SOA experiments (Engelhart et al., 2008; King et al., 2009) and speciated ambient aerosol (Bougiatioti et al., 2009; Dusek et al., 2010; Pöschl et al., 2010; Asa-Awuku et al., 2011). In both ambient and laboratory studies, the presence of SA caused a decrease in the hygroscopicity and CCN activity. This is likely

attributed to depressions in the droplet surface tension, and to a lesser extent changes in morphology (density) and molar volume (King et al., 2009; Asa-Awuku et al., 2010; Ruehl et al., 2012).

In the sub-saturated HDTMA experiments, we observed similar dependence of the hygroscopicity, κ_{HTDMA} on the seed type and SA condensation. The SSA mixtures showed higher hygroscopicity than BCSA. Although there was a modification in κ_{HTDMA} with aging, the biggest driver of the hygroscopicity in the sub-saturated regime appears to be aerosol dry size. In BCSA, κ_{HTDMA} increased with experimental evolution and increasing peak diameter. The solubility of BCSA is minimal in HTDMA (with short residence time and low RH) (Chan & Chan, 2005). The hygroscopicity is therefore constrained by the relatively more soluble SA fraction. In SSA the condensing SA is less soluble than the $(NH_4)_2SO_4$ seed, the κ_{HTDMA} is therefore depressed at higher dry aerosol sizes which have higher SA volume fractions. This susceptibility of sub-saturated hygroscopicity in salt and SOA mixtures to volume fractions and dry size has previously been reported in ambient and laboratory data sets. Mixtures of $(NH_4)_2SO_4$ and SOA in chamber studies showed a decrease in hygroscopicity based on the volume fraction of the SOA and the level of oxidation similar to our observations (Smith et al., 2012). The hygroscopicity has also been shown to be dependent on aerosol dry size, especially in multicomponent systems (Laskina et al., 2015). The weak closure observed between the κ_{HTDMA} and κ_{CCN} supports these assertions. Absent the solubility influences, a stronger convergence between κ_{HTDMA} and κ_{CCN} is expected especially in more soluble, $(NH_4)_2SO_4$ –seeded SSA. We however observe similar $\kappa_{HTDMA}/\kappa_{CCN}$ for BCSA (0.10 –

0.42) and SSA (0.13 - 0.27) indicating a higher dependence of the sub-saturated hygroscopicity on the condensing SA fraction than on the seed.

In terms of the droplet kinetics, we do not observe a significant modification due to either the condensing gases or seed. The TDGA analysis shows comparable final droplet diameters between BCSA, SSA and $(NH_4)_2SO_4$. The presence of the insoluble, un-wettable BC, even that which is internally mixed, does not modify the droplet growth significantly. This suggests that, post-activation, the solubility of the aerosol does not have a significant influence on the condensational growth of the droplet. The presence of the organics and sulfates do not also modify the droplet kinetics significantly, unlike in previously reported ambient CCN measurements of aged urban combustion aerosol (Asa-Awuku, Engelhart, et al., 2009; Asa-Awuku et al., 2011). The SA formed does however seem to modify the surface activity of the aerosol mixture in the $(NH_4)_2SO_4$-seeded SSA particles. The presence of surface-active, surface tension depressing organic components would have modified the mass transfer of water (characterized by the mass accommodation coefficient) and hence the smaller final droplet sizes (Ruehl et al., 2008; Ruehl et al., 2012; Noziere, 2016; Ruehl et al., 2016). The absence of distinguishable differences in droplet kinetics does not however conclusively indicate similar droplet kinetics considering the high supersaturation of the CCN (Engelhart et al., 2008) and the bin width of the CCNc optical particle counter (Fofie, Castellucio, et al., 2017).

The results from this study suggests that emissions from newer technology GDI engines form CCN active SA upon photochemical aging. The integration of gasoline

particulate filters (which removes up to 90% of BC) will modify the hygroscopicity and CCN activity of the emissions based on the point of dispersion. In supersaturated urban environments where BC is abundant, the SA formed from GPF fitted GDI vehicles are more likely to condense onto BC and increase the hygroscopicity. In supersaturated rural regions, the SA will form mixtures (internal or external) with salts (nitrates, sulfates) and reduce the hygroscopicity of the new particle. In BC-core-shell mixtures, our results suggest that the hygroscopicity may be significantly inhibited by the less hygroscopic volume fraction. When the BC is removed however, hygroscopicity of the resulting internal mixtures are largely dependent on the most soluble, hygroscopic fraction (such as the cases where sulfates are dominant). It is therefore important to constrain the available seed chemical composition when modelling the effects of anthropogenic combustion vehicle emissions on cloud indirect effects. In the subsaturated environments however, the delinquency is only influenced by the SA coating making the point of emission dispersion unimportant to modeling cloud indirect effects.

4.7 Acknowlegdements

The authors would like to thank the United States National Science Foundation (NSF) and the University of California Transportation Research Fellowship for their support in this work. Specifically, the publication of this work was supported by the NSF grant 1151893. Its contents are solely the responsibility of the grantees and do not necessarily represent the official views of the NSF or UCTC. Further, the NSF does not

endorse the purchase of any commercial products or services mentioned in the publication.

4.8 Literature Cited

Adachi, K., & Buseck, P. R. (2008). Internally mixed soot, sulfates, and organic matter in aerosol particles from Mexico City. *Atmospheric Chemistry and Physics, 8*(21), 6469-6481. doi:10.5194/acp-8-6469-2008

Adachi, K., Chung, S. H., & Buseck, P. R. (2010). Shapes of soot aerosol particles and implications for their effects on climate. *Journal of Geophysical Research-Atmospheres, 115*(D15). doi:Artn D15206

10.1029/2009jd012868

Alfarra, M. R., Good, N., Wyche, K. P., Hamilton, J. E., Monks, P. S., Lewis, A. C., & McFiggans, G. (2013). Water uptake is independent of the inferred composition of secondary aerosols derived from multiple biogenic VOCs. *Atmospheric Chemistry and Physics, 13*(23), 11769-11789. doi:10.5194/acp-13-11769-2013

Andreae, M. O., & Rosenfeld, D. (2008). Aerosol-cloud-precipitation interactions. Part 1. The nature and sources of cloud-active aerosols. *Earth-Science Reviews, 89*(1-2), 13-41. doi:10.1016/j.earscirev.2008.03.001

Asa-Awuku, A., Engelhart, G. J., Lee, B. H., Pandis, S. N., & Nenes, A. (2009). Relating CCN activity, volatility, and droplet growth kinetics of beta-caryophyllene secondary organic aerosol. *Atmospheric Chemistry and Physics, 9*(3), 795-812.

Asa-Awuku, A., Miracolo, M. A., Kroll, J. H., Robinson, A. L., & Donahue, N. M. (2009). Mixing and phase partitioning of primary and secondary organic aerosols. *Geophysical Research Letters, 36*(15). doi:Artn L15827

10.1029/2009gl039301

Asa-Awuku, A., Moore, R. H., Nenes, A., Bahreini, R., Holloway, J. S., Brock, C. A., . . . Huey, L. G. (2011). Airborne cloud condensation nuclei measurements during the 2006 Texas Air Quality Study. *Journal of Geophysical Research-Atmospheres, 116*(D11). doi:Artn D11201

10.1029/2010jd014874

Asa-Awuku, A., Nenes, A., Gao, S., Flagan, R. C., & Seinfeld, J. H. (2010). Water-soluble SOA from Alkene ozonolysis: composition and droplet activation kinetics inferences from analysis of CCN activity. *Atmospheric Chemistry and Physics, 10*(4), 1585-1597.

Bond, T. C., Doherty, S. J., Fahey, D. W., Forster, P. M., Berntsen, T., DeAngelo, B. J., . . . Zender, C. S. (2013). Bounding the role of black carbon in the climate system: A scientific assessment. *Journal of Geophysical Research-Atmospheres, 118*(11), 5380-5552. doi:10.1002/jgrd.50171

Bougiatioti, A., Fountoukis, C., Kalivitis, N., Pandis, S. N., Nenes, A., & Mihalopoulos, N. (2009). Cloud condensation nuclei measurements in the marine boundary layer

of the eastern Mediterranean: CCN closure and droplet growth kinetics. *Atmospheric Chemistry and Physics, 9*(18), 7053-7066.

Canagaratna, M. R., Jayne, J. T., Jimenez, J. L., Allan, J. D., Alfarra, M. R., Zhang, Q., . . . Worsnop, D. R. (2007). Chemical and microphysical characterization of ambient aerosols with the aerodyne aerosol mass spectrometer. *Mass Spectrom Rev, 26*(2), 185-222. doi:10.1002/mas.20115

Cappa, C. D., Onasch, T. B., Massoli, P., Worsnop, D. R., Bates, T. S., Cross, E. S., . . . Zaveri, R. A. (2012). Radiative Absorption Enhancements Due to the Mixing State of Atmospheric Black Carbon. *Science, 337*(6098), 1078-1081. doi:10.1126/science.1223447

Chan, M., & Chan, C. K. (2005). Mass transfer effects in hygroscopic measurements of aerosol particles. *Atmospheric Chemistry and Physics, 5*(10), 2703-2712.

Chan, M. N., & Chan, C. K. (2007). Mass transfer effects on the hygroscopic growth of ammonium sulfate particles with a water-insoluble coating. *Atmospheric Environment, 41*(21), 4423-4433. doi:10.1016/j.atmosenv.2007.01.047

Chan, T. W., Meloche, E., Kubsh, J., & Brezny, R. (2014). Black carbon emissions in gasoline exhaust and a reduction alternative with a gasoline particulate filter. *Environ Sci Technol, 48*(10), 6027-6034. doi:10.1021/es501791b

Chan, T. W., Meloche, E., Kubsh, J., Rosenblatt, D., Brezny, R., & Rideout, G. (2012). Evaluation of a gasoline particulate filter to reduce particle emissions from a gasoline direct injection vehicle. *SAE International Journal of Fuels and Lubricants, 5*(2012-01-1727), 1277-1290.

Chang, R. Y. W., Slowik, J. G., Shantz, N. C., Vlasenko, A., Liggio, J., Sjostedt, S. J., . . . Abbatt, J. P. D. (2010). The hygroscopicity parameter (kappa) of ambient organic aerosol at a field site subject to biogenic and anthropogenic influences: relationship to degree of aerosol oxidation. *Atmospheric Chemistry and Physics, 10*(11), 5047-5064. doi:10.5194/acp-10-5047-2010

Chirico, R., DeCarlo, P., Heringa, M., Tritscher, T., Richter, R., Prévôt, A., . . . Gysel, M. (2010). Impact of aftertreatment devices on primary emissions and secondary organic aerosol formation potential from in-use diesel vehicles: results from smog chamber experiments. *Atmospheric Chemistry and Physics, 10*(23), 11545.

Cocker, D. R., 3rd, Flagan, R. C., & Seinfeld, J. H. (2001). State-of-the-art chamber facility for studying atmospheric aerosol chemistry. *Environ Sci Technol, 35*(12), 2594-2601.

Cubison, M., Ervens, B., Feingold, G., Docherty, K., Ulbrich, I., Shields, L., . . . Jimenez, J. (2008). The influence of chemical composition and mixing state of Los Angeles urban aerosol on CCN number and cloud properties. *Atmospheric Chemistry and Physics, 8*(18), 5649-5667.

DeCarlo, P. F., Slowik, J. G., Worsnop, D. R., Davidovits, P., & Jimenez, J. L. (2004). Particle morphology and density characterization by combined mobility and aerodynamic diameter measurements. Part 1: Theory. *Aerosol Science and Technology, 38*(12), 1185-1205. doi:10.1080/027868290903907

Duplissy, J., DeCarlo, P. F., Dommen, J., Alfarra, M. R., Metzger, A., Barmpadimos, I., . . . Baltensperger, U. (2011). Relating hygroscopicity and composition of organic aerosol particulate matter. *Atmospheric Chemistry and Physics, 11*(3), 1155-1165. doi:10.5194/acp-11-1155-2011

Dusek, U., Frank, G., Curtius, J., Drewnick, F., Schneider, J., Kürten, A., . . . Pöschl, U. (2010). Enhanced organic mass fraction and decreased hygroscopicity of cloud condensation nuclei (CCN) during new particle formation events. *Geophysical Research Letters, 37*(3).

Dusek, U., Frank, G., Massling, A., Zeromskiene, K., Iinuma, Y., Schmid, O., . . . Andreae, M. (2011). Water uptake by biomass burning aerosol at sub-and supersaturated conditions: closure studies and implications for the role of organics. *Atmospheric Chemistry and Physics, 11*(18), 9519-9532.

Dusek, U., Frank, G. P., Hildebrandt, L., Curtius, J., Schneider, J., Walter, S., . . . Andreae, M. O. (2006). Size matters more than chemistry for cloud-nucleating ability of aerosol particles. *Science, 312*(5778), 1375-1378. doi:10.1126/science.1125261

Ellies, B., Schenk, C., & Dekraker, P. (2016). *Benchmarking and Hardware-in-the-Loop Operation of a 2014 MAZDA SkyActiv 2.0 L 13: 1 Compression Ratio Engine* (0148-7191). Retrieved from

Engelhart, G., Asa-Awuku, A., Nenes, A., & Pandis, S. (2008). CCN activity and droplet growth kinetics of fresh and aged monoterpene secondary organic aerosol. *Atmospheric Chemistry and Physics, 8*(14), 3937-3949.

Engelhart, G. J., Moore, R. H., Nenes, A., & Pandis, S. N. (2011). Cloud condensation nuclei activity of isoprene secondary organic aerosol. *Journal of Geophysical Research: Atmospheres, 116*(D2).

EPA. (2012). 2017 and later model year light-duty vehicle greenhouse gas emissions and corporate average fuel economy standards; final rule. *Federal Register, 77*(199), 62623-63200.

Fofie, E. A., Castellucio, V., & Asa-Awuku, A. (2017). Exploring CCN droplet kinetics with a higher sensitivity optical particle counter *Aerosol Sci Technol, in review*.

Fofie, E. A., Donahue, N. M., & Asa-Awuku, A. (2017). Cloud condensation nuclei activity and droplet formation of primary and secondary organic aerosol mixtures *Aerosol Sci Technol, under review*

Frosch, M., Bilde, M., DeCarlo, P., Juranyi, Z., Tritscher, T., Dommen, J., . . . Baltensperger, U. (2011). Relating cloud condensation nuclei activity and oxidation level of α-pinene secondary organic aerosols. *Journal of Geophysical Research: Atmospheres, 116*(D22).

Giordano, M., Espinoza, C., & Asa-Awuku, A. (2015). Experimentally measured morphology of biomass burning aerosol and its impacts on CCN ability. *Atmospheric Chemistry and Physics, 15*(4), 1807-1821. doi:10.5194/acp-15-1807-2015

Giordano, M. R., Chong, J., Weise, D. R., & Asa-Awuku, A. A. (2016). Does chronic nitrogen deposition during biomass growth affect atmospheric emissions from biomass burning? *Environmental Research Letters, 11*(3), 034007.

Gunthe, S., King, S., Rose, D., Chen, Q., Roldin, P., Farmer, D., . . . Martin, S. (2009). Cloud condensation nuclei in pristine tropical rainforest air of Amazonia: size-resolved measurements and modeling of atmospheric aerosol composition and CCN activity. *Atmospheric Chemistry and Physics, 9*(19), 7551-7575.

Gysel, M., McFiggans, G., & Coe, H. (2009). Inversion of tandem differential mobility analyser (TDMA) measurements. *Journal of Aerosol Science, 40*(2), 134-151.

Huff Hartz, K. E., Rosenørn, T., Ferchak, S. R., Raymond, T. M., Bilde, M., Donahue, N. M., & Pandis, S. N. (2005). Cloud condensation nuclei activation of monoterpene and sesquiterpene secondary organic aerosol. *Journal of Geophysical Research: Atmospheres, 110*(D14).

Hula, A., Bunker, A., & Alson, J. (2015). *Light-Duty Automotive Technology, Carbon Dioxide Emissions, and Fuel Economy Trends: 1975 Through 2015*. Retrieved from

Iwamoto, Y., Noma, K., Nakayama, O., Yamauchi, T., & Ando, H. (1997). *Development of gasoline direct injection engine* (0148-7191). Retrieved from

Jacobson, M. Z. (2001). Strong radiative heating due to the mixing state of black carbon in atmospheric aerosols. *Nature, 409*(6821), 695-697.

Jimenez, J., Canagaratna, M., Donahue, N., Prevot, A., Zhang, Q., Kroll, J. H., . . . Ng, N. (2009). Evolution of organic aerosols in the atmosphere. *Science, 326*(5959), 1525-1529.

Karavalakis, G., Short, D., Vu, D., Villela, M., Asa-Awuku, A., & Durbin, T. D. (2014). Evaluating the regulated emissions, air toxics, ultrafine particles, and black carbon from SI-PFI and SI-DI vehicles operating on different ethanol and iso-butanol blends. *Fuel, 128*, 410-421. doi:10.1016/j.fuel.2014.03.016

Khalizov, A. F., Lin, Y., Qiu, C., Guo, S., Collins, D., & Zhang, R. (2013). Role of OH-initiated oxidation of isoprene in aging of combustion soot. *Environmental science & technology, 47*(5), 2254-2263.

Khvorostyanov, V. I., & Curry, J. A. (2007). Refinements to the Köhler's theory of aerosol equilibrium radii, size spectra, and droplet activation: Effects of humidity and insoluble fraction. *Journal of Geophysical Research: Atmospheres, 112*(D5).

King, S. M., Rosenoern, T., Shilling, J. E., Chen, Q., & Martin, S. T. (2009). Increased cloud activation potential of secondary organic aerosol for atmospheric mass loadings. *Atmospheric Chemistry and Physics, 9*(9), 2959-2971.

Köhler, H. (1936). The nucleus in and the growth of hygroscopic droplets. *Transactions of the Faraday Society, 32*, 1152-1161.

Kreidenweis, S., & Asa-Awuku, A. (2014). 5.13-Aerosol hygroscopicity: Particle water content and its role in atmospheric processes.

Lamarque, J. F., Bond, T. C., Eyring, V., Granier, C., Heil, A., Klimont, Z., . . . Owen, B. (2010). Historical (1850–2000) gridded anthropogenic and biomass burning emissions of reactive gases and aerosols: methodology and application. *Atmospheric Chemistry and Physics, 10*(15), 7017-7039.

Lance, S., Nenes, A., Mazzoleni, C., Dubey, M. K., Gates, H., Varutbangkul, V., . . . Flagan, R. C. (2009). Cloud condensation nuclei activity, closure, and droplet growth kinetics of Houston aerosol during the Gulf of Mexico Atmospheric Composition and Climate Study (GoMACCS). *Journal of Geophysical Research: Atmospheres, 114*(D7).

Lance, S., Nenes, A., Medina, J., & Smith, J. N. (2006). Mapping the Operation of the DMT Continuous Flow CCN Counter. *Aerosol Science and Technology, 40*(4), 242-254. doi:10.1080/02786820500543290

Lance, S., Raatikainen, T., Onasch, T. B., Worsnop, D. R., Yu, X.-Y., Alexander, M., . . . Nenes, A. (2013). Aerosol mixing state, hygroscopic growth and cloud activation

efficiency during MIRAGE 2006. *Atmospheric Chemistry and Physics, 13*(9), 5049-5062.

Laskina, O., Morris, H. S., Grandquist, J. R., Qin, Z., Stone, E. A., Tivanski, A. V., & Grassian, V. H. (2015). Size matters in the water uptake and hygroscopic growth of atmospherically relevant multicomponent aerosol particles. *The Journal of Physical Chemistry A, 119*(19), 4489-4497.

Lathem, T. L., & Nenes, A. (2011). Water Vapor Depletion in the DMT Continuous-Flow CCN Chamber: Effects on Supersaturation and Droplet Growth. *Aerosol Science and Technology, 45*(5), 604-615. doi:10.1080/02786826.2010.551146

Ma, X., Zangmeister, C. D., Gigault, J., Mulholland, G. W., & Zachariah, M. R. (2013). Soot aggregate restructuring during water processing. *Journal of Aerosol Science, 66*, 209-219.

Malloy, Q. G., Nakao, S., Qi, L., Austin, R., Stothers, C., Hagino, H., & Cocker III, D. R. (2009). Real-time aerosol density determination utilizing a modified scanning mobility particle sizer—aerosol particle mass analyzer system. *Aerosol Science and Technology, 43*(7), 673-678.

Maricq, M. M., Szente, J. J., & Jahr, K. (2012). The impact of ethanol fuel blends on PM emissions from a light-duty GDI vehicle. *Aerosol Science and Technology, 46*(5), 576-583.

Massoli, P., Lambe, A., Ahern, A., Williams, L., Ehn, M., Mikkilä, J., . . . Jayne, J. (2010). Relationship between aerosol oxidation level and hygroscopic properties of laboratory generated secondary organic aerosol (SOA) particles. *Geophysical Research Letters, 37*(24).

Mikhailov, E., Vlasenko, S., Martin, S., Koop, T., & Pöschl, U. (2009). Amorphous and crystalline aerosol particles interacting with water vapor: conceptual framework and experimental evidence for restructuring, phase transitions and kinetic limitations. *Atmospheric Chemistry and Physics, 9*(24), 9491-9522.

Modini, R. L., Johnson, G. R., He, C., & Ristovski, Z. D. (2010). Observation of the suppression of water uptake by marine particles. *Atmospheric Research, 98*(2), 219-228.

Moffet, R. C., & Prather, K. A. (2009). In-situ measurements of the mixing state and optical properties of soot with implications for radiative forcing estimates. *Proceedings of the National Academy of Sciences, 106*(29), 11872-11877.

Moore, R. H., Nenes, A., & Medina, J. (2010). Scanning Mobility CCN Analysis—A Method for Fast Measurements of Size-Resolved CCN Distributions and

Activation Kinetics. *Aerosol Science and Technology, 44*(10), 861-871. doi:10.1080/02786826.2010.498715

Nakao, S., Shrivastava, M., Nguyen, A., Jung, H., & Cocker III, D. (2011). Interpretation of secondary organic aerosol formation from diesel exhaust photooxidation in an environmental chamber. *Aerosol Science and Technology, 45*(8), 964-972.

Noziere, B. (2016). Don't forget the surface. *Science, 351*(6280), 1396-1397.

Padró, L. T., Tkacik, D., Lathem, T., Hennigan, C. J., Sullivan, A. P., Weber, R. J., . . . Nenes, A. (2010). Investigation of cloud condensation nuclei properties and droplet growth kinetics of the water-soluble aerosol fraction in Mexico City. *Journal of Geophysical Research: Atmospheres, 115*(D9).

Petters, M. D., Carrico, C. M., Kreidenweis, S. M., Prenni, A. J., DeMott, P. J., Collett, J. L., & Moosmueller, H. (2009). Cloud condensation nucleation activity of biomass burning aerosol. *Journal of Geophysical Research: Atmospheres, 114*(D22).

Petters, M. D., & Kreidenweis, S. M. (2007). A single parameter representation of hygroscopic growth and cloud condensation nucleus activity. *Atmospheric Chemistry and Physics, 7*(8), 1961-1971.

Petters, M. D., & Kreidenweis, S. M. (2008). A single parameter representation of hygroscopic growth and cloud condensation nucleus activity–Part 2: Including solubility. *Atmospheric Chemistry and Physics, 8*(20), 6273-6279.

Piock, W., Hoffmann, G., Berndorfer, A., Salemi, P., & Fusshoeller, B. (2011). Strategies towards meeting future particulate matter emission requirements in homogeneous gasoline direct injection engines. *SAE International Journal of Engines, 4*(2011-01-1212), 1455-1468.

Pöschl, U., Martin, S., Sinha, B., Chen, Q., Gunthe, S., Huffman, J., . . . Helas, G. (2010). Rainforest aerosols as biogenic nuclei of clouds and precipitation in the Amazon. *Science, 329*(5998), 1513-1516.

Prenni, A. J., DeMott, P. J., Kreidenweis, S. M., Sherman, D. E., Russell, L. M., & Ming, Y. (2001). The effects of low molecular weight dicarboxylic acids on cloud formation. *The Journal of Physical Chemistry A, 105*(50), 11240-11248.

Prenni, A. J., Petters, M. D., Kreidenweis, S. M., DeMott, P. J., & Ziemann, P. J. (2007). Cloud droplet activation of secondary organic aerosol. *Journal of Geophysical Research: Atmospheres, 112*(D10).

Presto, A., Gordon, T., & Robinson, A. (2014). Primary to secondary organic aerosol: evolution of organic emissions from mobile combustion sources. *Atmospheric Chemistry and Physics, 14*(10), 5015-5036.

Pruppacher, H., & Klett, J. (1997). Microphysics of Clouds and Precipitation: With an Introduction to Cloud Chemistry and Cloud Electricity, 954 pp: Springer, New York

Qi, L., Nakao, S., Tang, P., & Cocker III, D. (2010). Temperature effect on physical and chemical properties of secondary organic aerosol from m-xylene photooxidation. *Atmospheric Chemistry and Physics, 10*(8), 3847-3854.

Rader, D., & McMurry, P. (1986). Application of the tandem differential mobility analyzer to studies of droplet growth or evaporation. *Journal of Aerosol Science, 17*(5), 771-787.

Ramanathan, V., & Carmichael, G. (2008). Global and regional climate changes due to black carbon. *Nature geoscience, 1*(4), 221-227.

Riemer, N., Vogel, H., & Vogel, B. (2004). Soot aging time scales in polluted regions during day and night. *Atmospheric Chemistry and Physics, 4*(7), 1885-1893.

Riipinen, I., Rastak, N., & Pandis, S. (2015). Connecting the solubility and CCN activation of complex organic aerosols: a theoretical study using solubility distributions. *Atmospheric Chemistry and Physics, 15*(11), 6305-6322.

Rissler, J., Messing, M. E., Malik, A. I., Nilsson, P. T., Nordin, E. Z., Bohgard, M., . . . Pagels, J. H. (2013). Effective density characterization of soot agglomerates from various sources and comparison to aggregation theory. *Aerosol Science and Technology, 47*(7), 792-805.

Robinson, E. S., Donahue, N. M., Ahern, A. T., Ye, Q., & Lipsky, E. (2016). Single-particle measurements of phase partitioning between primary and secondary organic aerosols. *Faraday discussions*.

Rose, D., Gunthe, S. S., Mikhailov, E., Frank, G. P., Dusek, U., Andreae, M. O., & Pöschl, U. (2008). Calibration and measurement uncertainties of a continuous-flow cloud condensation nuclei counter (DMT-CCNC): CCN activation of ammonium sulfate and sodium chloride aerosol particles in theory and experiment. *Atmospheric Chemistry and Physics, 8*(5), 1153-1179.

Ruehl, C., Chuang, P., Nenes, A., Cappa, C., Kolesar, K., & Goldstein, A. (2012). Strong evidence of surface tension reduction in microscopic aqueous droplets. *Geophysical Research Letters, 39*(23).

Ruehl, C. R., Chuang, P. Y., & Nenes, A. (2008). How quickly do cloud droplets form on atmospheric particles? *Atmospheric Chemistry and Physics, 8*(4), 1043-1055.

Ruehl, C. R., Davies, J. F., & Wilson, K. R. (2016). An interfacial mechanism for cloud droplet formation on organic aerosols. *Science, 351*(6280), 1447-1450. doi:10.1126/science.aad4889

10.1126/science.aad4889.

Sasser, E., Hemby, J., Adler, K., Anenberg, S., Bailey, C., Brockman, L., . . . Dawson, J. (2012). Report to Congress on Black Carbon. *Department of the Interior, Environment, and Related Agencies*.

Schwarz, J. P., Gao, R. S., Fahey, D. W., Thomson, D. S., Watts, L. A., Wilson, J. C., . . . Aikin, K. C. (2006). Single-particle measurements of midlatitude black carbon and light-scattering aerosols from the boundary layer to the lower stratosphere. *Journal of Geophysical Research, 111*(D16). doi:10.1029/2006jd007076

Seinfeld, J. H., & Pandis, S. N. (2006). Atmospheric Chemistry and Physics, A Wiley-Inter Science Publication: John Wiley & Sons Inc, New York

Shantz, N., Chang, R.-W., Slowik, J., Vlasenko, A., Abbatt, J., & Leaitch, W. (2010). Slower CCN growth kinetics of anthropogenic aerosol compared to biogenic aerosol observed at a rural site. *Atmospheric Chemistry and Physics, 10*(1), 299-312.

Smith, M., Bertram, A., & Martin, S. (2012). Deliquescence, efflorescence, and phase miscibility of mixed particles of ammonium sulfate and isoprene-derived secondary organic material. *Atmospheric Chemistry and Physics, 12*(20), 9613-9628.

Spracklen, D., Carslaw, K., Pöschl, U., Rap, A., & Forster, P. (2011). Global cloud condensation nuclei influenced by carbonaceous combustion aerosol. *Atmospheric Chemistry and Physics, 11*(17), 9067-9087.

Suda, S. R., Petters, M., Matsunaga, A., Sullivan, R., Ziemann, P., & Kreidenweis, S. (2012). Hygroscopicity frequency distributions of secondary organic aerosols. *Journal of Geophysical Research: Atmospheres, 117*(D4).

Tritscher, T., Jurányi, Z., Martin, M., Chirico, R., Gysel, M., Heringa, M. F., . . . Weingartner, E. (2011). Changes of hygroscopicity and morphology during ageing of diesel soot. *Environmental Research Letters, 6*(3), 034026.

Vaden, T. D., Song, C., Zaveri, R. A., Imre, D., & Zelenyuk, A. (2010). Morphology of mixed primary and secondary organic particles and the adsorption of spectator

organic gases during aerosol formation. *Proceedings of the National Academy of Sciences, 107*(15), 6658-6663.

Vu, D., Short, D., Karavalakis, G., Durbin, T., & Asa-Awuku, A. (2015). Integrating Cloud Condensation Nuclei Predictions with Fast Time Resolved Aerosol Instrumentation to Determine the Hygroscopic Properties of Emissions Over Transient Drive Cycles. *Aerosol Science and Technology, 49*(11), 1149-1159.

Vu, D., Short, D. Z., Karavalakis, G., Durbin, T. D., & Asa-Awuku, A. (2017). Will Aerosol Hygroscopicity Change with Biodiesel, Renewable Diesel Fuels and Emission Control Technologies? *Environmental science & technology*.

Wang, C., Xu, H., Herreros, J. M., Wang, J., & Cracknell, R. (2014). Impact of fuel and injection system on particle emissions from a GDI engine. *Applied Energy, 132*, 178-191.

Wang, J., Cubison, M., Aiken, A., Jimenez, J., & Collins, D. (2010). The importance of aerosol mixing state and size-resolved composition on CCN concentration and the variation of the importance with atmospheric aging of aerosols. *Atmospheric Chemistry and Physics, 10*(15), 7267-7283.

Whitaker, P., Kapus, P., Ogris, M., & Hollerer, P. (2011). Measures to reduce particulate emissions from gasoline DI engines. *SAE International Journal of Engines, 4*(2011-01-1219), 1498-1512.

Whitehead, J., Irwin, M., Allan, J., Good, N., & McFiggans, G. (2014). A meta-analysis of particle water uptake reconciliation studies. *Atmospheric Chemistry and Physics, 14*(21), 11833-11841.

Wittbom, C., Eriksson, A., Rissler, J., Carlsson, J., Roldin, P., Nordin, E., . . . Svenningsson, B. (2014). Cloud droplet activity changes of soot aerosol upon smog chamber ageing. *Atmospheric Chemistry and Physics, 14*(18), 9831-9854.

Xing, J., Pleim, J., Mathur, R., Pouliot, G., Hogrefe, C., Gan, C.-M., & Wei, C. (2013). Historical gaseous and primary aerosol emissions in the United States from 1990 to 2010. *Atmospheric Chemistry and Physics, 13*(15), 7531-7549.

Yi, J., Wooldridge, S., Coulson, G., Hilditch, J., Iyer, C. O., Moilanen, P., . . . VanDerWege, B. (2009). Development and optimization of the Ford 3.5 L V6 EcoBoost combustion system. *SAE International Journal of Engines, 2*(2009-01-1494), 1388-1407.

Zaveri, R. A., Barnard, J. C., Easter, R. C., Riemer, N., & West, M. (2010). Particle-resolved simulation of aerosol size, composition, mixing state, and the associated

optical and cloud condensation nuclei activation properties in an evolving urban plume. *Journal of Geophysical Research: Atmospheres, 115*(D17).

Zhang, J., Fan, X., Graham, L., Chan, T. W., & Brook, J. R. (2012). Evaluation of an annular denuder system for carbonaceous aerosol sampling of diesel engine emissions. *http://dx.doi.org/10.1080/10962247.2012.739582*. doi:J. Air & Waste Manage. Assoc., Vol. 63, No. 1, January 2013: pp. 87–99

Zhao, D., Buchholz, A., Kortner, B., Schlag, P., Rubach, F., Fuchs, H., . . . Watne, Å. (2016). Cloud condensation nuclei activity, droplet growth kinetics, and hygroscopicity of biogenic and anthropogenic secondary organic aerosol (SOA). *Atmospheric Chemistry and Physics, 16*(2), 1105-1121.

CHAPTER 5:MODIFICATIONS IN DROPLET KINETICS BY AMBIENT GASES

5.1 Introduction

The earth's radiation budget is modified by clouds. This is the cloud indirect effect and has a net cooling effect on the atmosphere (Haywood & Boucher, 2000; Bauer & Menon, 2012). Aerosols are the seeds on which water vapor condenses to form cloud droplets. When aerosol is exposed to a water vapor supersaturation higher than the critical supersaturations it activates into cloud droplets and is called cloud condensation nuclei (CCN) (Twomey, 1963; Seinfeld & Pandis, 2016). The activation of aerosol into CCN depends primarily on the dry aerosol dry size, chemistry and mixing state (Dusek et al., 2006; McFiggans et al., 2006; Cubison et al., 2008). Aerosol, especially secondary organic aerosol, exhibit various degrees of volatility and coexist with gas phase components (An et al., 2007; Lane et al., 2008). Gas phase components may be condensable or inert. Condensable semi-volatile organic vapours have been shown to enhance CCN concentrations through co-condensation (Topping et al., 2013; Connolly et al., 2014). In non-organic gases, such as ammonium nitrate, ammonia and nitric acid, laboratory and modelling studies suggest that at high concentrations these gases can enhance the CCN activity of even non-volatile aerosol and increases the CCN density (Kulmala et al., 1993; Hegg, 2000; Romakkaniemi et al., 2014).

In the atmosphere, volcanic eruptions are one of the common source of both condensable and non-condensable gases. During volcanic eruptions, aerosol (mainly ash and sulfate) is co-emitted with a diverse soup of gases (Andersson et al., 2013; Mills et al., 2016). The co-emitted gases include methane, nitrates, hydrogen, nitrogen, helium, argon and carbon dioxide (Giggenbach & Matsuo, 1991; Fedele et al., 2017; Shinohara et al., 2017). Volcanoes, be it active or passive, contribute to the uncertainty in estimating aerosol indirect effects. Efforts at estimating the CCN activity of volcanic aerosol involves the use of extracted satellites data (Ebmeier et al., 2014; McCoy & Hartmann, 2015) and ground based measurements of plumes near passive volcanoes (Martin et al., 2008). The presence of high amount of these gases may modify the droplet kinetics in addition to the CCN activity by modifying the mass accommodation coefficient (Ruehl et al., 2008; Ruehl et al., 2016). In evaluating the CCN contributions from volcanoes the effects of these co-emitted gases are rarely explicitly constrained.

To gain a greater understanding of the influence of gas-rich systems, such as during volcanoes, on cloud indirect effects it is important to constrain, in addition to the CCN activity, the droplet kinetics of such systems. Does the presence of these gases influence the final droplet sizes of the CCN formed? In this study we couple laboratory studies with a scaling analysis of the droplet growth equations to explore the influence of gases on the CCN droplet kinetics. We use a DMT Inc. cloud condensation nuclei counter (CCNc) to measure the CCN activity and final droplet sizes of ammonium sulfate aerosol in the presence of excess argon and carbon dioxide.

5.2 Theory and Scaling Analysis

Aerosol with a dry size, d_s will activate into CCN when exposed to a supersaturation, S greater than the critical supersaturation, S_c (Köhler, 1936). The thermodynamic relationships between the aerosol dry size, chemical properties and activation supersaturation is succinctly expressed by Köhler Theory. Köhler Theory can be defined as (Seinfeld & Pandis, 2006):

$$ln\, S_c = \left(\frac{4A^3\rho_w M_s}{27v\rho_s M_w d_s^3}\right)^{\frac{1}{2}} \qquad [\mathbf{5.1}]$$

Where A incorporates the Kelvin effects due to the curvature of the aerosol, ρ_s and ρ_w are the densities of the aerosol and water vapor, respectively. M_s and M_w are the molecular weights of the aerosol and water vapor, respectively. v is the molar volume. This thermodynamic relationship between aerosol dry sizes and the supersaturation is parametrized by a single parameter κ-hygroscopicity (Petters & Kreidenweis, 2007):

After activation, the droplet will continue to absorb water vapor by condensation so far as it is exposed to S_c. The growth of the droplet can be estimated from the diffusional growth equation (Roberts & Nenes, 2005; Seinfeld & Pandis, 2006):

$$D_p\frac{dD_p}{dt} = \frac{\left(S - S_R^{eq}\right)}{\frac{\rho_w R_g T}{4P_{H_2O}^o D_v' M_w} + \frac{\Delta H_v \rho_w}{4\kappa_a' T}\left(\frac{\Delta H_v \rho_w}{T R_g} - 1\right)} \qquad [5.2]$$

Where D_p is the droplet diameter, S is the local supersaturation, S_R^{eq} is the droplet equilibrium supersaturation, D_v' and κ_a' is the diffusivity of water vapor in air and thermal conductivity of air, respectively, both modified for non-continuum effects. R_g is the universal gas constant, T is temperature in Kelvin , ΔH_v is the enthalpy of evaporation of water. $P_{H_2O}^o$ is the equilibrium vapor pressure. The correction for non-continuum effects are necessary due to the very small diameter of the activating droplets (Fukuta & Walter, 1970). The corrected thermal conductivity coefficient, κ_a' is expressed as:

$$\kappa_a' = \frac{\kappa_a}{1 + \frac{2\kappa_a}{\alpha_T D_p \rho_a c_p}\sqrt{\frac{2\pi M_a}{R_g T}}} \quad [5.3]$$

Where κ_a is the thermal conductivity of air, M_a is the mean molar mass of air, c_p is the heat capacity of air, and α_T is the thermal accommodation coefficient. The diffusivity corrected by the mass accommodation coefficient is defined:

$$D_v' = \frac{D_v}{1 + \frac{2D_v}{\alpha D_p}\sqrt{\frac{2\pi M_w}{R_g T}}} \quad [5.4]$$

Where D_v is the diffusivity of water vapor in air, and α is the mass accommodation coefficient. The binary diffusivity coefficient D_v can be estimated from Chapman-Enskog theory (Chapman & Cowling, 1970; Brush, 2013):

$$D_v = \frac{0.00186T^{\frac{3}{2}}}{p\sigma_{ij}^2\Omega}\left(\frac{1}{M_i}+\frac{1}{M_j}\right)^{1/2} \quad [5.5]$$

Where p is the pressure in atmosphere, M_{ij} are molecular weights of the air and water vapor. The quantities Ω and σ are molecular property characteristics of the gas (Hirschfelder & Curtiss, 1954). σ is the collision diameter whiles Ω is a dimensionless quantity typically on the order of 1.

If the gas surrounding the aerosol is modified with an excess of another gas of significantly divergent molecular weight, the heat and mass transfer regime may change. The molecular interactions during CCN activation and droplet growth in the CCN counter is assumed to be between water vapor and air (volumetric air composition; 21% O_2, 78% N_2, 0.93% Ar, 0.03% CO_2, and the remaining fraction made of H_2, Ne, He, Kr, Xe). Thus the molecular diffusional and heat transfer regimes may change when the working gas is changed (Roberts & Nenes, 2005). The equilibrium water vapor supersaturation and hence droplet growth will be modified. From equation [5], with all other conditions being the same, the change from air to another gas will be constrained by the molecular weight of the gases. Due to changes in the relative molecular velocities with the introduction of other gases, the changes in supersaturation will be more dependent on modifications in mass transfer. This is characterized by the molecular diffusivity of water vapor in the gas, D_v' (Lance et al., 2006). A relative change, ΔS_{gas}in the water vapor supersaturation, S due to a change in the gas medium from air to another gas can therefore be estimated by:

$$\Delta S_{gas} \approx \left(\frac{M_j}{M_{air}}\right)^{\frac{1}{2}} \quad [5.6]$$

Where ΔS_{gas} is the change in supersaturation, *S* due to the introduction of another gas *j* with molecular weight M_j. Equation [5.4] assumes any changes in the supersaturation are due to the mass transfer alone.

From Köhler Theory (equation [5.1]) a critical diameter d_s can be estimated for each supersaturation. By default equation [5.1] uses air as the medium for CCN activation. If we modify the gas medium from air, an apparent critical diameter, d_s' will be measured by the cloud condensation nuclei counter. If no changes in the condensate, water vapor, and the aerosol is made then the difference in the supersaturation due to the gas can be expressed as:

$$\Delta S_{d_s'} \approx \left(\frac{d_s'}{d_s}\right)^{\frac{3}{2}} \quad [5.7]$$

Where $\Delta S_{d_s'}$ is the change in the supersaturation, *S* due to the presence of an excess gas. Here we assume that changes in the supersaturation can be attributed to mass transfer alone. If this is true, then equation [5.5] and [5.6] are equivalent. Here, we also assume negligible effects of the gas on heat transfer (comparable specific heat capacities). Heat transfer effects on the supersaturation due to change in the gas medium is therefore assumed negligible. Assuming negligible changes in heat transfer suggests that droplet growth (in equation [5.2]) will be affected by only the changes in the

diffusivity. The change in the gas medium from air may only not affect the diffusivity but also the non-continuum correction factor, α. The changes in the gas medium may therefore affect the droplet kinetics and final droplet sizes beyond the changes in the supersaturation.

5.3 Experimental Methods

Aerosol activation and droplet growth experiments were done with DMT Inc. cloud condensation nuclei counter (CCNc) coupled with a TSI Inc. scanning mobility particle sizer (SMPS) system. The SMPS consists of a differential mobility analyzer (DMA 3081) and a condensation particle counter (CPC 2776). The SMPS uses electrical mobility to classify the dry aerosol size and also provides dry aerosol concentration information (Wang & Flagan, 1990). The CCNc measures droplet size and concentration. A solution of $(NH_4)_2SO_4$ was aerosolized using a home-built constant flow Collison atomizer and dried. The dry aerosol is injected into a 1 m^3 fluorinated ethylene propylene film reactor. Excess gas, argon and carbon dioxide, was injected into the reactor such that the air to gas ratio is 1:9. The air to gas to air ratio is estimated from the initial assumed volumetric fraction of air and the volume of additional inert gas added.

The size distribution of $(NH_4)_2SO_4$ aerosol in excess argon was scanned by the SMPS and the dry aerosol exposed to a supersaturation (0.2 – 0.6%) at an instrument flowrate of 0.5 lpm. The dry aerosol data from the SMPS and the CCN spectrum data is synchronized and inverted with Scanning Mobility CCN Analysis (SCMA) algorithm (Moore et al., 2010). SMCA estimates a critical diameter, d_s beyond which more than

half the dry aerosol will activate into droplets ($\frac{CCN}{CN} \geq 0.5$) at a set instrument supersaturation, *S*. The instrument set *S* is corrected with calibration data and reported as S_c (*see Table B*-1). The reported S_c is derived from extended Köhler Theory and uses temperature modified surface tension corrections based on Pitzer dissolution correlations in water (Pruppacher & Klett, 1997; Seinfeld & Pandis, 2006). Thus changes in the gas phase are assumed to have no or little effect on the dissolution in the water phase. It should be stated that these calibrations are similar to the protocol suggested by *Rose et al*.(Rose et al., 2008).

In the Argon + $(NH_4)_2SO_4$ experiment, the dry diameter at the apparent aerosol critical supersaturation is the apparent critical dry diameter, d_s'. The apparent critical dry diameter, d_s' and the critical diameter, d_s from a standard calibration experiment (in which air is the gas medium) is used together with equation [6] to estimate the change in supersaturation due to the change in the critical diameter, $\Delta S_{d_s'}$. The average droplet sizes, D_p at each supersaturation exiting the CCNc optical particle counter are evaluated using threshold droplet growth analysis (TDGA). In TGDA the droplets exiting the optical particle counter are compared to the droplet diameters formed from a reference aerosol (Engelhart et al., 2008). $(NH_4)_2SO_4$ is used as the reference aerosol. TDGA has previously been applied to various ambient (Bougiatioti et al., 2009; Asa-Awuku et al., 2011; Padró et al., 2012; Asa-Awuku et al., 2015) and laboratory chamber studies (Asa-Awuku et al., 2009; Frosch et al., 2013).

In another setup the droplet sizes were evaluated for size selected 100 nm dry $(NH_4)_2SO_4$ aerosol. 100nm is selected because it is commonly considered a cut off size for CCN and droplet size measured by the CCNc. It can also be easily modified by dry particle size (Lathem & Nenes, 2011; Fofie et al., 2017). In this experiment CO_2 was the gas medium in which the aerosol was suspended. The 100 nm dry $(NH_4)_2SO_4$ + CO_2 was exposed to supersaturations from 0.1 to 0.8% at 0.5 lpm. The resultant droplet sizes, $D_{p_{CO_2}}$ are compared to those of 100 nm dry $(NH_4)_2SO_4$ in standard air, D_p at the same instrument conditions using TDGA. Using the scaling in superstations due to the change in medium gas and critical diameter (equation [6] and [7]) we model a new droplet diameter Dp_{gas} and $Dp_{d_s'}$ respectively, from prior experiments at the same supersaturation and flowrate.

Table 5.1. Gas Properties

Gas	Molecular weight [g/mol]	Diffusivity (H_2O in gas) [cm^2/s]
Air	28.97	0.28
Argon	39.95	0.29
CO_2	44.01	0.25

5.4 Results

The CCN activation experiments with excess argon gas showed a significant decrease in the critical diameter (Figure 5.1). Based on the molecular weights of argon and air the supersaturation is expected to increase by a maximum 18% ($\Delta S_{Ar} = 1.175$ in Fig. 5.1) with excess argon (equation [5.6] and table 5.1). From experimental observations however, the increase in supersaturation due to the excess argon, $\Delta S_{d_s'}$ ranged from 10 – 20%.

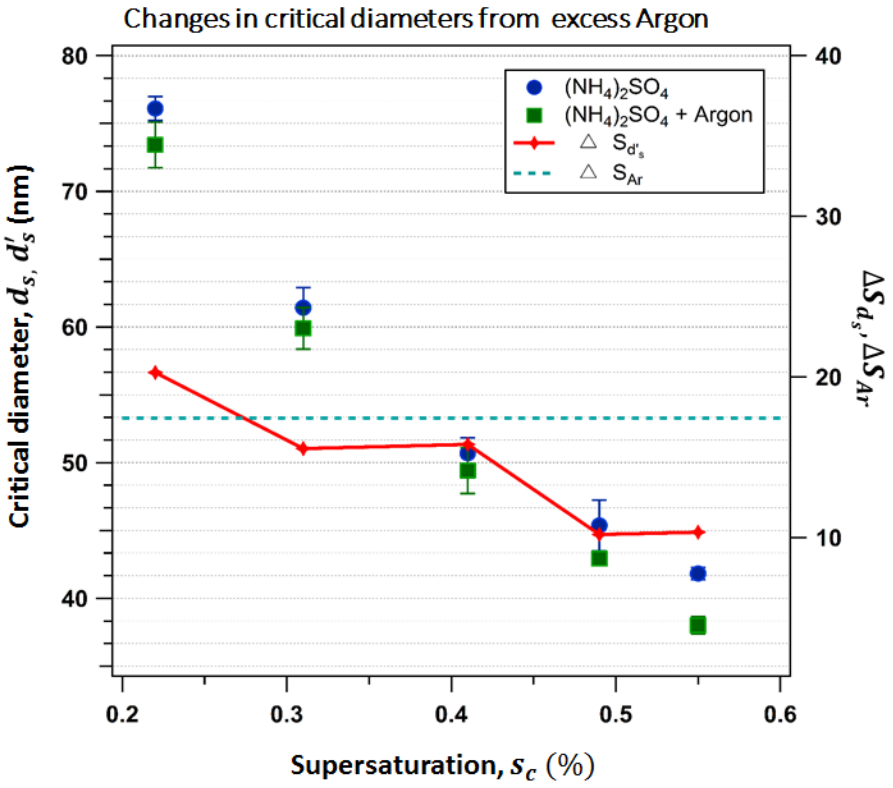

Figure 5.1. Measured $(NH_4)_2SO_4$ critical diameter (blue filled circles) compared to that of $(NH_4)_2SO_4$ + Argon (green filled squares). The red line shows the apparent increase in the supersaturation from estimated from SMCA due to the excess argon. The blue horizontal

dashed green line is the maximum increase in supersaturation due to molecular weight alone.

This is estimated from equation [5.7] based on the measured apparent increase in critical diameter from d_s to d_s'. The increase in supersaturation seem to be more pronounced at lower supersaturations.

In figure 5.2, droplet diameters measured from the droplet activation experiments are compared. The droplet diameter are estimated from the raw size and frequency of the droplets exiting the CCNc optical particle counter. The droplet diameters are an average of the total activated aerosol fraction. The droplet diameters show a gradual divergence when the standard $(NH_4)_2SO_4$ is compared with $(NH_4)_2SO_4$ + argon. The differences in the droplet diameters seem to be strongly dependent on supersaturation.

Below $s_c = 0.4$ the difference between the droplets diameters are all within one bin width; the droplets are statistically the same. At $s_c > 0.4$ however, the difference between the $(NH_4)_2SO_4$ droplets and the $(NH_4)_2SO_4$ + argon droplets are more significant. The droplet sizes increases to as much as 60% at 0.55%. We modelled droplet diameter based on ΔS_{Ar} and $\Delta S_{d_s'}$ supersaturations using previous CCNc experimental data. The modelled droplet diameters, $Dp_{d_s'}$ and $D_{p_{Ar}}$ converged. The modelled droplet diameters were statistically similar to those of the standard $(NH_4)_2SO_4$ experiments but less than those experimentally measured from the $(NH_4)_2SO_4$ + argon experiments.

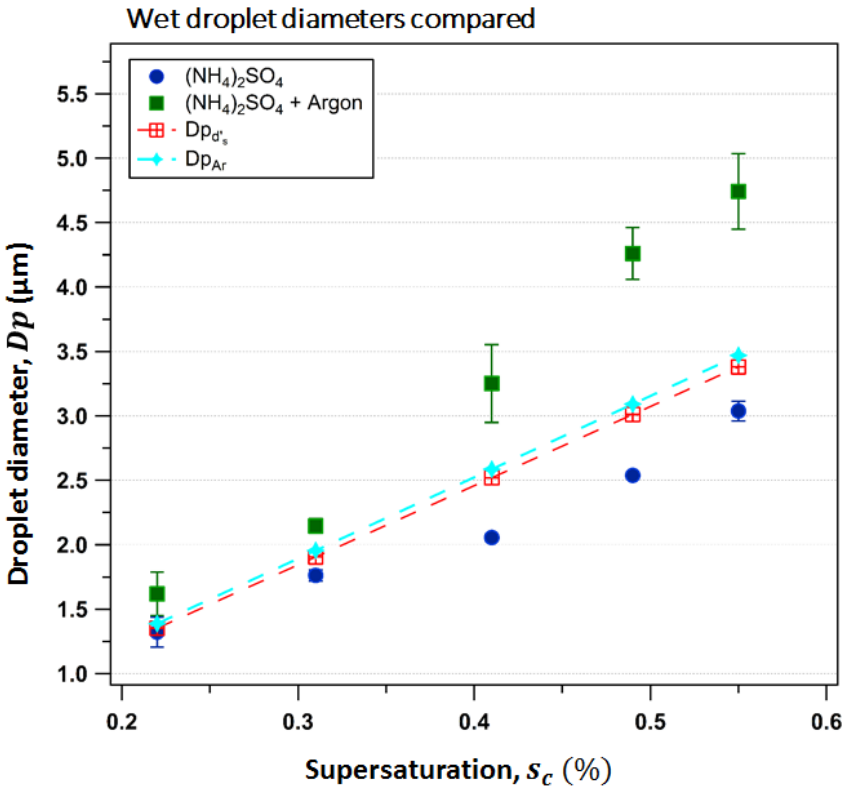

Figure 5.2. The average droplet diameters from the SMCA. Blue filled circles are $(NH_4)_2SO_4$ and green filled squares are $(NH_4)_2SO_4$ + argon.

In figure 5.3, the droplet diameters of 100nm $(NH_4)_2SO_4$ droplets and the $(NH_4)_2SO_4$ + CO_2. We also modelled droplet diameters based on the supersaturation scaling, ΔS_{CO_2}. The ΔS_{CO_2} used is calculated based on the molecular weights of air and CO_2. With excess CO_2, the droplets formed from size-selected 100nm $(NH_4)_2SO_4$ (filled

triangles), were significantly larger than those of $(NH_4)_2SO_4$ in standard air. The $(NH_4)_2SO_4 + CO_2$ droplet diameters were ~2 µm (4 bins) larger for all supersaturations (0.1 – 0.7 %). The modelled droplet diameters, although larger than the $(NH_4)_2SO_4$ in air system, is smaller than those of $(NH_4)_2SO_4 + CO_2$. There is a 2 bin difference between them.

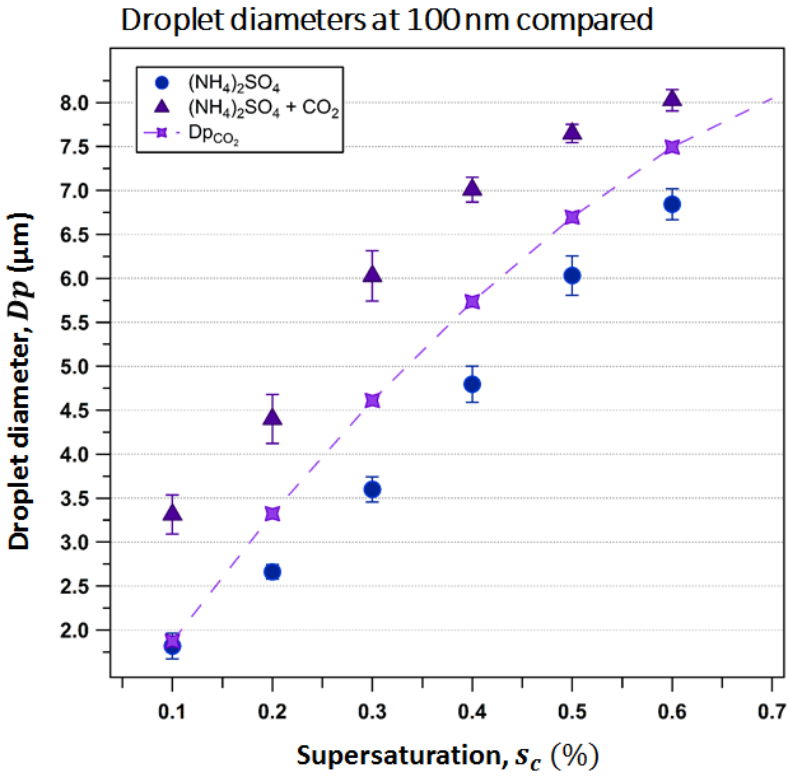

Figure 5.3. CCNc droplet diameters of 100nm $(NH_4)_2SO_4$ compared to $(NH_4)_2SO_4$ + excess CO_2 from SS = 0.1 – 0.7%. The CCNc measured droplet diameters are also compared to modelled droplet diameters based on the molecular weight-constrained supersaturation (Dp_{CO_2}).

5.5 Summary and Conclusions

The observations made from this study suggests the presence of excess gases that modify the volumetric ratio of air may have a significant influence on the apparent supersaturation and mass transfer. The decrease in the critical supersaturation suggested by the apparent decrease in critical diameter can be attributed to the presence of excess gas. Excess gas of higher molecular weight (argon and carbon dioxide) increases the relative molecular velocity of water vapor to the centerline of the instrument. This causes an apparent increase in the supersaturation. The observed change due to the critical diameter is however lower than the maximum predicted from molecular weight ratios alone. This suggests that, when the working gas is modified the changes in supersaturation may need to be constrained by water vapor mass transfer as well as the heat transfer (which we assumed negligible in our analysis).

The apparent increase in supersaturation causes an increase in the wet diameter of the droplets formed. In the size-selected droplet growth experiments there is a consistent, statistically significant increase in droplet diameter with the injection of excess carbon dioxide. In SMCA experiments however, the increase in droplet sizes is not significant at lower superstations (< 0.3 %). This may indicate a higher susceptibility to supersaturation depletion with the injection of the heavier gases (Lathem & Nenes, 2011; Fofie et al., 2017). In both size selected and SMCA droplets, the measured CCN droplet diameters do not converge with modelled droplet diameters based on molar mass and apparent critical diameter supersaturation scaling. This suggests that the scaling of the droplet growth by the molecular based-mass transfer (velocity ratio) is insufficient. In addition to an

increase in the droplet growth due to the increase in the supersaturation, the discrepancies in the final droplet sizes suggest that there may be higher a mass accommodation of water vapor (α) due to the modification of the volumetric ratio of air. Higher supersaturation plus higher mass transfer regime results in the formation of larger droplets.

The observations made here may provide new insights into previous ambient and laboratory observations of increases in the droplet diameters. In ambient aircraft measurements of urban, sulfates and organics dominated regions, 60% of droplets were smaller than the reference $(NH_4)_2SO_4$ (Asa-Awuku et al., 2011). In another study of chamber generated secondary organic aerosol from β-caryophyllene ozonolysis there was an observed change in droplet diameters with changes experimental time and water soluble organic fractions. The changes in droplet diameters was inadequately constrained by the mass accommodation coefficient (Asa-Awuku et al., 2009). From the observations in this study we propose that potential changes in mass transfer due to significant presence of volatile gasses (such as in the case of secondary organic aerosol partitioning) may cause an apparent modifications in the supersaturation of the CCNc. This coupled with higher mass transfer rates may explain the unresolved increase in droplet diameters observed.

This study demonstrates a modification in CCN activity and droplet growth kinetics when activating aerosol coexist with condensable and non-condensable gases. These gases may modify the operation of the CCNc instrument. It is therefore imperative

to also quantify the volumetric composition of gases when measuring CCN in both laboratory studies and ambient environments with high gas concentrations.

5.6 Acknowledgements

The authors would like to thank the United States National Science Foundation (NSF) and the University of California Transportation Research Fellowship for their support in this work. Specifically, the publication of this work was supported by the NSF grant 1151893. Its contents are solely the responsibility of the grantees and do not necessarily represent the official views of the NSF or UCTC. Further, the NSF does not endorse the purchase of any commercial products or services mentioned in the publication.

5.7 Literature Cited

An, W. J., Pathak, R. K., Lee, B.-H., & Pandis, S. N. (2007). Aerosol volatility measurement using an improved thermodenuder: Application to secondary organic aerosol. *Journal of Aerosol Science, 38*(3), 305-314.

Andersson, S., Martinsson, B., Friberg, J., Brenninkmeijer, C., Rauthe-Schöch, A., Hermann, M., . . . Zahn, A. (2013). Composition and evolution of volcanic aerosol from eruptions of Kasatochi, Sarychev and Eyjafjallajökull in 2008–2010 based on CARIBIC observations. *Atmospheric Chemistry and Physics, 13*(4), 1781-1796.

Asa-Awuku, A., Engelhart, G. J., Lee, B. H., Pandis, S. N., & Nenes, A. (2009). Relating CCN activity, volatility, and droplet growth kinetics of beta-caryophyllene secondary organic aerosol. *Atmospheric Chemistry and Physics, 9*(3), 795-812.

Asa-Awuku, A., Moore, R. H., Nenes, A., Bahreini, R., Holloway, J. S., Brock, C. A., . . . Huey, L. G. (2011). Airborne cloud condensation nuclei measurements during the 2006 Texas Air Quality Study. *Journal of Geophysical Research-Atmospheres, 116*(D11). doi:Artn D11201

10.1029/2010jd014874

Asa-Awuku, A., Sorooshian, A., Flagan, R. C., Seinfeld, J. H., & Nenes, A. (2015). CCN properties of organic aerosol collected below and within marine stratocumulus clouds near Monterey, California. *Atmosphere, 6*(11), 1590-1607.

Bauer, S. E., & Menon, S. (2012). Aerosol direct, indirect, semidirect, and surface albedo effects from sector contributions based on the IPCC AR5 emissions for preindustrial and present-day conditions. *Journal of Geophysical Research: Atmospheres (1984–2012), 117*(D1).

Bougiatioti, A., Fountoukis, C., Kalivitis, N., Pandis, S. N., Nenes, A., & Mihalopoulos, N. (2009). Cloud condensation nuclei measurements in the marine boundary layer of the Eastern Mediterranean: CCN closure and droplet growth kinetics. *Atmospheric Chemistry and Physics, 9*, 7053.

Brush, S. G. (2013). *Kinetic Theory: The Chapman–Enskog Solution of the Transport Equation for Moderately Dense Gases* (Vol. 3): Elsevier.

Chapman, S., & Cowling, T. G. (1970). *The mathematical theory of non-uniform gases: an account of the kinetic theory of viscosity, thermal conduction and diffusion in gases*: Cambridge university press.

Connolly, P., Topping, D., Malavelle, F., & McFiggans, G. (2014). A parameterisation for the activation of cloud drops including the effects of semi-volatile organics. *Atmospheric Chemistry and Physics, 14*(5), 2289-2302.

Cubison, M., Ervens, B., Feingold, G., Docherty, K., Ulbrich, I., Shields, L., . . . Jimenez, J. (2008). The influence of chemical composition and mixing state of Los Angeles urban aerosol on CCN number and cloud properties. *Atmospheric Chemistry and Physics, 8*(18), 5649-5667.

Dusek, U., Frank, G. P., Hildebrandt, L., Curtius, J., Schneider, J., Walter, S., . . . Andreae, M. O. (2006). Size matters more than chemistry for cloud-nucleating ability of aerosol particles. *Science, 312*(5778), 1375-1378. doi:10.1126/science.1125261

Ebmeier, S., Sayer, A. M., Grainger, R., Mather, T., & Carboni, E. (2014). Systematic satellite observations of the impact of aerosols from passive volcanic degassing on local cloud properties. *Atmospheric Chemistry and Physics, 14*(19), 10601-10618.

Engelhart, G. J., Asa-Awuku, A., Nenes, A., & Pandis, S. N. (2008). CCN activity and droplet growth kinetics of fresh and aged monoterpene secondary organic aerosol. *Atmospheric Chemistry and Physics, 8*(14), 3937-3949.

Fedele, A., Pedone, M., Moretti, R., Wiersberg, T., Somma, R., Troise, C., & De Natale, G. (2017). Real-time quadrupole mass spectrometry of hydrothermal gases from the unstable Pisciarelli fumaroles (Campi Flegrei): Trends, challenges and processes. *International Journal of Mass Spectrometry*.

Fofie, E. A., Castellucio, V., & Asa-Awuku, A. (2017). Exploring CCN droplet kinetics with a higher sensitivity optical particle counter *Aerosol Sci Technol, in review*.

Frosch, M., Bilde, M., Nenes, A., Praplan, A., Jurányi, Z., Dommen, J., . . . Baltensperger, U. (2013). CCN activity and volatility of β-caryophyllene secondary organic aerosol. *Atmospheric Chemistry and Physics, 13*(4), 2283-2297.

Fukuta, N., & Walter, L. (1970). Kinetics of hydrometeor growth from a vaper-spherical model. *Journal of the Atmospheric Sciences, 27*(8), 1160-1172.

Giggenbach, W., & Matsuo, S. (1991). Evaluation of results from Second and Third IAVCEI field workshops on volcanic gases, Mt Usu, Japan, and White Island, New Zealand. *Applied Geochemistry, 6*(2), 125-141.

Haywood, J., & Boucher, O. (2000). Estimates of the direct and indirect radiative forcing due to tropospheric aerosols: A review. *REVIEWS OF GEOPHYSICS-RICHMOND VIRGINIA THEN WASHINGTON-, 38*(4), 513-543.

Hegg, D. A. (2000). Impact of gas-phase HNO3 and NH3 on microphysical processes in atmospheric clouds. *Geophysical Research Letters, 27*(15), 2201-2204.

Hirschfelder, J., & Curtiss, C. (1954). RB Bird Molecular theory of liquids and gases: John Wiley and Sons, Inc., New York

Köhler, H. (1936). The nucleus in and the growth of hygroscopic droplets. *Transactions of the Faraday Society, 32*, 1152-1161.

Kulmala, M., Laaksonen, A., Korhonen, P., Vesala, T., Ahonen, T., & Barrett, J. (1993). The effect of atmospheric nitric acid vapor on cloud condensation nucleus activation. *Journal of Geophysical Research: Atmospheres, 98*(D12), 22949-22958.

Lance, S., Nenes, A., Medina, J., & Smith, J. N. (2006). Mapping the Operation of the DMT Continuous Flow CCN Counter. *Aerosol Science and Technology, 40*(4), 242-254. doi:10.1080/02786820500543290

Lane, T. E., Donahue, N. M., & Pandis, S. N. (2008). Simulating secondary organic aerosol formation using the volatility basis-set approach in a chemical transport model. *Atmospheric Environment, 42*(32), 7439-7451.

Lathem, T. L., & Nenes, A. (2011). Water Vapor Depletion in the DMT Continuous-Flow CCN Chamber: Effects on Supersaturation and Droplet Growth. *Aerosol Science and Technology, 45*(5), 604-615. doi:10.1080/02786826.2010.551146

Martin, R., Mather, T., Pyle, D., Power, M., Allen, A., Aiuppa, A., . . . Ward, E. (2008). Composition-resolved size distributions of volcanic aerosols in the Mt. Etna plumes. *Journal of Geophysical Research: Atmospheres, 113*(D17).

McCoy, D. T., & Hartmann, D. L. (2015). Observations of a substantial cloud-aerosol indirect effect during the 2014–2015 Bárðarbunga-Veiðivötn fissure eruption in Iceland. *Geophysical Research Letters, 42*(23).

McFiggans, G., Artaxo, P., Baltensperger, U., Coe, H., Facchini, M. C., Feingold, G., . . . Lohmann, U. (2006). The effect of physical and chemical aerosol properties on

warm cloud droplet activation. *Atmospheric Chemistry and Physics, 6*(9), 2593-2649.

Mills, M. J., Schmidt, A., Easter, R., Solomon, S., Kinnison, D. E., Ghan, S. J., . . . Bardeen, C. G. (2016). Global volcanic aerosol properties derived from emissions, 1990–2014, using CESM1 (WACCM). *Journal of Geophysical Research: Atmospheres, 121*(5), 2332-2348.

Moore, R. H., Nenes, A., & Medina, J. (2010). Scanning Mobility CCN Analysis—A Method for Fast Measurements of Size-Resolved CCN Distributions and Activation Kinetics. *Aerosol Science and Technology, 44*(10), 861-871. doi:10.1080/02786826.2010.498715

Padró, L., Moore, R., Zhang, X., Rastogi, N., Weber, R., & Nenes, A. (2012). Mixing state and compositional effects on CCN activity and droplet growth kinetics of size-resolved CCN in an urban environment. *Atmospheric Chemistry and Physics, 12*(21), 10239-10255.

Petters, M. D., & Kreidenweis, S. M. (2007). A single parameter representation of hygroscopic growth and cloud condensation nucleus activity. *Atmospheric Chemistry and Physics, 7*(8), 1961-1971.

Pruppacher, H., & Klett, J. (1997). Microphysics of Clouds and Precipitation: With an Introduction to Cloud Chemistry and Cloud Electricity, 954 pp: Springer, New York

Roberts, G. C., & Nenes, A. (2005). A continuous-flow streamwise thermal-gradient CCN chamber for atmospheric measurements. *Aerosol Science and Technology, 39*(3), 206-221.

Romakkaniemi, S., Jaatinen, A., Laaksonen, A., Nenes, A., & Raatikainen, T. (2014). Ammonium nitrate evaporation and nitric acid condensation in DMT CCN counters. *Atmospheric Measurement Techniques, 7*(5), 1377-1384.

Rose, D., Gunthe, S., Mikhailov, E., Frank, G., Dusek, U., Andreae, M. O., & Pöschl, U. (2008). Calibration and measurement uncertainties of a continuous-flow cloud condensation nuclei counter (DMT-CCNC): CCN activation of ammonium sulfate and sodium chloride aerosol particles in theory and experiment. *Atmospheric Chemistry and Physics, 8*(5), 1153-1179.

Ruehl, C. R., Chuang, P. Y., & Nenes, A. (2008). How quickly do cloud droplets form on atmospheric particles? *Atmospheric Chemistry and Physics, 8*(4), 1043-1055.

Ruehl, C. R., Davies, J. F., & Wilson, K. R. (2016). An interfacial mechanism for cloud droplet formation on organic aerosols. *Science, 351*(6280), 1447-1450. doi:10.1126/science.aad4889

10.1126/science.aad4889.

Seinfeld, J. H., & Pandis, S. N. (2006). Atmospheric Chemistry and Physics, A Wiley-Inter Science Publication: John Wiley & Sons Inc, New York

Seinfeld, J. H., & Pandis, S. N. (2016). *Atmospheric chemistry and physics: from air pollution to climate change*: John Wiley & Sons.

Shinohara, H., Geshi, N., Matsushima, N., Saito, G., & Kazahaya, R. (2017). Volcanic gas composition changes during the gradual decrease of the gigantic degassing activity of Miyakejima volcano, Japan, 2000-2015. *Bulletin of Volcanology, 79*(2), 21.

Topping, D., Connolly, P., & McFiggans, G. (2013). Cloud droplet number enhanced by co-condensation of organic vapours. *Nature geoscience, 6*, 443-446. doi:doi:10.1038/ngeo1809

Twomey. (1963). Measurements of natural cloud nuclei. *J. Rech. Atmos, 1*, 101-105.

Wang, S. C., & Flagan, R. C. (1990). Scanning electrical mobility spectrometer. *Aerosol Science and Technology, 13*(2), 230-240.

CHAPTER 6:CONCLUSIONS AND FUTURE DIRECTIONS

The objectives of this dissertation were to characterize the CCN droplet growth kinetics, and constrain the CCN activity and droplet kinetics of combustion emissions with aging, mixing states and chemical composition.

We investigated the droplet kinetics with a re-engineered, higher sensitivity CCNc optical particle counter, OPC-β. The higher sensitivity OPC-β data was coupled with the continuous flow streamwise thermal gradient CCNc (CFSTGC) model to estimate the mass accommodation coefficient, α. For inorganic and organic aerosol, a mass accommodation coefficient, $\alpha >> 0.2$ yielded modelled droplet diameters consistent with experimental and ambient observations. The droplet kinetics, and hence final droplet diameters are suppressed by ~ 0.2 μm for every $1000\ cm^{-3}$ CCN, even at CCN concentrations less than $5000\ cm^{-3}$. Using modified gas medium in the CCN chamber we demonstrated that the CCN activity and droplet kinetics of aerosol can be modified due to excess condensable or non-condensable gases. These gases change the heat and mass transfer regime in the CCNc and modify the supersaturation and mass transfer rate in the CCNc. It is therefore imperative to constrain droplet kinetics with volumetric gas phase composition data when measuring CCN in both laboratory studies and ambient environments with high and varying gas concentrations.

In vehicular emissions, we evaluated the hygroscopicity and droplet kinetics of fresh and aged emissions from new generation gasoline direct injection engines

retrofitted with a gasoline particulate filter (GPF). The chemical composition and morphology of the SA formed from the aging was measured with an HR-TOF-AMS and a custom-built APM-SMPS system. The supersaturated and subsaturated hygroscopicity of the fresh and aged emission was measured with a DMT Streamwise Thermal Gradient CCN counter and a hygroscopicity tandem differential mobility analyzer (HTDMA), respectively. The measurements show that the fresh gasoline emissions were only slightly hygroscopic in both supersaturated and subsaturated environments. Photochemical aging and subsequent condensation of the SOA formed from the co-emitted gas phase SOA precursors increases the hygroscopicity of gasoline emissions. In the stock engine setup (without the GPF), both subsaturated and supersaturated hygroscopicity increased. When the engine was retrofitted with the GPF, the SA experiments were seeded with $(NH_4)_2SO_4$. In these experiments the presence of the condensing SA depressed the hygroscopicity of the salt-SOA mixture. The hygroscopicity was also depressed in the subsaturated regime with time. These changes in the hygroscopicity with aging were additionally sensitive to aerosol dry size distribution. Based on the CCN, HTDMA and AMS data we inferred that the aerosol mixture formed from the aging process is either internally mixed (in $(NH_4)_2SO_4$-seeded experiments) or formed core shell structures from the stock configuration emissions. We also used threshold droplet growth analysis (TDGA) to evaluate the effects of the condensing SA on droplet kinetics. There were no significant, observable modifications in the droplet sizes of all the aerosol mixtures formed due to aging.

The effects of mixing states of anthropogenic primary (diesel or motor oil-fuel POA) and biogenic secondary organic aerosol (α-pinene SOA) on CCN activity and droplet kinetics was explored. In the α-pinene SOA + diesel POA mixture, the CCN activity, characterized by κ-hygroscopicity, decreased after an initial injection of the POA but increased after mixing equilibrium was established. The α-pinene SOA + motor oil-fuel POA mixture formed a weak mixture whose CCN activity increased with aging. An empirical model using unit mass resolution (UMR) AMS data predicts CCN activity. The model captures the complex CCN activity from both anthropogenic and biogenic mixing systems.

From this thesis we can make these novel inferences which have important implications for the assessment of cloud-aerosol indirect effects from anthropogenic emissions:

i. The current understanding of aerosol CCN formation and droplet kinetics may be dependent on the sensitivity of the optical particle counter in the CCN counter used for measurements.
ii. The final droplet diameters of CCN are independent of aerosol hygroscopicity (hence chemical composition) but strongly dependent on the CCN concentration.
iii. CCN droplet diameters can be modified by gas-phase vapors
iv. A similarity in the CCN activity of organic aerosol may be indicative of its propensity to mix.

v. CCN data coupled with UMR AMS information maybe a promising tool to gain additional insight into mixtures of organic aerosol and its interactions with water vapor.

vi. Emissions from new technology gasoline direct injection (GDI) light duty vehicles fitted with gasoline particulate filters (GPF) form CCN active SOA upon photochemical aging.

vii. In GDI with GPF vehicles, the point of emission may influence the chemical composition, and mixing states of the SA formed and subsequently hygroscopicity and delinquency.

Future work should be focused on further improving the sensitivity of currently available CCN measurement tools. With an improved sensitivity and size measuring range, more robust ambient and laboratory data will be derived to better refine cloud models. A more thorough understanding of CCN density and gas-phase volumetric ratio effects on droplet kinetics also needs to be pursued. These will contribute to a more robust prediction of aerosol-indirect effects.

APPENDIX A

A.1 Droplet Growth

CCN droplets grow indefinitely after activation provided the supersaturation, *SS,* is higher the critical supersaturation of the dry aerosol. After activation, the condensational or evaporation growth rate of an atmospheric droplet that forms clouds and fog is described by the equation (Fukuta & Walter, 1970; Seinfeld & Pandis, 2006):

$$\frac{dm}{dt} = 2\pi D_p D_v \left(c_{w,\infty} - c_w^{eq}\right) \quad [1]$$

where m is the droplet mass, D_p is droplet diameter, D_v is the water vapor diffusivity, $c_{w,\infty}$ is the concentration of water vapor far from the droplet and c_w^{eq} is the equilibrium concentration of water vapor. Equation 1 neglects the non-continuum effects of smaller droplets. The correction is made by introducing the water uptake coefficient, α, the probability of a water vapor sticking to the surface of the droplet, into the diffusivity equation. This accounts for the kinetic limitations of the droplets that may be due to the solute-solvent interactions. The modified diffusivity D_v' by (Fukuta & Walter, 1970; Seinfeld & Pandis, 2006)

$$D'_v = \frac{D_v}{1 + \frac{2D_v}{\alpha}\left(\frac{2\pi M_w}{RT}\right)^{0.5}} \quad [2]$$

After rearrangement, the growth of a droplet of initial diameter D_p, can be described as. For aerosols grown in the DMT CCN counter the final droplets diameters are determined by the aerosol flowrate, supersaturation (relative humidity) and the CCN concentration. The growth of the droplets is inversely proportional to the aerosol flowrates;

higher CCN sample flowrates reduce the residence time for droplet growth (Lance et al., 2006).

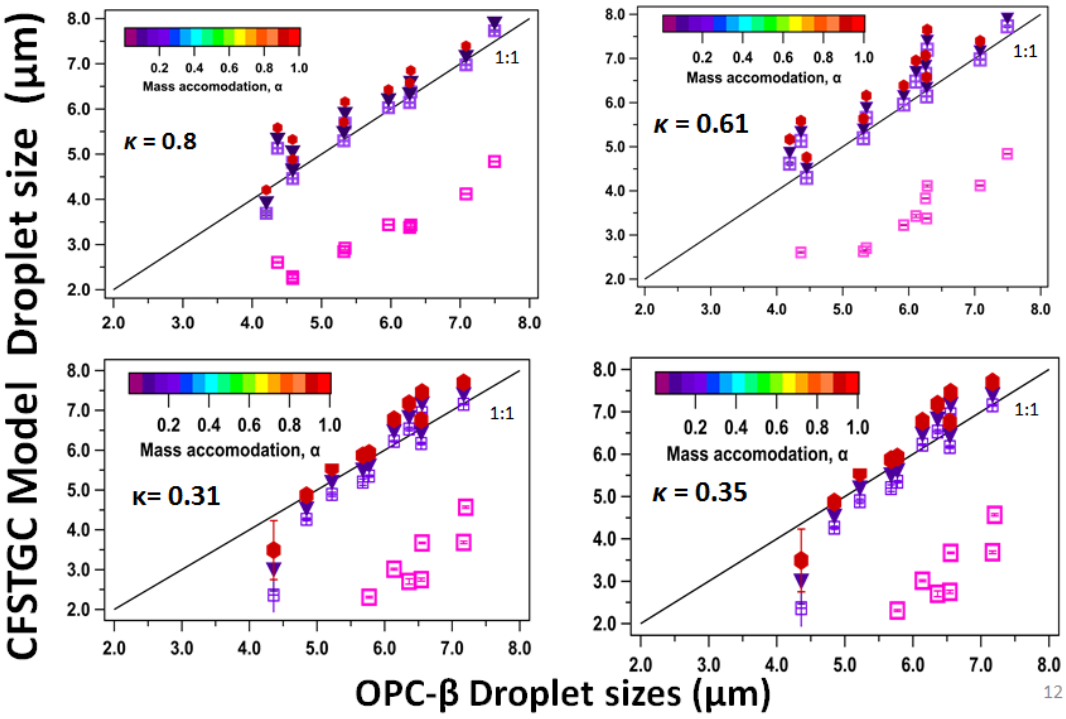

Figure A - 1. Droplet simulated with the CFSTGC for different solute composition (represented by κ) and mass accommodation coefficient from 0.01 – 1 and compared with the experimentally

APPENDIX B

Tabble B - 1. Calibration of DMT CCN counter. The calibration was done at 0.5 lpm instrument flowrate, SS is the supersaturation and Stdev is the standard deviation.

Instrument SS [%]	Dp_{50} [nm]	Stdev Dp_{50} [nm]	Calibrated SS [%]
0.2	72.96	0.62	0.23
0.3	59.41	1.11	0.32
0.3	61.01	15.63	0.31
0.4	49.04	1.88	0.42
0.6	41.71	0.53	0.54
0.6	41.14	0.75	0.55
0.7	36.22	1.85	0.67
0.8	35.02	0.94	0.7
0.9	31.81	0.2	0.81
1	28.93	0.01	0.94
1.2	24.73	0.03	1.23
1.5	22	0.02	1.42

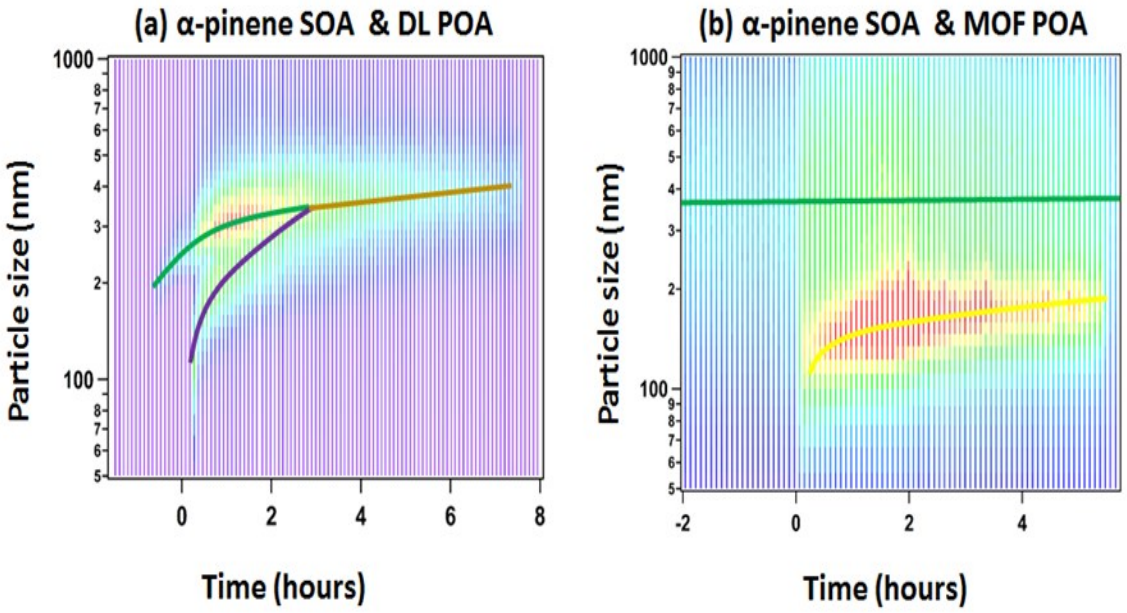

Figure B - 1. AMS PToF Particle size distribution over the experiment duration. (a) α-pinene SOA and DL POA. Distinct distributions for α-pinene SOA (green line) and DL POA (violet line) exist before equilibrium mixing is attained after (brown). (b) In the α-pinene SOA (green) and MOF POA (yellow) distinct chemical modes exist throughout the experiment.

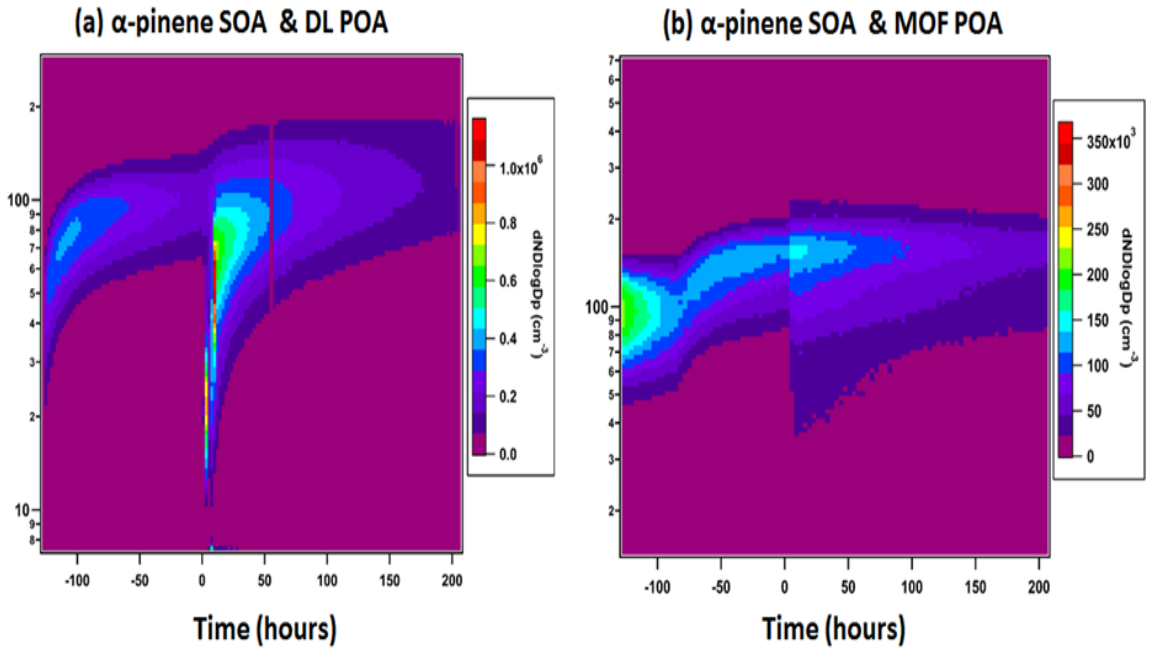

Figure B - 2. SMPS size distribution over the experiment duration. (a) α-pinene SOA and DL POA. The injection of the DL POA (at time = 0 hour) shifts the aerosol distribution. There is a significant amount of aerosol with a dry diameter between 10-60 nm. More volatile components of the injected DL POA condense onto the smaller particles as the experiment evolves. The initial bimodal distribution merges with time. (b) α-pinene SOA and MOF POA. Injected MOF POA has a similar size distribution compared to the α-pinene SOA and form a single size distribution.

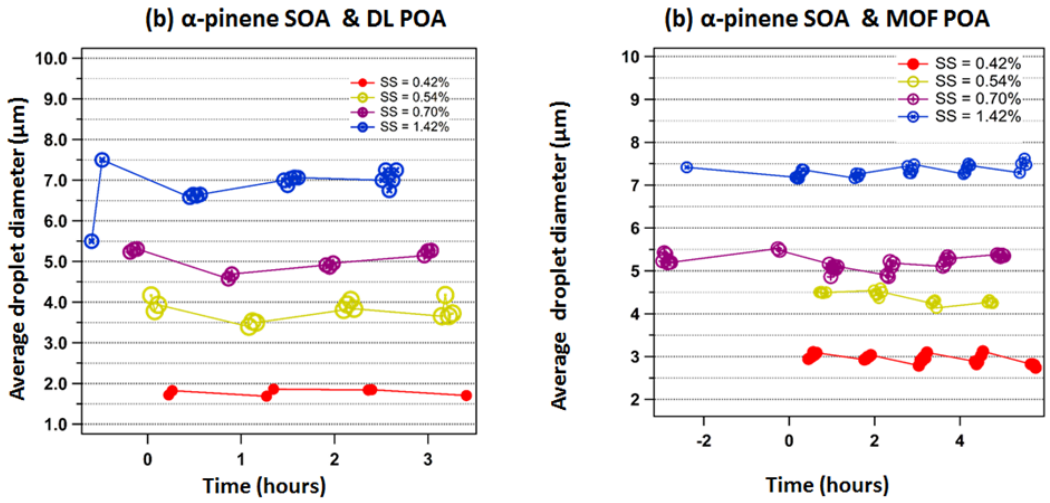

Figure B - 3. Average droplet sizes for (a) α-pinene SOA and DL POA and (b) α-pinene SOA and MOF POA. In both mixtures the average droplet sizes do not change significantly with time. And where changes do occur they are within the measuring uncertainty of the OPC sensitivity and hence may be insignificant.

Literature Cited

Fukuta, N., & Walter, L. (1970). Kinetics of hydrometeor growth from a vaper-spherical model. *Journal of the Atmospheric Sciences, 27*(8), 1160-1172.

Lance, S., Nenes, A., Medina, J., & Smith, J. (2006). Mapping the operation of the DMT continuous flow CCN counter. *Aerosol Science and Technology, 40*(4), 242-254.

Seinfeld, J. H., & Pandis, S. N. (2006). Atmospheric Chemistry and Physics, A Wiley-Inter Science Publication: John Wiley & Sons Inc, New York